# CHARACTERIZATION OF HB9 INTERNEURONS: BEHAVIOUR AND ANATOMY

by

Lina Mohamed Koronfel

Submitted in partial fulfilment of the requirements
for the degree of Master of Science

at

Dalhousie University
Halifax, Nova Scotia
March 2015

إلى أمى و أبى لتشجيعهما الدائم، و حبهما الذى لا ينتهى

# TABLE OF CONTENTS

# LIST OF TABLES

# LIST OF FIGURES

# ABSTRACT

Central pattern generators (CPGs) are neuronal circuits that are responsible for the generation of rhythmic behaviours such as locomotion. It has been suggested that a population of spinal interneurons (INs), known as Hb9 INs, are possible rhythm generators of the locomotor CPG. Whether these glutamatergic INs (expressing vesicular glutamate transporter vGluT2) are indeed involved in generating the rhythm of locomotion remains unknown. To address this question, we used genetic strategies to silence the output of Hb9 INs. Hb9::CreER$^{T2}$ animals were crossed for two generations with vGluT2$^{flox/flox}$ animals. Injection of tamoxifen generated animals that lack vGluT2 in the terminals of Hb9 expressing cells (Hb9 -VGluT2$^{OFF}$). There were no significant differences observed in treadmill locomotion of Hb9-VGluT2$^{OFF}$ animals compared to heterozygotes and wild-type littermates. To further assess their possible role, the distribution of glutamatergic boutons of Hb9 INs was analyzed in Hb9::CreER$^{T2}$; Rosa26$^{fs\text{-}synaptophysin\text{-}Td\text{-}tomato}$ mouse model. The boutons of Hb9 INs were distributed in the rostrocaudal axis of the spinal cord, and selectively in medial lamina VIII, lamina IX and ventral lamina X of upper lumbar segments. While their role appears to be limited in locomotor activity, the locations of Hb9 IN boutons may provide insight into the role of these interneurons.

A similar, non-published abstract was submitted to the spinal cord injury meeting (2015), for an accompanying poster presentation.

# LIST OF ABBREVIATIONS AND SYMBOLS USED

| | |
|---|---|
| µl | microliter |
| µm | micrometer |
| $^{o}C$ | degree Celsius |
| 2D | two dimensional |
| 3D | three dimensional |
| 5-HT | 5-hydroxytryptamine |
| Ab | antibody |
| ANOVA | analysis of variance |
| C.V. | coefficient of variation |
| $Ca^{2+}$ | calcium ion |
| CaV3 | T-type voltage gated calcium channel |
| ChAT | choline acetyltransferase |
| cm | centimeter |
| CPG | central pattern generator |
| cps | centimeters per second |
| Cre | cyclization recombination enzyme |
| CreER | cyclization recombination enzyme fused with estrogen receptor |
| $CreER^{T2}$ | cyclization recombination enzyme fused with estrogen receptor highly sensitive to Tamoxifen |
| $d.H_2O$ | distilled water |
| Dbx1 | developing brain homeobox protein 1 |
| $dI3^{OFF}$ | mouse model of mutant vGluT2 in Isl1 expressing cells |
| DNA | deoxyribonucleic acid |

| | |
|---|---|
| DIG | digoxigenin |
| dsPBS | double salt phosphate buffer solution |
| EM | electron microscopy |
| EMG | electromyogram |
| ER | estrogen receptor |
| floxP or flox | flanked by loxP sites |
| fs | stop sequence flanked by loxP sites |
| GFP | green fluorescent protein |
| Hb9 | homeodomain protein product of HB9 gene |
| HB9 | homeobox gene B9 |
| Hb9::CreER$^{T2}$ | transgenic mouse model that express CreER$^{T2}$ in Hb9 cells |
| Hb9::eGFP | transgenic mouse model that express eGFP in Hb9 cells |
| Hb9$^{Cre/+}$ | knock-in mouse model that express Cre in Hb9 cells |
| Hb9 -VGluT2$^{OFF}$ | mouse model of mutant vGluT2 in Hb9 expressing cells |
| HCl | hydrochloric acid |
| HD | homeodomain protein |
| HeNe | helium neon |
| IF | immunoflourescent |
| IgG | immunoglobulin G |
| IML | intermediolateral |
| IMM | intermediomedial |
| IN | interneuron |
| IP | intra-peritoneal |
| Isl1 | insuline gene enhancer protein Isl1 |
| Kde2d | two dimensional kernel density estimation |

| | |
|---|---|
| L (#) | lumbar segment (#) |
| lacZ | structural gene lacZ of lactose operon |
| Lhx3/6 | LIM/homeoboxprotein Lhx3/6 |
| LMC | lateral motoneuron column |
| loxP | loxus of X over of P1 bacteriophage DNA |
| M | molar |
| ml | milliliter |
| MIP | maximum intensity projection |
| MMC | medial motoneuron column |
| MN | motoneuron |
| mRNA | messenger ribonuclic acid |
| MΩ | mega ohm |
| NaOH | sodium hydroxide |
| NMDA | N-methyl-D-aspartate |
| nNOS | neuronal nitric oxide synthase |
| OCT | optimal cutting temprature compound |
| P(#) | postnatal day (#) |
| P20s | postnatal days 21-23 mouse group |
| P30s | postnatal days 35-38 mouse group |
| PAP | peroxidase-antiperoxidase |
| PB | phosphate buffer |
| PBST | phosphate buffer solution with triton X |
| pF | pico Farad |
| PFA | paraformaldehyde |
| PIR | post inhibitory rebound |

| | |
|---|---|
| RGB | red green blue |
| Rosa26 | Gt(ROSA)26Sor gene locus |
| RT | room temperature |
| SC | sub-cutaneous |
| SD | standard deviation |
| SHH | sonic hedgehog protein |
| SPN | sympathetic preganglionic neuron |
| SSC | saline sodium citrate buffer |
| Td tomato | tandem dimeric (pseudo monomeric) derivative of dsRed |
| TNB | tris sodium blocking buffer |
| V0 | postmitotic cells of progenitor p0 |
| V1 | postmitotic cells of progenitor p1 |
| V2 | postmitotic cells of progenitor p2 |
| V3 | postmitotic cells of progenitor p3 |
| VGluT2 | vesicular glutamate transporter 2 |
| W10s | postnatal week 9-11 mouse group |
| YFP | yellow fluorescent protein |

# ACKNOWLEDGEMENTS

I would like to express my deepest gratitude to my supervisor, Dr. Robert Brownstone, for his excellent guidance that kept me motivated, and for providing me with an excellent atmosphere to enjoy scientific research. Despite his busy schedule, he was always present whenever I had a question or needed to stimulate a discussion. His answers and intelligent point of views opened my mind and raised my curiosity towards neuroscience in general, and the field of neural circuits in particular.

I would like to thank my graduate committee, Dr. Ying Zhang and Dr. Steven Barnes for their advices, inside and outside of the meeting room. I thank them for guiding me throughout my thesis and for their reassurance that I'm on the right direction.

I thank Dr. Kazue Semba for being in my final thesis defence committee, for being a generous and kind graduate co-ordinator, and for helping me throughout my years as a Masters student.

I also want to thank Kevin Kanning in the Henderson lab (University of Columbia, USA) for providing the Hb9::CreER$^{T2}$ transgenic mouse, and the Todd lab (University of Glasgow, Scotland) for answering our questions using the electron microscope.

A special thanks to Angelita Alcos for teaching me many of the techniques behind the results presented in this thesis, for her patience in guiding me if I had no luck with an experiment, and for contributing with the *in situ* hybridization experiments. A deep thank you to Nadia Farbstein for providing the genotyping results of the animals used in this study, and to Stephen Whitefield for his assistance with the confocal microscope. I'm so glad I worked hand by hand with such cheerful, friendly and patient people.

I want to thank my lab members, past and present, for their help and friendship, they filled the lab with cheer, and the lab was always an exciting place in their presence. In particular, I want to thank Nicolas Stifani and Izabela Panek for being so generous in providing and offering their time and knowledge whenever needed. They have been colleagues whom I hold respect and appreciation to their generosity and intelligence. I also want to thank Abi Thana for her insightful comments.

To the graduate students of the department of Medical Neuroscience whom I considered friends more than colleagues. I'm so lucky to have known such wonderful people whom our relationship was not limited by lab hours or campus borders. A special thanks to Han Zhang for his generosity, and for being always willing to share his knowledge throughout my years in the department.

I want to thank my family and friends around the globe who despite our distance, continued to support and encourage me. A special thanks to Dr. Younes Anini in the department of Physiology and Biophysics who mentored me in my coursework and gave me precious advices on being a productive graduate student. Thanks to Dr. Wael El-Shemey (Cairo University, Egypt) and Dr. Hossam Kareem (Research institute of Opthalmology in Giza, Egypt) for supporting me while achieving my academic goals.

And before all, I want to thank God for guiding me throughout my journey. For giving me strength, patience and wisdom., for helping me to develop on all levels, and for providing me with the insight and faith that led me to where I'm now. Alhamdullah.

**وَتَحْسَبُ أنَّكَ جُرْمٌ صَغِيرٌ ،، وفيك إنطَوَى العالمُ الأكبرَ**

الإمام علي أبن أبي طالب
٥٩٩-٦٦١م

A little body thyself thou deem, while the great universe in thee dwells.

Ali ibn Abi Talib

599-661 AD

# CHAPTER 1 INTRODUCTION

## 1.1 GENERATION OF LOCOMOTOR PATTERN

Locomotion, described as an active shift of body in space, is a basic behaviour that is essential for the survival of living organisms. Locomotor behaviour comes in a variety of forms such as undulation, swimming and walking. The more complex is the animal, the more complex its locomotor behaviour. The core details of the central circuits that generate locomotor rhythm in mammals are still not known. Nevertheless, in the early1900s, Brown (1911) suggested that all the neurons responsible for generating and maintaining the locomotor rhythm in vertebrates reside within the spinal cord. Decerbrated animals with all peripheral sensory inputs removed were still capable of maintaining the locomotor pattern. Later, scientists were able to record locomotor output from an isolated spinal cord preparation by adding neurotransmitter agonists (5-HT, NMDA and Dopamine) or by electric stimulation of the spinal cord (or brain stem) and recording the output activity discharged in the ventral roots that correspond to flexor and extensor MN pools (Whelan *et al.,* 2000; Hinckley *et al.,* 2005; Kwan *et al.,* 2009; Brownstone *et al.,* 2011). Furthermore, researchers found that the locomotor speed can be regulated within the spinal cord (Cazalets *et al.,* 1998; Gosgnach *et al.,* 2006), which means that in addition to the ability of generating locomotor pattern that is rhythmic in nature, the spinal cord exhibits different modalities that allow flexibility in modulating the locomotor output autonomously and without the influence of external components (i.e. supraspinal and sensory feedback). The ability of the spinal cord to generate rhythmic locomotor pattern is an evolutionarily conserved phenomenon that is observed

in lower vertebrates, such as in the generation of swimming pattern based on the flexion and extension of trunk muscles in lamprey and *Xenopus* tadpole (Buchanan, 1982; Roberts *et al.,* 1998), as well as in the more complicated mammalian locomotor pattern which is based on alternative flexion and extension between right and left limb muscles (Brown, 1911; Carr *et al.,* 1995; Dai *et al.,* 2005; Kwan *et al.,* 2009). The work presented in this thesis aims to identify the cellular basis of rhythmicity which is important in order to understand the complex mammalian locomotor behaviour.

## 1.2 SPINAL LOCOMOTOR NETWORKS

### 1.2.1 Central pattern generators (CPGs)

The central nervous system contains neuronal circuits that are arranged in such a way to serve various functions vital to the needs of the organism. These circuits were phylogenetically modified over the course of evolution to meet the demand of more complicated behaviours and functions required for the survival of higher organisms. However, the more evolved the animal, the more complex is the understanding of the construction of its neural networks. Circuits that can independently generate an output pattern which is repeated over a period of time without sensory feedback are called central pattern generators (CPGs; Hughes and Wiersma, 1960; Wilson 1961). CPGs are capable of manipulating the locomotor activity through initiating rhythmic activity and shaping the pattern delivered to motoneurons (MNs) that subsequently project to target muscles during the swing and stance phases of the locomotor cycle (Kiehn and Butt, 2003). Several models have been proposed to represent the mammalian CPGs; For

example, the half center model suggested that interneurons responsible for stimulating flexion and extension throughout a limb reciprocally inhibit each other, but intrinsic activation was not acknowledged in that model (Brown, 1912; Lundberg *et al.,* 1981; Stuart and Hultborn, 2008). In another model, researchers proposed that interneurons are organized in units, called unit burst generators, which are interconnected to coordinate flexion and extension of muscles that control the movement of a specific joint, and are further connected with unit burst generators that control the activity of muscles around other joints (Edgerton *et al.,* 1976). A recent study (Hagglund *et al.,* 2013) used optogenetic techniques to specifically stimulate neurons in an isolated spinal cord. Their results demonstrated that the locomotor pattern can be recorded in left and right hemicords independently, as well as in different MN pools within the same hemicord, suggesting that each CPG consists of its own rhythm generating kernel as well as pattern forming cells. However, a coordinated and intact locomotor output requires interconnection of these modules via excitatory, inhibitory and modulatory mechanisms (Grillner and Jessell, 2009; Nishimaru and Kakizaki, 2009; Hagglund *et al.,* 2013).

Interneurons (INs) that constitute the CPGs are interconnected through chemical synapses and/or electronic coupling (Brownstone and Wilson, 2008; Su *et al.,* 2012; Sasaki *et al* 2013; Sieling *et al.,* 2014). Although the anatomy of and interconnection between the neurons that constitute the CPG were identified in invertebrates and lower vertebrates (Grillner *et al.,* 1995; Lansner *et al.,* 1998; Roberts *et al.,* 1998; Sasaki *et al.,* 2013), the details of the mammalian CPG are yet to be identified.

### 1.2.2 Rhythm generation and pattern formation

Until this date, there is still much to unravel about the rhythm generating and pattern forming cells in the mammalian locomotor CPG. In invertebrates and lower vertebrates, it has been shown that rhythm generation and pattern formation can be initiated in the same cell type (Lansner *et al.,* 1998; Roberts *et al.,* 1998), which is not the case in mammalian CPG that require different rhythm generating and pattern forming cells (Brownstone and Wilson, 2008). Scientists suggested hypothetical models to allow easier understanding of the underlying components of the rhythm generating and pattern forming layers and how they are connected. In one of these models (McCrea and Rybak, 2008), INs that are active during locomotion were divided into two functional levels; rhythm generating (level 1) and pattern forming (level 2) INs. The difference between the two levels as the name implies is that rhythm generating cells are responsible for generating the rhythm and for setting a defined frequency for network oscillation, whereas pattern forming INs which are activated downstream of rhythm generating INs, control the duration and amplitude of MN activation, in other words, the locomotor pattern (McCrea and Rybak, 2008; Brownstone and Wilson, 2008).

In a recent study, Griener *et al.* (2013) illustrated that there are morphological differences between rhythm generating and pattern forming cells. In addition to confirming that rhythm generating INs are medially located compared to pattern forming INs (Kiehn and Kjaerulff, 1998), they showed that rhythm generating cells possessed relatively shorter axons that extended medially and caudally while pattern forming cells possessed longer axons that projected laterally and toward the MN pools. Rhythm generating cells were also shown to be located in the thoracolumbar segments of the

spinal cord (Cowley and Schmidt, 1997), whereas this observation was not critical for pattern forming cells. Thus, it is generally accepted that the mammalian CPG, unlike invertebrates or lower vertebrates, consist of rhythm generating INs and pattern forming INs.

## 1.3 CLASSIFICATION OF SPINAL INS

The mammalian spinal cord contains a variety of neurons and interneurons that differ anatomically, morphologically, and electrophysiologically. During embryonic development, cellular diversification occurs along the rostrocaudal as well as the dorsoventral axis of the neural tube under the effect of several factors, to generate several types of neurons, each possessing a unique set of properties and characteristics (Tanabe and Jessell, 1996). In the spinal cord, premitotic cells known as progenitor domains are aligned throughout the dorsoventral axis along the wall of the neural tube (Jessell, 2000; Pierani *et al.,* 2001). The position of the progenitor domains is critical in determining the postmitotic fate that they establish later in development; for example, dorsally located INs develop from dorsal progenitor domains, and ventrally located INs (and MNs) develop from ventral progenitor domains.

Paying close attention to the ventral half of the neural tube, previous studies have shown that a factor named sonic hedgehog (SHH) is responsible for the differentiation of ventral progenitor domains early in the developmental stage (Johnson and Tabin, 1995; Marigo and Tabin, 1996; Tanabe and Jessell, 1996). SHH is produced by the notochord and allows the formation of floor plate cells in the ventral most part of the spinal cord.

Together, the notochord and floor plate cells produce SHH that acts on the progenitor cells via its graded concentration (i.e. the more ventral, the more SHH signal the cell receives) to initiate the expression of upstream homeodomain (HD) proteins. As the concentration of SHH will depend on the position of the progenitor cells, diversification of INs will occur at an early stage of development (Jessell, 2000; Pierani *et al.,* 2001). According to their position and type of HD protein they possess, ventral progenitor domains are identified as p0, p1, p2, pMN and p3 that later develop into distinct types of post-mitotic ventral INs (V0, V1, V2 and V3) as well as MNs (Alaynick *et al.,* 2011; Jessell, 2000). Post-mitotic ventral INs are further divided into subtypes, with each interneuronal subtype possessing unique HD protein expression profile, intrinsic properties as well as neurotransmitter phenotype. For example, downstream HD protein Dbx1 is critical in the formation of V0 INs which are further subdivided into excitatory V0e, inhibitory V0i, cholinergic V0c, and medial glutamatergic V0g INs (Lanuza *et al.,* 2004; Zagoraiou, 2009; Arber, 2012), each interneuronal subtype possess a unique set of HD proteins in addition to Dbx1. Similarly, Lhx3/6 HD proteins are responsible for the differentiation of V2 INs which are further subdivided into excitatory V2a, inhibitory V2b, and V2c INs (Briscoe *et al.,* 2000; Pierani *et al.,* 2001; Panayi *et al.,* 2010; Arber, 2012). Moreover, the Hb9 HD protein is expressed in pMNs and is critical in the formation of MNs (Harrison *et al.,* 1994; Saha *et al.,* 1997; Arber *et al.,* 1999; Thaler *et al.,* 1999). Its absence during embryonic development leads to the formation of a chimeric neuron that expresses morphological properties of MNs yet shows molecular properties of V2 INs (Arber *et al.,* 1999; Thaler *et al.,* 1999). Thus, HD protein

expression provides diversity in spinal IN populations, and the inter-connections between different types of ventral INs forms the basis of spinal networks (i.e. CPGs).

One subset of ventral cells that was later discovered and expresses the HD protein Hb9 is referred to as Hb9 INs (Wilson *et al.,* 2005; Hinckley *et al.,* 2005). While the progenitor origin of Hb9 INs has not been identified, it is known that they are a small subset of excitatory INs located ventral to the central canal throughout the cervical to upper lumbar spinal cord segments. The progenitor origin of these INs and how they are formed during embryonic development is still unknown and their discovery raised questions ranging from how they developed to what role they play in the spinal cord (Wilson *et al.,* 2005; Hinckley *et al.,* 2005; Brownstone and Wilson, 2008).

## 1.4 PROPERTIES OF RHYTHMICALLY ACTIVE INS THAT CONTRIBUTE TO LOCOMOTOR OUTPUT

### 1.4.1 Characteristics of INs that contribute to locomotor output

Over the past century, multiple studies have suggested that a set of characteristics is required for an IN to be eligible for rhythm generation or pattern formation (Brownstone and Wilson, 2008). Most of these characteristics are conserved in organisms that undergo locomotion. Each IN in the CPG exhibits a unique set of anatomical, synaptic and intrinsic characteristics. The characteristics of some defined INs involved in pattern formation have been identified. For example, both V0e and V0i INs have roles in right-left alternation and their absence led to hopping behaviour in experimental animals

(Talpalar *et al.,* 2013). Inhibitory V1 interneurons were found to have a prominent effect on the speed of locomotion (Gosgnach *et al.,* 2006), and V2a INs were shown to be required for alternation of left-right limb at high speeds only (Crone *et al.,* 2009; Ausborn *et al.,* 2012). Also, elimination of V3 INs disrupts the regularity of the rhythm and the balance between the right and left halves of the spinal cord during locomotion (Zhang *et al.,* 2008). The mechanisms by which these INs affect the spinal CPGs are not known.

One outstanding question is how locomotor rhythm is generated. In addition to showing firing activity during locomotion, anatomical studies have suggested that INs involved in rhythm generation are located in the ventromedial region of the lower thoracic-upper lumbar spinal cord (Kiehn and Kjaerulff, 1998; Cowley and Schmidt, 1997). Since stimulation of the locomotor rhythm requires inputs from supraspinal, and sensory afferent sources, it was suggested that rhythm-generating cells receive chemical inputs from these sources (Conway *et al.,* 1987; Ohta and Grillner; 1989; MacLean *et al.,* 1998). In addition, rhythm generating cells are suggested to possess an excitatory phenotype and to form recurrent synaptic connections in order to initiate mutual excitation (Lundberg, 1981; Feldman and Del Negro, 2006). Recently, researchers showed that silencing glutamatergic transmission in the spinal cord abolished rhythmicity of the locomotor output, whereas silencing inhibitory transmission did not (Hagglund *et al.,* 2010; Hagglund *et al.,* 2013). Another characteristic of rhythm generating INs, as discussed above, is that their axons may not form monosynaptic connections with MNs (Burke *et al.,* 2001; Kiehn, 2006). Moreover, electrophysiological studies showed that rhythm generating INs possess intrinsic properties that make them capable of generating the rhythm; endogenous (conditional) bursting, spike frequency adaptation, plateau

potentials and post-inhibitory rebound were all suggested to be necessary for rhythm generation (Perkel and Mulloney, 1974; Russell and Hartline, 1978; El-Manira *et al.,* 1994; Brownstone and Wilson, 2008). Although some INs involved in locomotor pattern formation have been identified, INs that generate the rhythm are still unknown.

### 1.4.2 Characteristics of Hb9 INs

Hb9 INs are a group of glutamatergic INs that were first reported a decade ago in the Hb9::eGFP mouse model (Wilson *et al.,* 2005; Hinckley *et al.,* 2005). They are small in size (8-10 μm somatic diameter) and have correspondingly low whole cell capacitance (10 ± 1.5 pF) and high input resistance (9903.2 ± 226.9 MΩ; Wilson *et al.,* 2005). A disadvantage of using the Hb9::eGFP mouse model was that it showed ectopic expression of GFP including in a group of Hb9 negative cells called type 2 interneurons (Wilson *et al.,* 2005; Hinckley *et al.,* 2005). In this mouse, Hb9 INs were characterized by their location, morphology and electrophysiological properties. Hb9 INs fulfill many of the characteristics that were suggested for rhythm generation; for example, they are active in fictive locomotion and are located in the ventromedial region of the thoracolumbar segments. They also receive supraspinal, and primary afferent inputs (Wilson *et al.,* 2005; Hinckley *et al.,* 2005; Brownstone and Wilson, 2008; Kwan *et al.,* 2009). Although processes of Hb9 INs projected to regions between the LMC and MMC in the ventral horn and were suggested to form contacts with somata and proximal dendrites of MNs (Hinckley *et al.,* 2005), it is possible that these projections synapse on ventrally projecting Hb9 IN dendrites to initiate mutual excitation, on distal dendrites of ventral horn MNs and/or on unidentified neurons in the ventral horn region.

Moreover, electrophysiological recording from Hb9 INs in a non-locomoting preparation showed prominent post-inhibitory rebound (PIR) that form doublet spikes mediated by T-type calcium channel (CaV3; Wilson *et al.,* 2005; Masino *et al.,* 2012). In some Hb9 INs, voltage independent oscillations were observed (Wilson *et al*., 2005) that suggested they are electronically coupled (Hinckley and Ziskind-Conhaim, 2006; Wilson *et al.,* 2007; Ziskind-Conhaim *et al.*, 2008). Electronic coupling is another important characteristic for rhythm generation as shown in simpler animal models (Saint-Amant and Drapeau, 2001; Li *et al*., 2009; Sasaki *et al.,* 2013). Thus, Hb9 INs have many of the characteristics of rhythm generating neurons.

A previous study questioned the hypothesis that Hb9 INs are involved in locomotion (Kwan *et al.,* 2009). These investigators showed that the onset of activity in Hb9 INs occurred after the onset of activity in ipsilateral ventral roots when inducing fictive locomotion in an isolated spinal cord. Thus, they suggested that Hb9 INs are not the sole pacemakers of locomotor rhythm. However, their rhythmic nature and firing in phase with ventral root output suggested that they may have a role in the rhythm generation circuit, even if they are not the sole pacemakers that initiate the rhythm. These observations together showed that Hb9 INs are capable of generating oscillations without receiving synaptic inputs and suggests a possible role in rhythm generation.

## 1.5 PRE-SYMPATHETIC INS

Sympathetic preganglionic neurons (SPNs) are innervated by supraspinal inputs as well as neurons that reside within the spinal cord. Bath application of 5-HT, NMDA

and dopamine to an isolated spinal cord preparation, showed rhythmic activity in the SPNs output (Madden & Morrison, 2006; Marina *et al*. 2006). The sympathetic spinal networks, similar to locomotor networks, consist of INs that fire in phase (sympathoexcitatory) or out of phase (sympathoinhibitory) with the sympathetic output pattern (McCall *et al*. 1977; Chau *et al*. 2000; Miller *et al*. 2001; Tang *et al*. 2003). These spinal pre-sympathetic INs connect to SPNs in the intermediomedial (IMM) and intermediolateral (IML) columns and function to manipulate and regulate sympathetic outflow (Deuchars, 2007). Evidence for the presence of intrinsic components within the spinal cord that are capable of synchronising both sympathetic and locomotor outputs was presented by Chizh *et al.* (1998). In their study, they used *in vitro* spinal cord preparations to record locomotor and autonomic outflows simultaneously and showed obvious synchronization between the two outputs in the absence of supraspinal influence. In another study, researchers showed a group of neurons in the pontomedullary reticular formation that send direct axonal collaterals to gastrocnemius MNs as well as to SPNs (Kerman *et al.,* 2003). This indicates the possibility of a single component to couple the two rhythmic outputs.

An important region in the spinal cord that contains pre-sympathetic INs is the central autonomic area located around the central canal near the IMM column (Deuchars, 2005). Hb9 INs are located near the central canal in a location similar to the putative pre-sympathetic INs (Wilson *et al.,* 2005; Deuchars *et al.,* 2005; Deuchars, 2007). The position of Hb9 INs from a sympathetic point of view, in addition to their hypothesized role in locomotion as discussed earlier, makes them possible candidates in the neural circuit responsible for synchronizing the autonomic and motor outputs.

## 1.6 THESIS OBJECTIVES

The main purpose of this thesis was to characterize the role of glutamatergic transmission by Hb9 INs in locomotion, and to map their projections throughout the spinal cord. In doing so, we first tested the reliability of a newly introduced mouse model Hb9::CreER$^{T2}$ to conditionally express and mutate selective genes in Hb9 expressing neurons (Chapter 2). We then tested the effect of silencing glutamatergic transmission by Hb9 INs on locomotor behaviour (Chapter 3). We also identified the projections and synapses of Hb9 INs terminals (Chapter 4). Collectively, our results suggest that glutamatergic transmission by Hb9 INs is not critical for treadmill locomotion. The distribution of their terminals throughout the spinal cord provides a map which provides a basis to direct further studies into the function of Hb9 INs.

# CHAPTER 2 THE HB9::CREER$^{T2}$ MOUSE MODEL

## 2.1 SUMMARY

Hb9 expressing interneurons (INs) are a small subset of spinal INs that reside in the ventromedial region near the central canal. Although Hb9 INs were suggested to play a role in rhythm generation, further investigation of their role was limited due to the inability to manipulate these neurons specifically. We therefore used inducible mouse genetic techniques (Hb9::CreER$^{T2}$) to conditionally manipulate target genes. We first aimed to express fluorescent proteins to label Hb9 expressing neurons in order to validate the strategy. Next, we used this strategy to conditionally knock out vesicular glutamate transporter 2 (vGluT2), the gene responsible for glutamatergic transmission by Hb9 INs. By crossing Hb9::CreER$^{T2}$ mice with appropriate transgenic mouse strains, we demonstrated excellent CreER mediated recombination in Hb9 expressing neurons. We conclude that this Hb9::CreER$^{T2}$ mouse model is reliable for studying Hb9 expressing neurons.

## 2.2 INTRODUCTION

The HB9 homeobox gene encodes the nuclear homeodomain protein Hb9 which is expressed in motoneurons (MNs), spinal preganglionic neurons (SPNs) and a small subset of glutamatergic spinal INs ventral to the central canal (Arber *et al.,* 1999; Thaler *et al.,* 1999; Wilson *et al.,* 2005; Hinckley *et al.,* 2005). Hb9 was shown to be essential for the consolidation of MN identity, migration of axons of MNs, and topological

organization of MN columns during embryonic stages (Arber *et al.,* 1999; Thaler *et al.*, 1999). The identification of Hb9 expression in INs led to a number of investigations, but the role of these Hb9 INs remained ambiguous (reviewed in Brownstone and Wilson, 2008). Due to their location in locomotor rhythmogenic regions of the spinal cord, their glutamatergic phenotype, and their electrophysiological properties, a number of studies have suggested that Hb9 INs may play a role in locomotor rhythm generation (Wilson *et al.,* 2005; Hinckley *et al.,* 2005; Hinckley *et al.,* 2006; Wilson *et al.,* 2007; Han *et al.,* 2007; Brownstone and Wilson, 2008; Ziskind-Conhaim *et al.,* 2008; Kwan *et al.,* 2009; Anderson *et al.,* 2012; Masino *et al.,* 2012). However, because Hb9 is expressed in MNs, and because there is "ectopic" expression of green fluorescent protein (GFP) in transgenic Hb9::eGFP animals used in previous studies, it has not been possible to selectively visualise or manipulate these neurons to test their necessity or sufficiency for locomotion.

Cre/lox site specific recombination is a technique that is used to selectively manipulate specific genes in the cells of transgenic animals (Sauer and Hendrson, 1989). The process of Cre mediated recombination consists of two elements: a protein called Cre recombinase and specific sites on the DNA called loxP sites. Cre mediates the excision of the DNA sequence flanked by two loxP sites (Austin *et al.,* 1981; Hoess *et al.,* 1982; Hoess *et al.,* 1984). To induce expression of a certain gene in transgenic mouse models, a transcriptional stop codon is flanked by loxP sites preceding the gene of interest and is excised only in the cells that express Cre. This leads to expression of the gene of interest in the cells of interest (Lakso *et al.,* 1992). Similarly, Cre mediated recombination can be used to knock out or mutate a certain gene in a specific cell type by flanking sequences of

the gene between the loxP sites (Gu *et al.,* 1994). Nevertheless, the Cre/loxP recombination strategy has its limitations, for example when targeting genes that are activated during development. In some conditions, excising specific genes during development leads to death of the animal, and in other conditions leads to compensatory mechanisms (Betz *et al.,* 1996).

In seeking to circumvent these issues of developmental excision, researchers introduced a Cre recombinase that could be induced via administration of an estrogen receptor (ER) antagonist (Metzger *et al.,* 1995; Feil *et al.,* 1996; Indra *et al.,* 1999). This CreER fusion protein provided a method to temporally and conditionally control the expression and/or knock out of the gene(s) of interest. The ability to temporally control the activation of Cre led to a substantial reduction in adverse effects observed when Cre is developmentally expressed (Betz *et al.,* 1996), thus allowing for anatomical, behavioural and physiological studies of various genetically identified cells.

In this study, we aimed to validate Cre mediated recombination in a newly introduced Hb9::CreER$^{T2}$ mouse model by examining both CreER mediated expression of fluorescent proteins and CreER mediated knockout of vGluT2 from Hb9 expressing cells. Results showed successful recombination in Hb9::CreER$^{T2}$ mouse model.

## 2.3 METHODS

### 2.3.1 Animals

To assess the recombination in the Hb9::CreER$^{T2}$ mouse model, kindly provided by Kevin Kanning and Christopher Henderson at Columbia University, Hb9::CreER$^{T2}$ mice were crossed for two generations with mice possessing the knock-in genes vGluT2$^{flox/flox}$ (Hnasko *et al.,* 2010) and Rosa26 $^{fs\text{-}Td\text{-}tomato/+}$, Rosa26 $^{fs\text{-}YFP/+}$, or both (Figure 2.1.). In additional experiments, Hb9::CreER$^{T2}$ mice were crossed with Rosa26$^{fs\text{-}Td\ tomato/+}$ and Hb9 $^{lacZ/+}$ mice. Two different lines of Hb9::CreER$^{T2}$ mice were used initially and were found to be similar. We therefore focused on one of the lines ("line 8"), using it for the experiments described herein. We also crossed Hb9$^{Cre/+}$ with Rosa26$^{fs\text{-}Td\ tomato/+}$ to compare conditional versus non-conditional expression of reporters. All animals were of C57BL/6J background and were used in the experiments regardless of sex. Experimental procedures were approved by the University Committee on Laboratory Animals and were in accordance with the Canadian Council on Animal Care guidelines.

### 2.3.2 Preparation and administration of Tamoxifen

To prepare a stock of 20 mg/ml, 100 mg Tamoxifen (T5648-1G) was warmed in 400 µl of 100% ethanol at 37$^{o}$ C for 5 minutes followed by dilution in 5 ml sunflower oil (w530285). The solution was incubated at 37$^{o}$ C $\geq$ 1 hour; vigorous shaking was required during incubation to dissolve Tamoxifen. Aliquots of 1-2 ml of Tamoxifen solution were stored at -20$^{o}$ C and warmed up to 37$^{o}$ C prior to injection. Mice were injected between

postnatal day 5 and 7 (P5-7) with a dose of 0.1- 0.2 ml of Tamoxifen solution. Injection was performed subcutaneously into the dorsal fat pad on the back of the neck using a 30G needle. It was notable that the actual absorbed dose of Tamoxifen was variable and less than the dose injected due to post injection leakage at the injection site. Pups were transferred to a clean cage during the injection session (approximately 30 minutes) and were injected by separate needles to avoid inter-individual infection. They were left in the cage for few minutes to allow leakage of excess Tamoxifen through the injection site before returning to their home cage to recover and be nursed.

### 2.3.3 Perfusion and tissue preparation

#### *2.3.3.1 Perfusion*

Before perfusion, mice were injected intraperitoneally (IP) with approximately 0.1 ml of anaesthetic solution (3 ml Ketamine HCl, 1.88 ml Xylocaine, and 5.12 ml saline per 10 ml solution). The effect of anaesthesia was confirmed by the disappearance of hind feet reflexes. The heart was then exposed by cutting along both sides of the ribs to allow insertion of a butterfly needle in the apex of the left ventricle, and a small incision was made in the right atrium to ensure that the administered solutions would flow through the entire cardiovascular system. First, Ringer's solution (containing 0.5 % Xylocaine) was administrated to clear the blood. Success of this procedure was determined by visual cues such as change in color of the liver from dark red to yellowish brown, and leaking of ringer's solution from the tail vein. This was followed by administration of approximately 200 ml of a 4% paraformaldehyde PFA solution in 0.2M

PB. Following perfusion, the spinal cords were extracted, cleaned from meninges, post-fixed in PFA at 4ºC overnight, and then transferred to a 30 % sucrose solution for 24-48 hours before sectioning.

#### *2.3.3.2 Sectioning*

Spinal cords blocks were frozen in agarose gel and mounted on a vibratome cutting stage using super glue and 4% agar block for support. 50-60 µm floating sections were collected in a rostral to caudal order in 0.1 M PB solution at 2º C, and stored in glass vials specified for the position from which the sections were collected. Sections were processed for immunohistochemistry on the same day or stored in glycerol at -20ºC for later use.

### 2.3.4 Immunohistochemistry

Floating sections were washed in PBS for 10 minutes and incubated in 50% ethanol to enhance antibody penetration. After 30 minutes of ethanol incubation, sections were washed with double salt PBS (dsPBS) 3 x 10 minutes and transferred to blocking solution containing 10% donkey serum in 0.3 M Triton X and PBS solution (PBST) for 30 minutes at RT to block non-specific staining. Tissues were quickly transferred to a solution containing the primary antibodies of interest, 1% donkey serum, and PBST, and incubated for 48-72 hours at 4º C. After incubation, sections were washed in dsPBS 3 x 10 minutes, transferred to secondary antibody solution, and incubated overnight at 4ºC.

Secondary antibodies were diluted in a solution containing 1% donkey serum and PBST. Finally sections were washed in PBS 1 x 10 minutes and mounted using Vectashield mounting medium (Vector laboratories, Burlingame, CA) on a microscope slide using a fine tip brush. Details of antibodies and their concentrations are presented in Table 2.1.

### 2.3.5 In situ hybridization

Tissues were processed for combined fluorescent *in situ* hybridization and immunohistochemistry as previously described (Wilson *et al*., 2005; Bui *et al.,* 2013). The primer for antisense digoxigenin (DIG) riboprobe for vGluT2 was provided by the Jessell lab (Columbia University, USA), and the probe was kindly prepared by the Fawcett lab (Dalhousie University, NS, Canada). Briefly, sections were fixed in 4% PFA for 10 minutes at RT followed by washing in PBS 3 x 3 minutes and incubation in Proteinase K solution for 5 minutes. Sections were acetylated for 10 minutes in an acetic anhydride buffer and transferred to a hybridization solution at RT overnight. Sections were then heated in a diluted hybridization solution for 5 minutes at 80$^{o}$C and quickly transferred to ice before being incubated in a 72$^{o}$C oven overnight. On day three, sections were incubated in 0.2x saline sodium citrate buffer (SSC) at 72$^{o}$C 2 x 30 minutes followed by equilibrating the sections in 0.2x SSC for 5 minutes at RT. Sections are incubated in tris NaCl blocking (TNB) buffer for 1 hour at RT and overnight in a solution containing donkey serum, riboprobe for vGluT2: sheep anti-DIG-POD (1:100) and primary antibody rabbit anti-GFP (1:100) at 4$^{o}$C. On day four, sections were blocked in a 1% blocking reagent solution (10 mg/ml) for 30 minutes followed by incubation in

streptavidin HRP solution for 30 minutes, then tyramide solution for 10 minutes at RT. Sections were incubated in secondary antibody solution (Table 2.1.) for 3 hours in PBS before examining.

### 2.3.6 Image acquisition

Confocal images were acquired with Zeiss LSM 710 - Laser Scanning Confocal Microscope, which includes Argon, HeNe and red diode lasers. Images were captured either in 2D as a snapshot, or in 3D as a z-stack up to approximately 30 µm in thickness. Interval between consecutive optical sections was 0.8-1.88µm. Pinhole size was set at 1 airy unit for all channels.

### 2.3.7 Image analysis

Images were analysed with the supplied software (Zen 2012 SP1-black edition-64 bit, Zeiss), ImageJ 1.49o to generate maximum intensity projection (MIP) image of the 3D z-stack, and IMARIS 8.0.1 software (Bitplane, Oxford Instruments, CT, USA) to detect the colocalization of labeling proteins in the cells. We created artificial spots that represent the expression of the specific labeling proteins being studied. To detect the colocalization of the two labeling proteins in the cells, a distance threshold between the spot centers was set, such that if the centers of any two spots are located within the threshold distance, the two spots were considered colocalized. To identify the regions where the different neurons are expressed in the spinal cord, we generated a reference

figure (Figure 2.2*Bii*) that represents the topological organization of the laminae and other landmarks in the spinal cord. The reference figure was generated based on Allen institute spinal cord map (Website: ©2012 Allen Institute for Brain Science. Allen Spinal Cord Atlas [Internet]. Available from: http://mousespinal.brain-map.org/) and Todd *et al.* (2003).

## 2.4 RESULTS

### 2.4.1 Cre mediated recombination in $Hb9^{Cre/+}$mouse model

In order to manipulate gene expression or excision in Hb9 neurons, we studied Cre versus CreER mediated recombination to express the fluorescent protein Td-tomato. In $Hb9^{Cre/+}$ mice, there was non-specific expression of Td-tomato in numerous Hb9 negative cells throughout laminae I-X of the upper lumbar segment as well as in Hb9 positive cells (Figure 2.2*A-B;* n=2). In comparison, Hb9::$CreER^{T2}$ mice showed expression of Td-tomato which appeared to be limited to MNs in lamina IX, SPNs in laminae VI-VII and Hb9 INs in lamina X and medial lamina VIII (Figure 2.2*C*). These results indicate the importance of controlling the time at which Cre is expressed in Hb9 neurons.

### 2.4.2 Specificity of CreER mediated recombination in Hb9 expressing cells of Hb9::CreER$^{T2}$ mouse model

Since Hb9 is expressed in MNs throughout the spinal cord segments, we first examined CreER recombination in MN pools of Hb9::CreER$^{T2}$; Rosa26 $^{fs\text{-}Td\text{-}tomato/+}$ or Rosa26 $^{fs\text{-}YFP/+}$ mice. We compared the CreER dependent expression of fluorescent proteins and the expression of choline acetyltransferase (ChAT), the enzyme responsible for synthesis of the MN neurotransmitter acetylcholine, and observed co-labelling of Hb9::CreER$^{T2}$ reporter proteins and ChAT in the MN pools (Figure 2.3). We found that 98.6 % (71/72) of Td-tomato positive MNs in the ventral horn (n=3 sections/animal) expressed ChAT, and 95.9 % (71/75) of ChAT positive MNs expressed Td-tomato (Figure 2.3*A*; n=1 animal). Similarly, YFP was expressed in ChAT positive MNs (Figure 2.3*B*). As this is a surrogate marker for Hb9, we proceeded to quantify the expression of CreER dependent fluorescent proteins in Hb9 expressing neurons by crossing Hb9::CreER$^{T2}$; Rosa26 $^{fs\text{-}Td\text{-}tomato/+}$ with Hb9$^{lacZ/+}$ animals, in which lacZ with a nuclear localising sequence is expressed in Hb9 expressing neurons. That led to the expression of two tracer proteins in Hb9 expressing cells: the fluorescent protein Td-tomato (via CreER recombination) and β-gal which reliably label Hb9 expressing cells (via the lacZ knockin). We found that 95 % (205/216) of the neurons that expressed Td tomato, expressed the nuclear protein β-gal (Figure 2.4*A*; n=3 animals). Colocalization was observed in Hb9 expressing INs located in medial laminae VIII and X (Figure 2.4*B*), MNs located in lamina IX (Figure 2.4*C*) and SPNs of intermediolateral as well as intermediomedial cell columns in laminae VI-VII (Figure 2.4 *D*). The inability to observe β-gal experession in the remaining 5% of Td-tomato positive neurons may be due to the

absence of the nuclei in the image taken, while counting only the apex of the Td-tomato positive cell body. Thus, it was clear that this genetic strategy led to effective recombination in Hb9 expressing neurons.

### 2.4.3 Conditional knockout of vGluT2 in Hb9::CreER$^{T2}$ mouse model

We next aimed to use the Hb9::CreER$^{T2}$ mice to drive excision of vGluT2 in Hb9 INs. We therefore crossed Hb9::CreER$^{T2}$ with vGluT2$^{flox/flox}$ and Rosa26 $^{fs\text{-}YFP/+}$ mice. In comparison to surrounding non-Hb9 glutamatergic neurons, combined fluorescent *in situ* hybridization and immunohistochemistry revealed pronounced reduction of vGluT2 mRNA in Hb9 expressing INs (Figure 2.5*;* n=3). This expression contrasts with our previously published study (Wilson *et al*., 2005) that showed strong expression of vGluT2 mRNA in control Hb9 INs.

## 2.5 DISCUSSION

In this study, we demonstrate successful CreER mediated recombination in the Hb9::CreER$^{T2}$ mouse model. We revealed that, following CreER activation at P5-7, there was successful recombination in 96 % of ChAT positive MNs. Successful recombination was also seen in Hb9 INs and SPNs by colocalization of the tracer proteins Td-tomato and β-gal. This recombination was specific to Hb9 expressing cells, as opposed to that seen in Hb9$^{Cre/+}$ mice, which demonstrated recombination in many Hb9 negative spinal

interneurons. Furthermore, the specificity of recombination provides a route by which Hb9 INs can be genetically manipulated, which will be useful in studying how spinal microcircuits produce motor behaviour.

Hb9 INs were first defined in transgenic Hb9::eGFP mice (Wilson *et al.,* 2005; Hinckley *et al.,* 2005), in which eGFP is expressed in α-motoneurons, Hb9 INs, a group of Hb9 negative INs called type 2 INs in close proximity to Hb9 INs, and other Hb9 negative INs in the ventral spinal cord. In Hb9::eGFP mice, Hb9 INs can be identified in slice preparations by their location, morphology, and electrophysiological properties (Wilson *et al.,* 2005; Hinckley *et al.,* 2005; Kwan *et al.,* 2009). The use of Hb9::CreER$^{T2}$ mice provides definitive identification of Hb9 INs in this region, without the need to rely on first recording the putative neuron's properties. That is, the use of these mice results in a significant improvement in the ability to identify Hb9 expressing cells.

Moreover, successful mutation of the vGluT2 gene in the transgenic offspring of Hb9::CreER$^{T2}$, Rosa 26 $^{fs\text{-}YFP/+}$ and vGluT2$^{flox/flox}$ was observed. VGluT2 mRNA was abolished or clearly reduced in the majority of the Hb9 INs examined. The reason for the observation of traces of vGluT2 mRNA in Hb9 INs may be due to two reasons: 1) defects in the staining process of combined fluorescent *in situ* hybridization-immunohistochemistry, such as pronounced increase in the background noise signal, and/or 2) the antisense riboprobe used in *in situ* hybridization which targets exon 1 of the vGluT2 gene, whereas the loxP sites flank exon 2 (Hnasko *et al.,* 2010). This is a similar result to that shown in Isl1$^{Cre/+}$; vGluT2$^{flox/flox}$ (dI3$^{OFF}$) mice, in which glutamatergic transmission from dI3 neurons was eliminated and the gripping behaviour of animals was disrupted (Bui *et al*., 2013). The successful recombination shown above, the elimination

or reduction of vGluT2 mRNA in Hb9 INs in comparison to neighbouring vGluT2 positive neurons and control Hb9 INs (Wilson *et al*., 2005), and the successful previous use of these vGluT2$^{flox/flox}$ animals in which there were significant differences in behaviour (Hnasko *et al.,* 2010; Scherrer *et al.,* 2010; Bui *et al.,* 2013), all point to the utility of Hb9::CreER$^{T2}$ mediated excision of vGluT2 to produce Hb9 -VGluT2$^{OFF}$ mice, in which glutamatergic transmission by Hb9 INs would be curtailed.

In summary, these findings demonstrate that Hb9::CreER$^{T2}$ mice are reliable for identifying and manipulating Hb9 expressing neurons.

**Table 2.1. List of antibodies and their sources**

| Antigen (Ag) | 1ry Ab | 1ry Ab host | 1ry Ab dilution | 1ry Ab Source | Flourescent label for 2ry Ab | 2ry Ab host | 2ry Ab dilution | 2ry Ab Sourc |
|---|---|---|---|---|---|---|---|---|
| Tandem dimer tomato (Td-tomato) | Anti-DsRed | Rabbit | 1:2000 | Rockland antibodies and assays (PA, USA) | Alexa 546 | Donkey anti-rabbit | 1:400 | Invetrogen (Oregon, USA) |
| Choline acetyltransferase (ChAT) | Anti-ChAT | Goat | 1:200 | Millipore (CA, USA) | Alexa 647 | Donkey anti-goat | 1:400 | Invetrogen (Oregon, USA) |
| β-galactosidase (β-gal or lacZ) | Anti-β-gal | Goat or Mouse | 1:500 | Santa Cruz Biotechnology, Inc. (Dallas, TX, USA) | Alexa 488 | Donkey anti-goat (or anti-mouse) | 1:400 | Invetrogen (Oregon, USA) |
| Yellow flourescent protein (YFP) | Anti-GFP | Sheep or Mouse | 1:500 | GenWay Biotech, Inc. (San Diego, CA, USA) & Novus Biologicals inc. (Littleton, CO, USA) | Alexa 488 | Donkey anti-sheep (or anti-mouse) | 1:400 | Invetrogen (Oregon, USA) |

**Figure 2.1.** CreER mediated recombination in Hb9::CreER$^{T2}$ mouse model. Inactive CreER is located in the cytoplasm. Once activated by Tamoxifen binding, CreER is translocated to the nucleus and mediates recombination of the DNA sequences flanked between the loxP sites to activate or excise target genes. Diagram is based on Sauer, 1998.

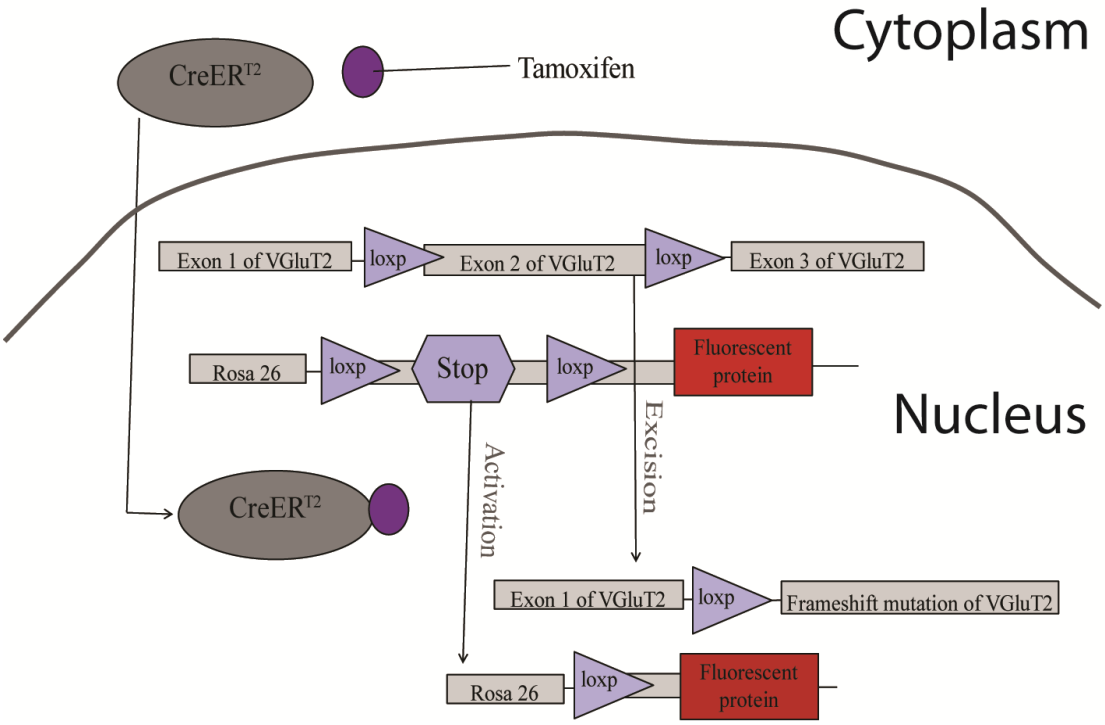


**Figure 2.1. CreER mediated recombination in Hb9::CreER$^{T2}$ mouse model.**

**Figure 2.2.** Comparison between non-conditional and conditional Cre recombination in Hb9 expressing cells. Non-specific expression of Td-tomato throughout the upper lumbar segment in $Hb9^{Cre/+}$mouse model **(A)**. Regions of cells expressing Td-tomato as a result of Cre mediated recombination are enlarged **(Bi)**, and the designation of the laminar regions in the upper lumbar segment is outlined in **(Bii).** On the other hand, conditional expression of Td-tomato in Hb9::$CreER^{T2}$ mouse model, **(C)** is confined to Hb9 expressing cells; SPNs in lamina VI-VII, MNs in lamina IX, and Hb9 INs in laminae VIII and X (arrows). CC: central canal, IML: intermedilateral column, MMC: medial motoneuron column and LMC: lateral motoneuron column. Dashed oval represents central canal. Scale bars: 50 μm for A and C and 30 μm for Bi.

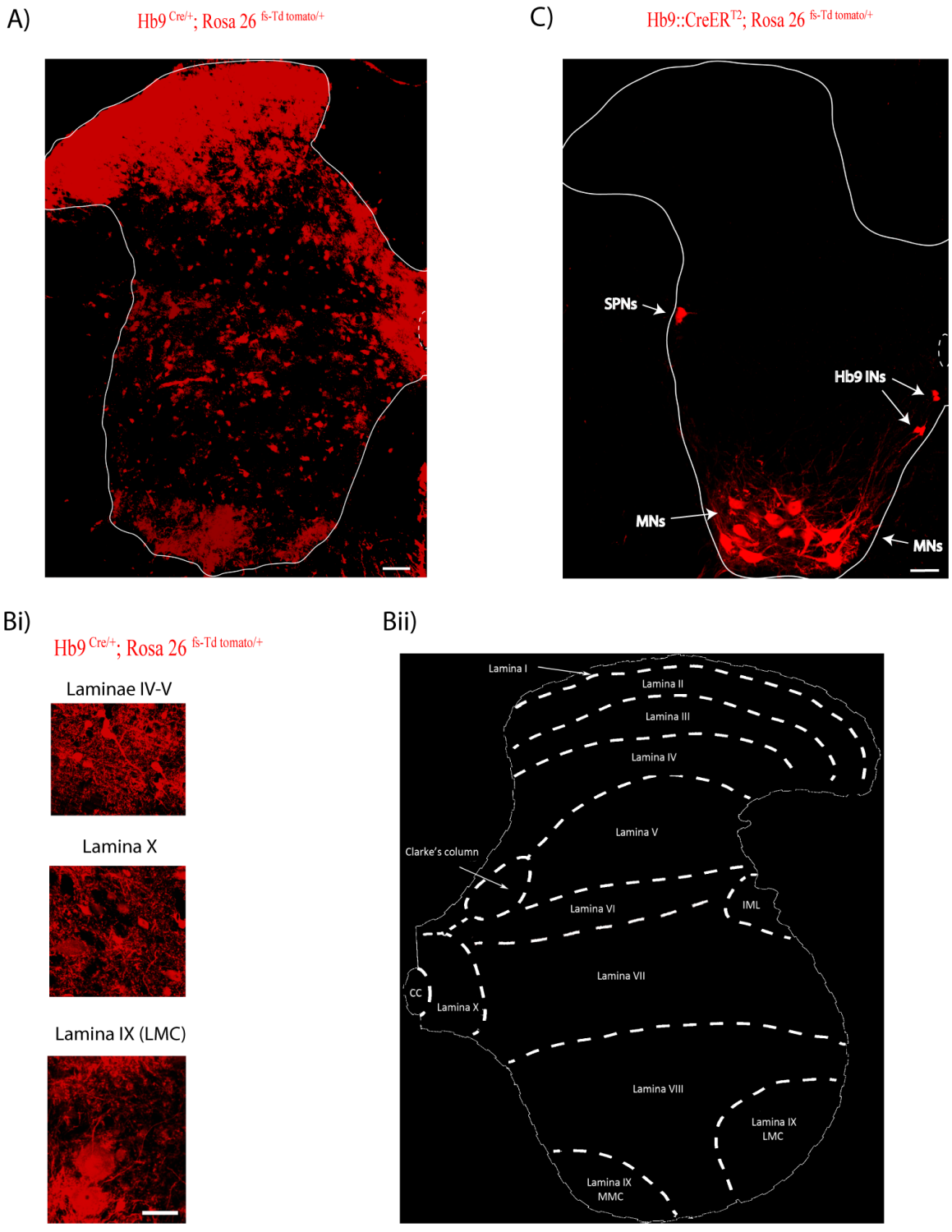


**Figure 2.2. Comparison between non-conditional and conditional Cre recombination in Hb9 expressing cells.**

**Figure 2.3.** Conditional expression of fluorescent protein in ChAT positive MNs. CreER derived expression of Td-tomato **(A)** and YFP **(B)**, is observed in ChAT expressing MNs of the MMC and LMC. It is also noticeable that although recombination was successful in the majority of ChAT expressing MNs, the intensity of Td-tomato or YFP was not uniform in all MNs. This may have resulted from different expression levels of Cre recombinase, different cytoplasmic volumes, or different turnover rates of the reporter proteins, for example. Refer to Figure 2.2Bii for the designation of MMC and LMC. Dashed oval represents the central canal. Scale bar: 50 μm for A and B.

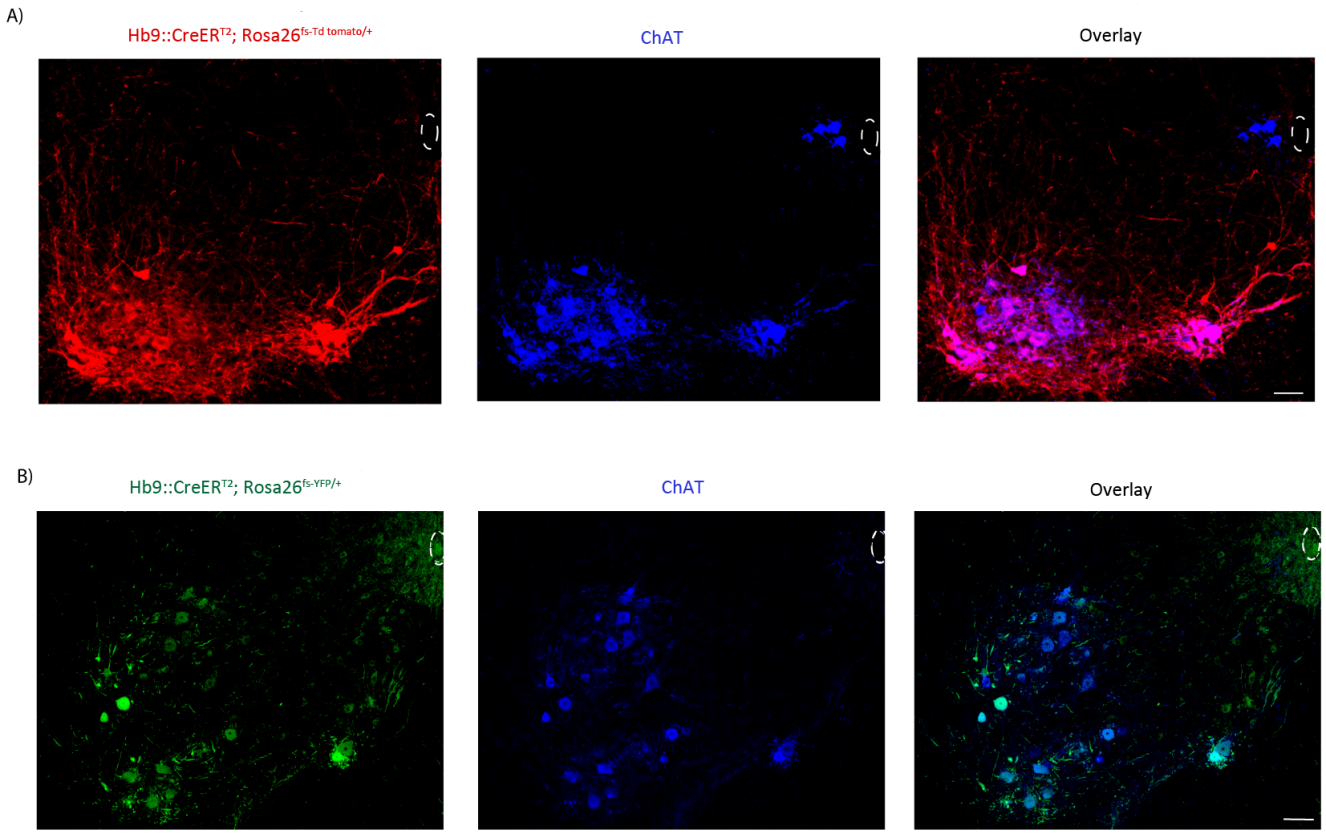


**Figure 2.3. Conditional expression of fluorescent protein in ChAT positive MNs.**

**Figure 2.4**.Conditional expression of fluorescent protein in Hb9 expressing cells. **(A)** Lower magnification of spinal cord section shows co-labelling of CreER derived expression of Td-tomato and Hb9 derived expression of β-gal in Hb9::CreER$^{T2}$; Rosa26$^{fs\text{-}Td\text{-}tomato/+}$; Hb9$^{lacZ/+}$ mouse. Double expression of tracer proteins is seen in: **(B)** Hb9 INs in medial lamina VIII and lamina X, **(C)** MNs in lamina IX and **(D)** SPNs of the IML as well as IMM columns in laminae VI-VII. Refer to Figure 2.2*Bii* for the designation of laminae. Dashed oval represent central canal; vertical line represents midline of the spinal cord section ventral to the central canal. Scale bar: 100 μm for A, 20 μm for B, 40 μm C-D.

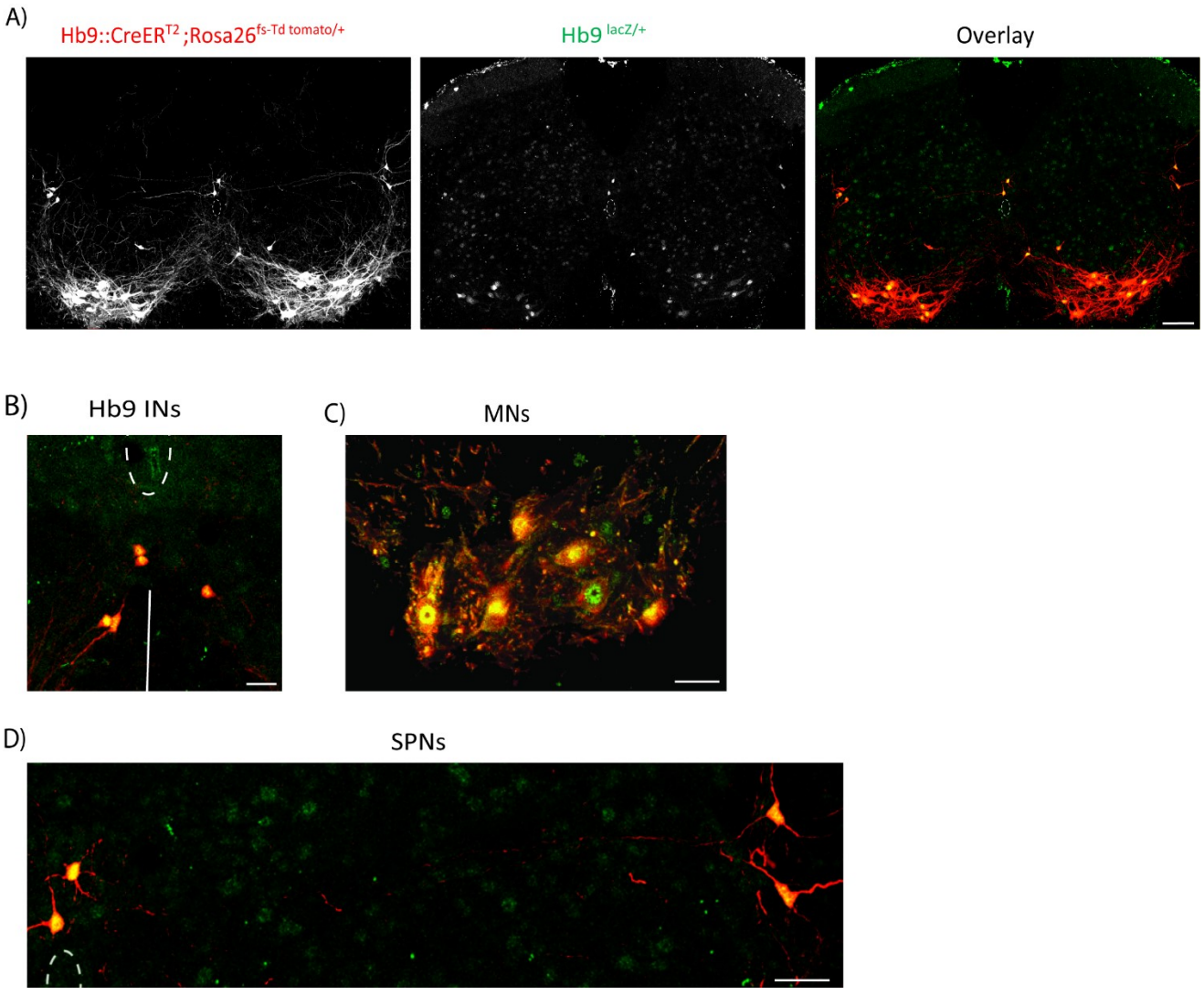


**Figure 2.4. Conditional expression of fluorescent protein in Hb9 expressing neurons.**

**Figure 2.5.** Conditional mutation of vGluT2 mRNA in Hb9 expressing INs. Combined fluorescent *in situ* hybridization-immunohistochemistry of Hb9 INs after CreER mediated mutation of vGluT2 in two animals **(A)** and **(B).** VGluT2 mRNA is eliminated or clearly reduced in the majority of Hb9 INs (arrowheads) compared to neighbouring glutamatergic neurons in laminae VIII and X. Hb9 INs that have vGluT2 mRNA are marked in asterisks. Refer to Figure 2.2*Bii* for the designation of laminae. Dashed oval represents the central canal; line represents midline of the spinal cord section ventral to the central canal. Scale bar: 50 μm for A and 20 μm for B.

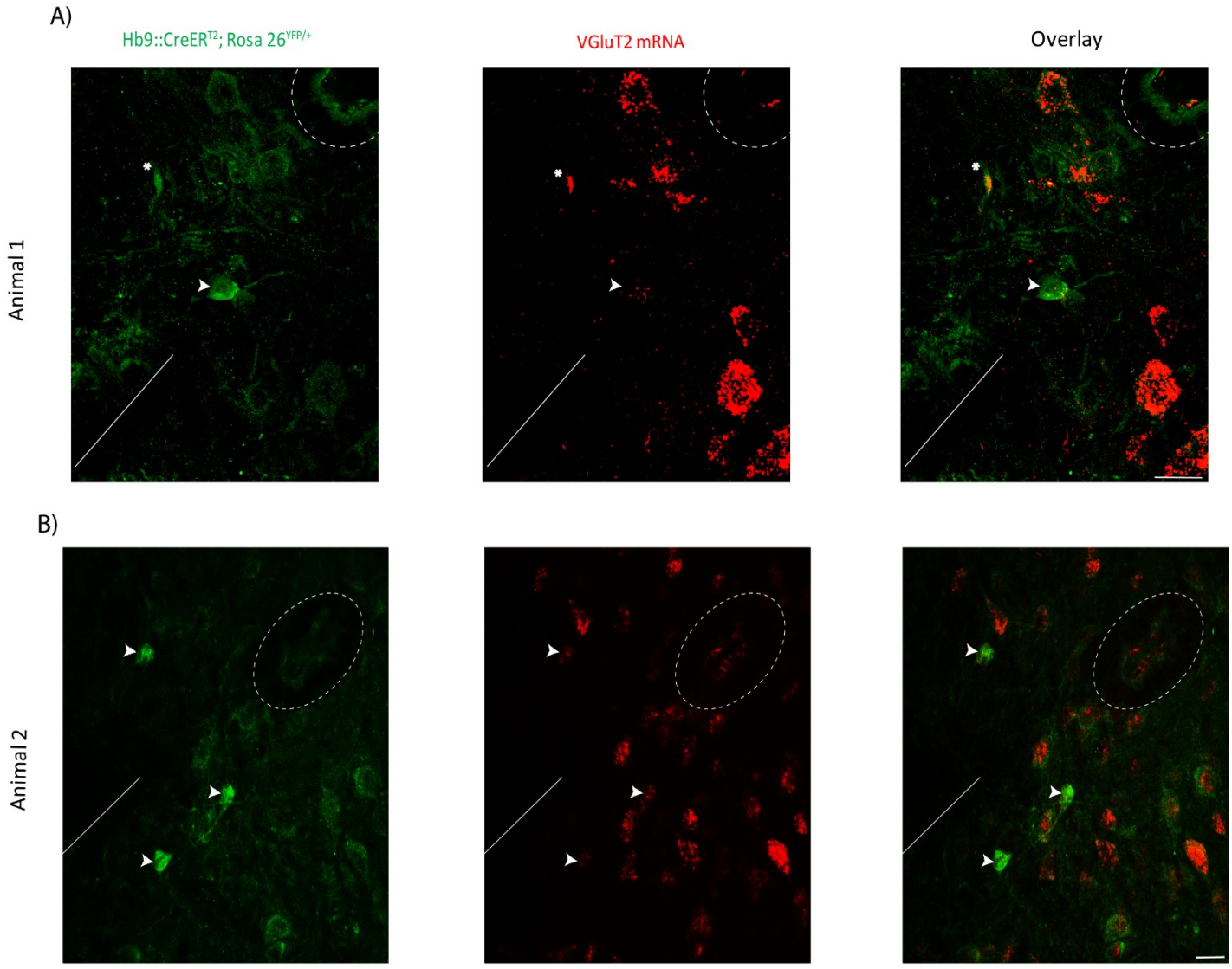


**Figure 2.5. Conditional mutation of vGluT2 mRNA in Hb9 expressing INs.**

# CHAPTER 3 EFFECTS OF SILENCING CHEMICAL TRANSMISSION BY HB9 INS ON LOCOMOTION

## 3.1 SUMMARY

Hb9 interneurons (INs) are a small group of glutamatergic cells located in the spinal cord ventral to the central canal from cervical to upper lumbar segments. In lower thoracic-upper lumbar segments, Hb9 INs are located in medial lamina VIII and lamina X. Their morphological, anatomical, and electrophysiological properties have led to the suggestion that they are involved in generating the rhythm of locomotion. To study this, we eliminated glutamatergic transmission by Hb9 INs using inducible mouse genetics; vesicular glutamate transporter 2 (vGluT2) expressed in Hb9 INs was excised by crossing Hb9::CreER$^{T2}$ with vGluT2$^{flox/flox}$ mice, and treating the offspring with the ER antagonist, Tamoxifen. In these conditional knockout mice at various postnatal stages, we studied treadmill locomotion at walking, and slow and fast running speeds. Analysis of various gait parameters including cycle duration, swing time, stance time, and their variability revealed that there were no significant differences between knockouts, heterozygotes, or wild-type littermate mice at any of the ages examined. We conclude that glutamatergic transmission by Hb9 INs is not required for treadmill locomotion.

## 3.2 INTRODUCTION

Neurons responsible for generating mammalian locomotor rhythm have not been positively identified. However, the kernel responsible for generating the locomotor

rhythm and the circuits required to maintain the rhythmic pattern are located within the spinal cord (Brown, 1911). These circuits are called central pattern generators (CPGs; Grillner and Zangger, 1975). The structure of spinal locomotor CPGs is not known yet, but there is evidence that there are a number of circuits that can generate rhythm independently, though interconnections between these circuits are required to maintain rhythmic motor output (Grillner *et al.,* 1991; Cohen *et al.,* 1992; Hagglund *et al.,* 2013). While INs responsible for locomotor rhythmogenesis have not been identified, properties that provide the capacity to generate rhythm have been outlined (Brownstone and Wilson, 2008).

Hb9 INs possess anatomical properties that make them candidates for locomotor rhythm generation. One important property is their location in ventro-medial laminae in the lower thoracic and upper lumbar segments (Wilson *et al.,* 2005; Hinckley *et al.,* 2005; Kiehn, 2006). They also exhibit intrinsic electrophysiological properties that support rhythm generation, such as post-inhibitory rebound and conditional bursting in the absence of synaptic inputs (Wilson *et al.,* 2005; Hinckley *et al.,* 2005; Tazerert *et al.,* 2008; Ziskind-Conhaim *et al* 2008; Masino *et al.,* 2012). Moreover, stable and consistent rhythmic bursts of action potential were observed when recording from Hb9 INs in response to chemical stimuli that initiate fictive locomotion and in response to increasing excitability by blocking potassium channels (Taccola and Nistri, 2004; Wilson *et al.,* 2005; Wilson *et al.,* 2007). In addition, Hb9 INs are glutamatergic and receive supraspinal and sensory afferent inputs (Wilson *et al.,* 2005; Hickley *et al.,* 2005; Hinckley *et al.,* 2010). All these characteristics may be required for rhythmogenesis (Brownstone and Wilson, 2008; Ziskind-Conhaim *et al.,* 2010). Nevertheless, using an *in*

*vitro* preparation to simultaneously record rhythmic discharges from ventral roots and $Ca^{2+}$ signals from Hb9 INs, it was observed that the onset of rhythmic discharge recorded from ipsilateral ventral roots occurred before the onset of activity in Hb9 INs located in adjacent segmental levels (Kwan *et al.,* 2009). This finding suggested a limited, if any, role of Hb9 INs as sole pacemakers for locomotor rhythm generation. Nevertheless, pacemaking properties of Hb9 INs and their stable and consistent rhythms suggest that they may affect the variability of the locomotor rhythm by manipulating the timing of firing in the locomotor network. Tests on the sufficiency or necessity of these neurons in locomotion have not been done.

In this study, we tested the hypothesis that chemical transmission by Hb9 INs contributes to locomotor rhythm generation. Using genetic techniques to knock out vGluT2 from Hb9 INs, we examined various gait parameters as well as intra-individual variability in step cycle duration of Hb9 -VGluT2$^{OFF}$ mice. Results showed no significant differences between Hb9 -VGluT2$^{OFF}$, heterozygote, and wild-type littermate mice, suggesting that chemical transmission by Hb9 INs is not necessary for locomotor rhythm generation or pattern formation.

## 3.3 METHODS

### 3.3.1 Animals

Hb9::CreER$^{T2}$ were crossed with vGluT2$^{flox/flox}$ and Rosa26$^{fs\text{-}YFP/+}$ mice (Figure 3.1.). Administration of Tamoxifen to the offspring resulted in activation of Cre

recombinase in cells expressing the homeobox gene HB9 (see Chapter 2), which excises the DNA between the loxP sites flanking exon 2 of the vGluT2 gene (Hnasko *et al.,* 2010), hence, preventing vGluT2 expression (i.e. conditional deletion). It also acts on floxed transcriptional stop sites in the Rosa 26 gene leading to expression of YFP (i.e. conditional expression; Sauer, 1998). All mice were of C57BL/6J background and were used in the experiments regardless of sex. Three age groups studied; Postnatal days P21-23 (or group P20s; weight: 7.71 $\pm$ 1.90 g; n=14), postnatal days P35-38 (or group P30s; weight: 15.92 $\pm$ 1.71 g; n=23) and postnatal weeks 11-12 (or group W10s; weight: 21.09 $\pm$ 1.56 g; n=14).All experimental procedures were approved by the University Committee on Laboratory Animals and were in accordance with the Canadian Council on Animal Care guidelines.

### 3.3.2 Preparation and administration of Tamoxifen

To prepare a stock of 20 mg/ml, 100 mg Tamoxifen (T5648-1G) was warmed in 400 µl of 100% ethanol at 37$^{o}$ C for 5 minutes followed by dilution in 5 ml sunflower oil (w530285). The solution was incubated at 37$^{o}$ C $\geq$ 1 hour; vigorous shaking was required during incubation to dissolve Tamoxifen. Aliquots of 1-2 ml of Tamoxifen solution were stored at -20$^{o}$ C and warmed up to 37$^{o}$ C prior to injection. Mice were injected between postnatal day 5 and 7 (P5-7) with a dose of 0.1- 0.2 ml of Tamoxifen solution. Injection was performed subcutaneously into the dorsal fat pad on the back of the neck using a 30 G needle. It was notable that the actual absorbed dose of Tamoxifen was variable and less than the dose injected due to post injection leakage at the injection site. Pups were

transferred to a clean cage during the injection session (approximately 30 minutes) and were injected by separate needles to avoid inter-individual infection. They were left in the cage for few minutes to allow leakage of excess Tamoxifen through the injection site before returning to their home cage to recover and be nursed.

### 3.3.3 Treadmill experiments

Locomotor behaviour was studied on a treadmill (Cleversys, Inc.) equipped with a transparent belt and a high speed camera (Basler). Mice were placed in a 161.1 $cm^2$ chamber (Figure 3.2*A*) and gait was recorded with the supplied software (BCam Capture Version 2.00, Cleversys, Inc.). The treadmill belt and chamber were cleaned with Peroxigard before each daily session, and between training mice from different cages. Locomotor behaviour was examined at belt speeds of 10, 15, and 20 cm/s (cps) for age group P20s, speeds of 15, 20, 27, and 30 cps for age groups P30s and speeds of 15, 20, and 30 cps for age group W10s. In some cases, faster speeds were attempted, but mice could not maintain locomotion at those speeds (e.g. 40 cps and 50 cps). The speeds were chosen to represent low, medium and high speeds respectively (Beare *et al.,* 2009). In age group P30s, 27 cps and 30 cps showed similar results, so the data at 30 cps were selected to represent the high speed. Video recording started after the belt speed was accelerated to the speed of interest. Recording duration was 20 seconds per trial. We created two methods to encourage the mouse to move in the front half of the treadmill chamber. The first was through olfactory stimulation by placing Enviro-dry from the mouse home cage behind the front wall of the chamber, and the second was through auditory stimulation by

tapping the lid of the treadmill chamber. Mice were allowed to rest for 1-2 minutes between each trial. In some cases, they were studied on a second day to confirm observations.

### 3.3.4 Analysis of gait

Gait parameters (Table 2) were analyzed using TreadScan Version 3.00 (Cleversys, Inc.). An artificial foot model was created by drawing a polygon over the foot of interest at different frames and saving the RGB ratios that represent each foot. To exclude the instances when the mouse did not keep up with speed (e.g. when rearing or grooming), we included only frames during which the mouse was at the front portion of the treadmill chamber. Analysis parameters included the stance time, swing time, and stride length for each step (Figure 3.2*B*). The reliability of each step was confirmed manually before proceeding to further analysis in order to delete false positive and accept false negative steps. All raw data were exported to an EXCEL file for further analysis.

### 3.3.5 Statistical analysis

Statistical analysis was performed using GraphPad Prism 5. Differences between the three experimental groups were evaluated using one-way analysis of variance (ANOVA). Bonferroni test was used for post hoc analysis. We used Degrees of freedom (DF) = 2. Probabilities ($P$) $< 0.05$ were considered significant.

## 3.4 RESULTS

### 3.4.1 Effect of silencing chemical synapses by Hb9 INs on variability of step cycle duration

To study the variability in locomotor cycle duration after silencing chemical transmission by Hb9 INs, we measured the time intervals between rear foot strikes, and constructed frequency plots of cycle duration. This demonstrated that, regardless of experimental group, as treadmill speed increased, the variability in cycle duration decreased, and the cycle duration became more consistent (Figure 3.3). To examine the difference between experimental groups, the coefficient of variation (C.V. = SD/Mean) of the cycle duration was calculated for each mouse, and results were compared at each speed for each age group. No significant differences were observed (Figure 3.4).

Since cycle duration is composed of two phases, stance and swing, phase variability in the hind limb was also studied, and also found to be similar across all groups (Figure 3.5). In comparing the mean and SD of cycle duration, stance time, and swing time between the experimental groups, no group differences were found at any of the speeds (Figure 3.6), suggesting that the absence of chemical transmission by Hb9 INs did not affect locomotor rhythmicity.

### 3.4.2 Effect of silencing chemical synapses by Hb9 INs on hind limb gait parameters

In order to study the role of chemical transmission by Hb9 INs on hind limb locomotion, various gait parameters were examined (Table 2). These parameters have been shown to be affected in other genetically modified mouse models (Gosgnach *et al.,* 2006; Crone *et al.,* 2009; Ausborn *et al.,* 2012; Talpalar *et al.,* 2013). To consider intra-individual as well as inter-individual variability within one experimental group, C.V. was calculated for instantaneous running speed and showed no significant difference between the experimental groups examined (Figure 3.6*A*). Average values of coupling between hind foot and ipsilateral front foot (homolateral coupling) and coupling between contralateral hind feet (homologous coupling) showed no significant differences between the experimental groups (Figure 3.6 *B*-*C*).

The number of total step cycles divided by total duration of locomotion (i.e. stride frequency) was not different between the experimental groups at low, medium, or high speeds (Figure 3.7*A*). Rear track width (i.e. distance between the two hind feet during locomotion), as well as the distance travelled by foot per step cycle (i.e. stride length) was similar in all experimental groups at low, medium, and high belt speeds (Figure 3.7*B*-*C*). Analysis of mean and S.D. values for all gait parameters were also conducted and showed no significant difference between the experimental groups at any of the speeds examined. These results suggested that chemical transmission by Hb9 INs is not necessary for maintaining the locomotor pattern.

## 3.5 DISCUSSION

In this study, we used mouse genetic techniques to silence glutatamatergic transmission by Hb9 INs in post-natal animals. Our goal was to investigate whether Hb9 INs have an important role in locomotor activity. We have demonstrated that silencing chemical transmission in Hb9 INs had no appreciable effects on locomotion.

We postulated that the conditional bursting properties of Hb9 INs could represent a pacemaker type function of spinal locomotor networks. By silencing Hb9 INs, the reduction of a pacemaker function may lead to greater variability in the locomotor cycle duration. In all mice, there was an inversely proportional relationship between variability of step cycle duration and treadmill belt speed which may have arisen as a result of a reduced chance of locomotor discontinuity when exploring and/or grooming at higher speeds compared to lower speeds. However, when eliminating glutamatergic transmission by these neurons, there was no change in this variability in conditional knock-out mice compared to littermate controls.

We also investigated whether silencing of glutamatergic transmission by Hb9 INs affected other gait parameters, but found there was no effect on stride frequency, rear track width, or stride length. This is in contrast to previous studies of other spinal INs that showed their roles in shaping the pattern of locomotor output by manipulating the locomotion speed such as inhibitory V1 INs (Gosgnach *et al.,* 2006), or by co-ordinating right-left alternation of the limbs such as V2a and V3 INs (Zhang *et al.,* 2008; Crone *et al.,* 2009; Ausborn *et al.,* 2012; Talpalar *et al.,* 2013). Thus, we were unable to

demonstrate that glutamatergic transmission by Hb9 INs is necessary for normal locomotor output.

The lack of observable effect does not mean that Hb9 INs are not involved in locomotor rhythm generation (Wilson *et al.,* 2005; Hinckley *et al.,* 2005; Wilson *et al.,* 2007; Tazerert *et al.,* 2008; Brownstone and Wilson, 2008; Kwan *et al.,* 2009; Ziskind-Conhaim *et al.,* 2010; Masino *et al.,* 2012). Firstly, we activated Cre recombinase at a young age (postnatal days 5-7), at a time when locomotor CPGs for mice are still developing (Iizuka *et al.,* 1997; Wilson *et al.*, 2007). Their locomotor activity was studied some weeks later at an age when mice can bear weight and walk (Jiang *et al.,* 1999). These results raise the possibility that neuroplastic mechanisms in these developing animals have compensated for the loss of vGluT2 in Hb9 INs, thus masking any effect on locomotor CPGs. *In vitro* recording of fictive locomotion from isolated spinal cords of young Hb9 -VGluT2$^{OFF}$ pups would provide an answer to this question. This preparation also has the advantage that sensory and descending inputs are eliminated, allowing study of the central circuitry in isolation.

The genetic strategy we used does not completely eliminate Hb9 IN activity. In addition to glutamatergic transmission, Hb9 INs are electrically coupled to other neurons (Hinckley and Ziskind-Conhaim, 2006; Wilson *et al.,* 2007). It is conceivable that this electric coupling is critical for rhythm generation. Rhythm generating cells in previously studied animal models were shown to be electrically coupled and to generate rhythm upon synchronous firing (Traub, 1995; Rekling *et al.,* 2000; Sasaki *et al.,* 2013). Moreover, a recent study showed that the regularity of rhythmic behaviour observed in Aplysia's buccal motor pattern is mediated by electrical rather than chemical

transmission between rhythm generating cells in feeding CPGs (Sieling *et al.,* 2014). Silencing electrical transmission by Hb9 INs could be done using a similar strategy as in this thesis, by crossing Hb9::CreER$^{T2}$ with Cx36$^{flox/flox}$ mice. That is, the intrinsic regular rhythmic nature of Hb9 INs may be critical for locomotor rhythmogenesis through electrical connectivity with neighbouring cells that are involved in locomotion, rather than via chemical transmission.

In conclusion, these results indicate that silencing glutamatergic transmission by Hb9 INs has no observable effect on locomotor rhythm generation or locomotor pattern formation in juvenile and adult mice.

**Table 3.1. Gait parameters measured**

| Gait parameter | Definition |
|---|---|
| Stride time | Locomotor cycle duration |
| Stance time | Duration of the stance phase |
| Swing time | Duration of the swing phase |
| Stride frequency | Number of step cycles per total duration of locomotion |
| Rear track width | Distance between the two hind feet during locomotion |
| Stride length | Distance travelled by hind limb per single locomotor cycle duration |
| Instantaneous running speed | Distance travelled by hind limb per second |
| Homolateral coupling | Right-left alternation |
| Homologous coupling | Right-left alternation |

**Figure 3.1.** Breeding strategy to generate Hb9 -VGluT2$^{OFF}$ mice. Genetically modified mice were crossed for two generations to generate Hb9 -VGluT2$^{OFF}$ mice. To produce the first generation, Hb9::CreER$^{T2}$ was crossed with a mouse strain possessing the knock-in genes vGluT2$^{flox/flox}$ and Rosa26 $^{+/+}$ to produce vGluT2$^{flox/+}$, Rosa26 $^{+/+}$ and Hb9::CreER$^{T2}$ offspring, which was then crossed with vGluT2$^{flox/flox}$ and Rosa26 $^{fs\text{-}YFP/+}$ mouse to generate a second generation of 4 genotyping possibilities: triple transgenic Hb9 -VGluT2$^{OFF}$, triple transgenic heterozygote and double transgenic wild-types.

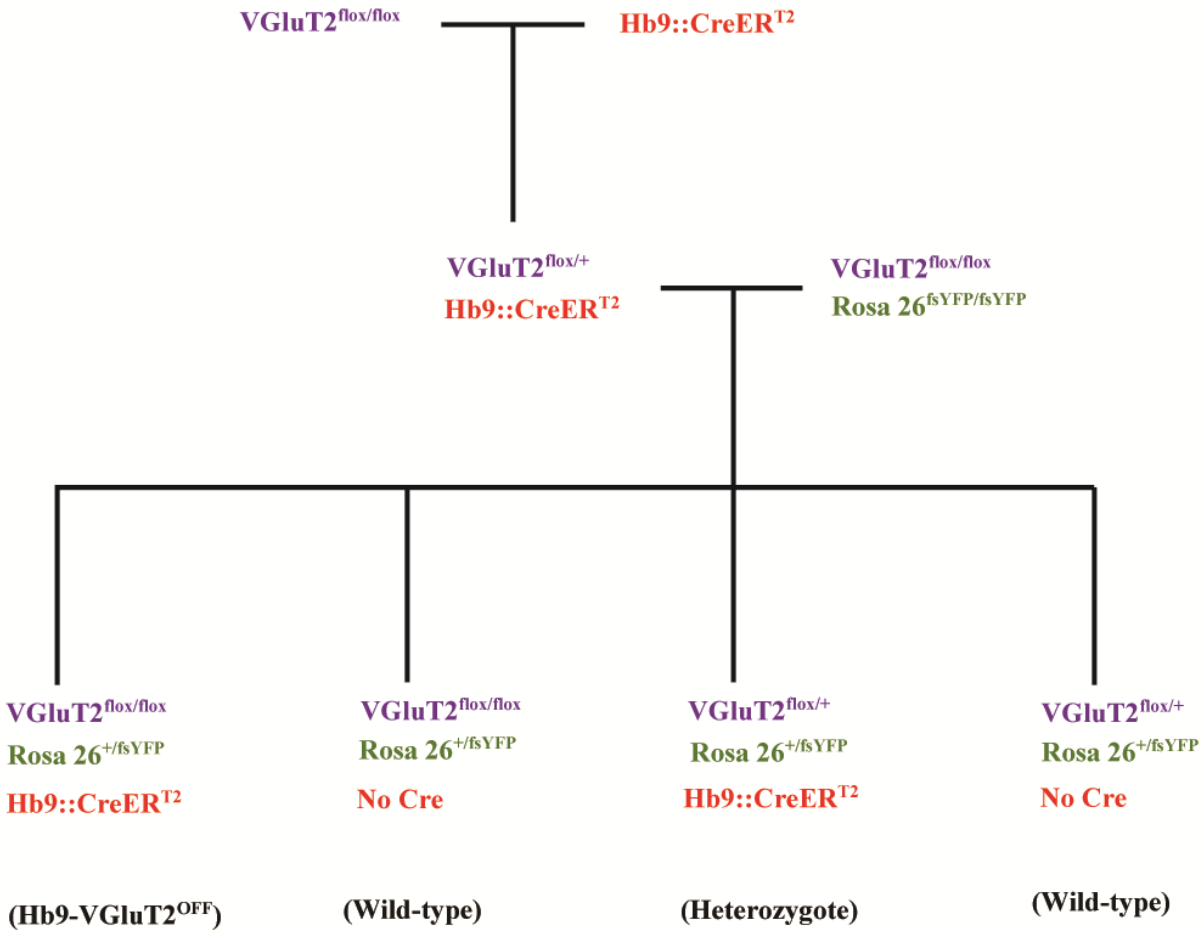


**Figure 3.1. Breeding strategy to generate Hb9-VGluT2$^{OFF}$ mice**

**Figure 3.2.** Treadmill training and recording of gait. **(A)** Experimental setup of the treadmill, with imaging from below the transparent belt. **(B)** Animal's steps are detected for all feet and processed for analysis. Each line represents the duration of the foot touching the belt (stance). The gaps between consecutive lines represents the duration when the foot is away from the belt (swing). FR: front right, FL: front left, RR: rear right and RL: rear left. X axis: recording duration (ms).

A)

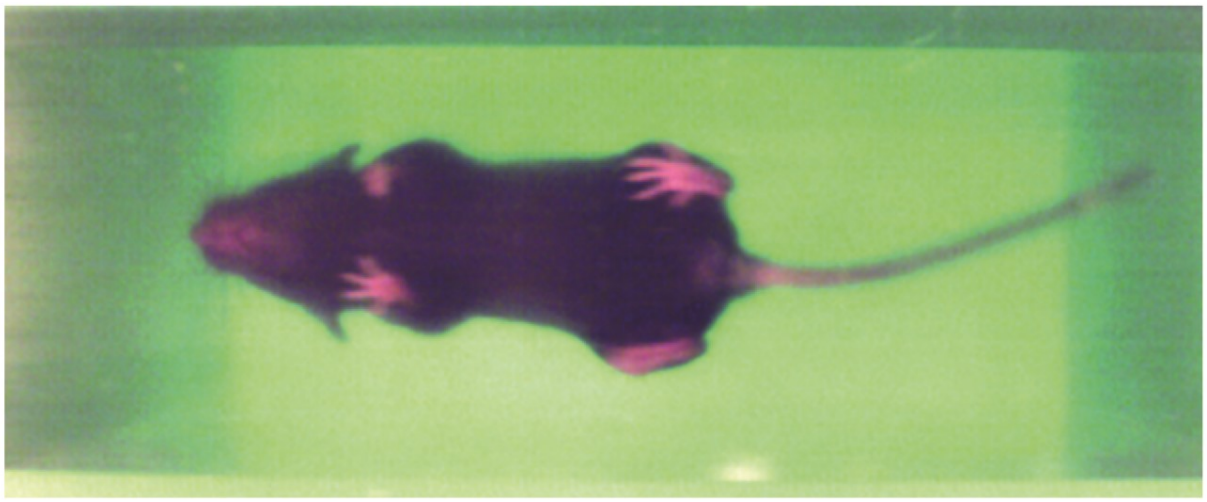

B)

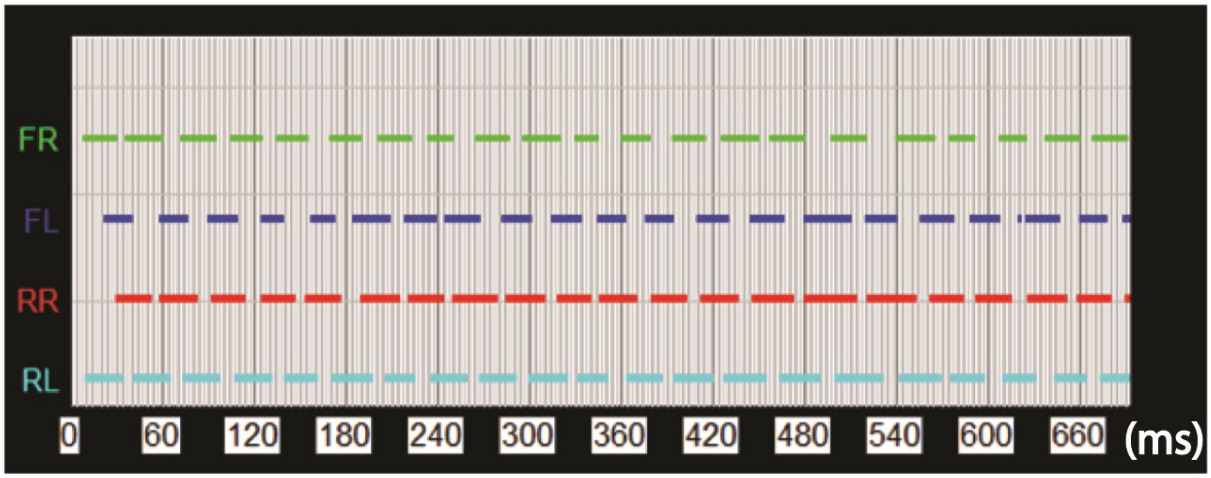


**Figure 3.2. Treadmill training and recording of gait.**

**Figure 3.3.** Frequency polygons of locomotor cycle duration. Frequency polygons outline the variability of the cycle duration per animal for age groups **(A)** P20s and **(B)** P30s. Each curve represents the behaviour of one animal. The frequency of a single event (i.e. cycle duration) is shown in percentage. Peaks represent the cycle duration at which maximum number of steps occurred. WT: wild-types, HZ: heterozygotes and Hb9-VG2OFF: Hb9 -VGluT2$^{OFF}$.

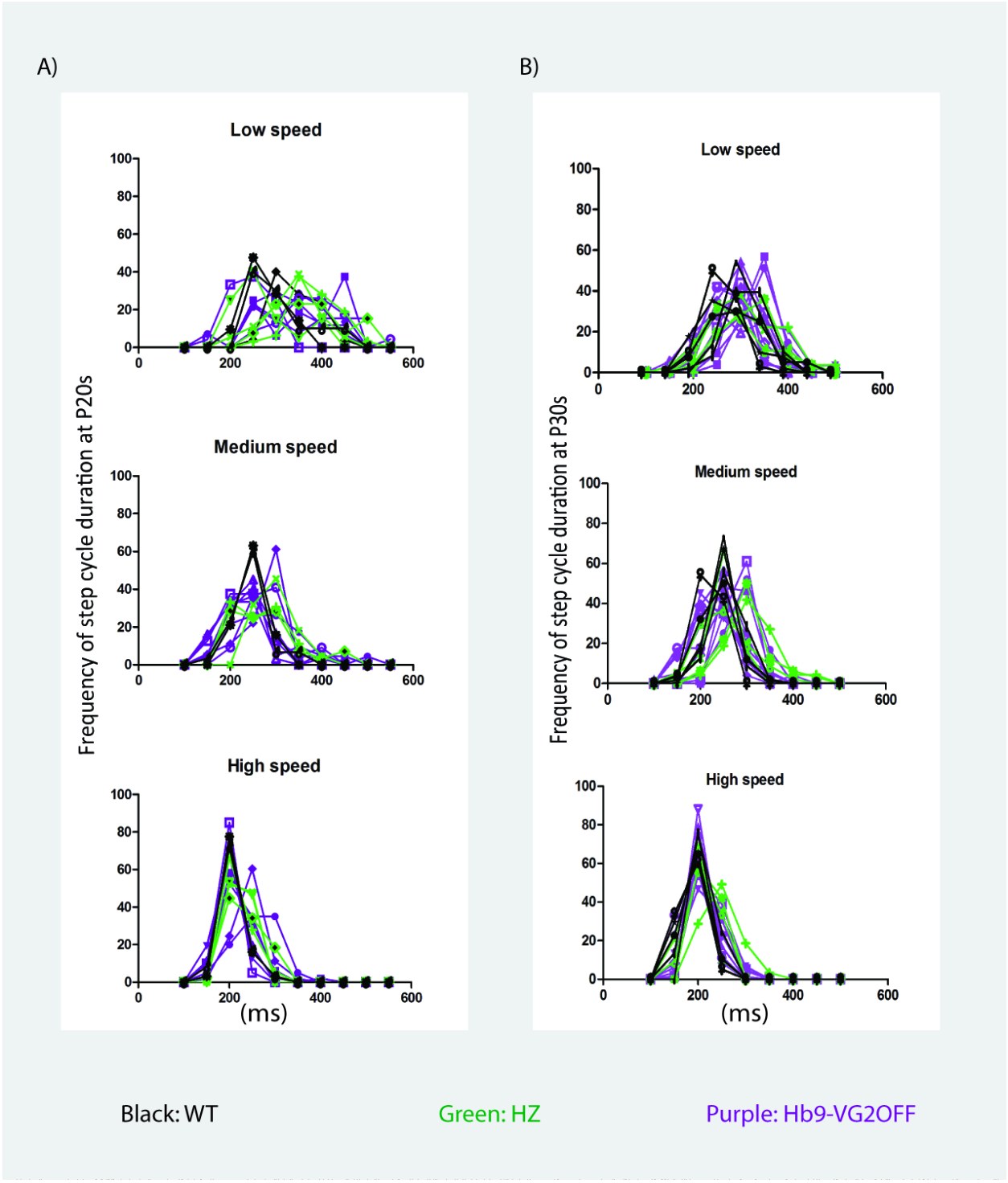


**Figure 3.3. Frequency polygons of locomotor cycle duration**

**Figure 3.4.**Variability of locomotor cycle duration in different age groups. No significant difference was observed between the experimental groups for variability of locomotor cycle duration measured in C.V. in age groups **(A)** P20s, **(B)** P30s and **(C)** W10s at walking, trotting and running speeds. WT: wild-type, HZ: heterozygotes and Hb9-VG2OFF: Hb9 -VGluT2$^{OFF}$. Each single value represents the intra-individual variability of one animal. P> 0.05.

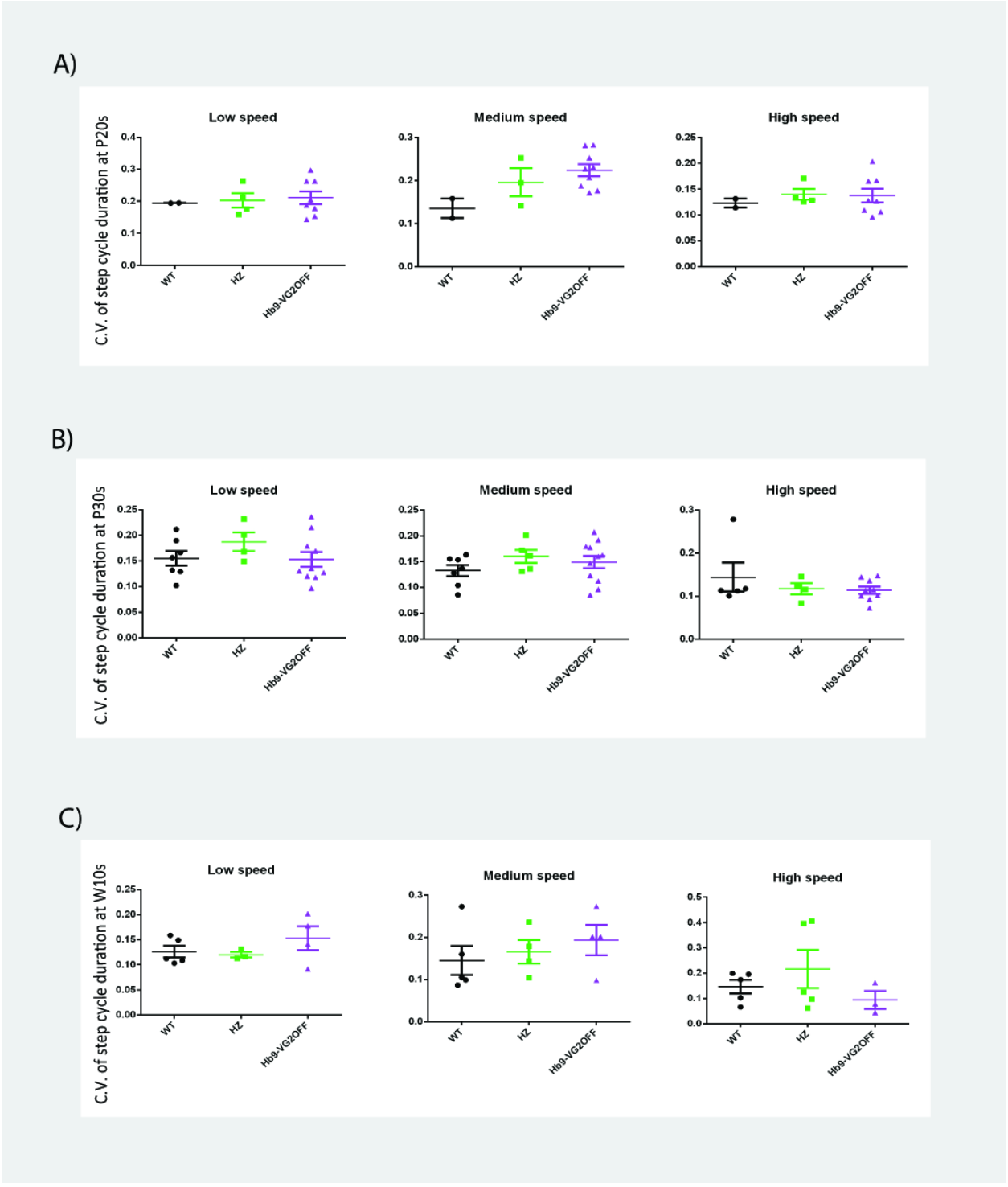


**Figure 3.4. Variability of locomotor cycle duration in different age groups**

**Figure 3.5.** Variability of swing and stance durations. No significant difference was observed between the experimental groups for **(A)** swing phase and **(B)** stance phase measured in C.V. at walking, trotting and running speeds. WT: wild-type, HZ: heterozygotes and Hb9-VG2OFF: Hb9 -VGluT2$^{OFF}$. Each single value represents the intra-individual variability of one animal. $P > 0.05$

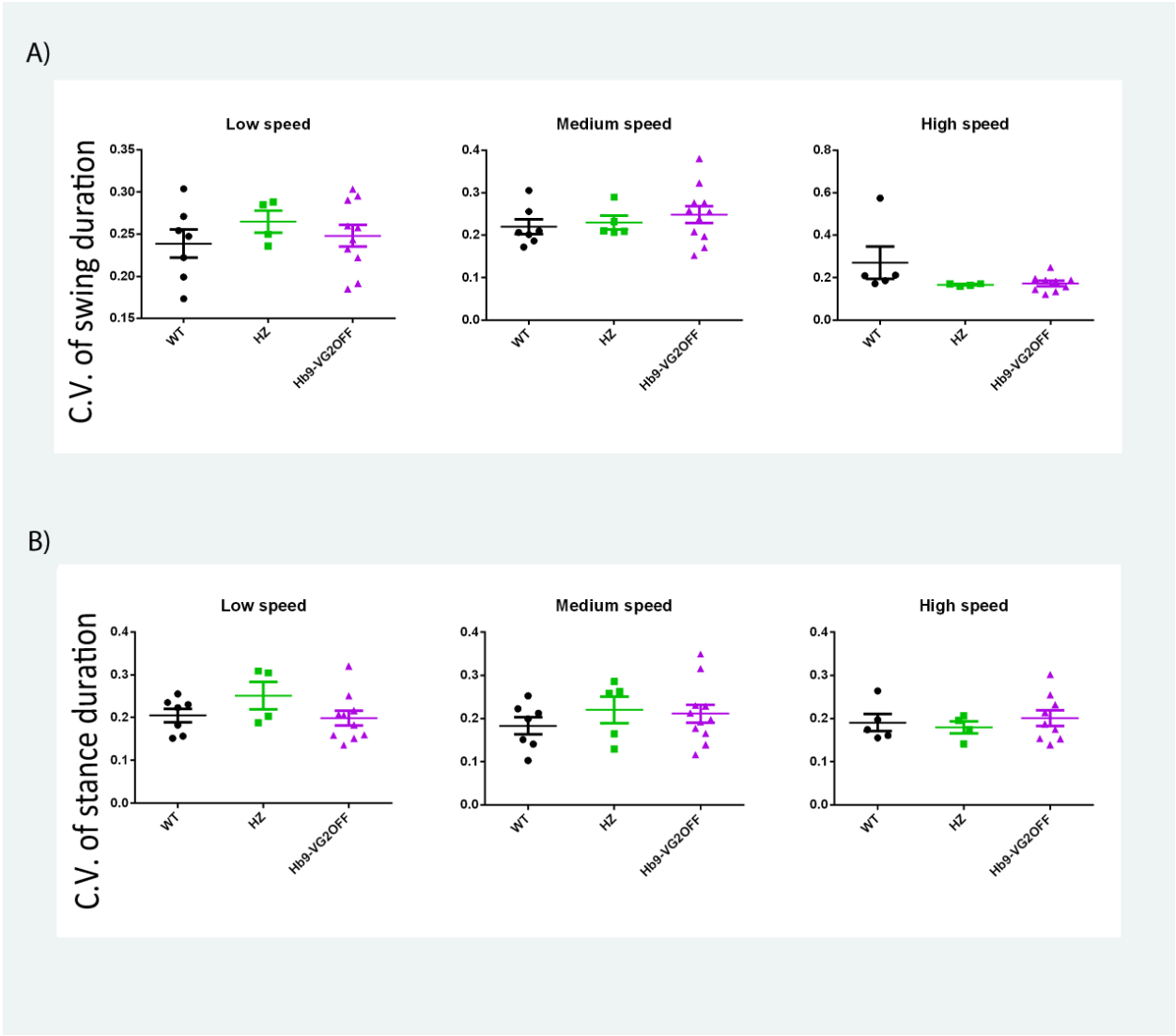


**Figure 3.5. Variability of swing and stance durations**

**Figure 3.6.** Comparing mean and SD values of cycle duration and its components**.** Average values of step cycle duration were compared between the experimental groups regardless of intra-individual variability **(A),** and variability measured in S.D. **(B)** showed no significant difference at all speeds examined. **(C)** Average values of stance and swing durations per treadmill speed is plotted against mean values of step cycle duration at the same speeds (X axis). Average and SD values of stance duration and swing duration showed no significant difference between the experimental groups. WT: wild-type, HZ: heterozygotes and Hb9-VG2OFF: Hb9 -VGluT2$^{OFF}$. P> 0.05.

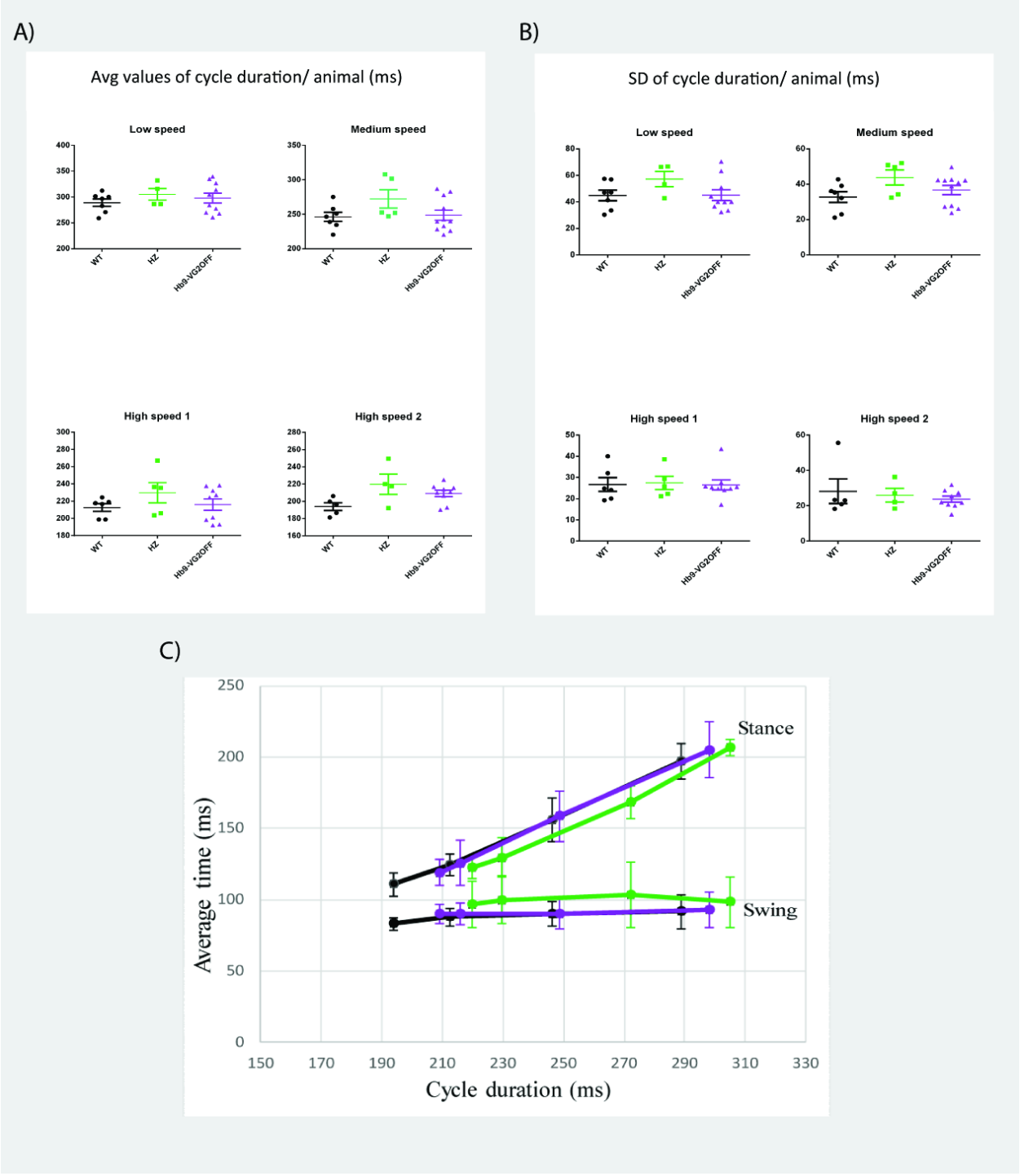


**Figure 3.6. Comparing mean and SD values of cycle duration and its components**

**Figure 3.7.** Analysis of locomotor speed and right-left alternation. **(A)** Variability in locomotor speed is presented as the variability in the distance travelled by hind foot per unit time of step cycle event (i.e. instantaneous running speed), and measured in C.V. Right- left alternation is presented as **(B)** coupling between ipsilateral front and hind feet (i.e. homolateral coupling) and **(C)** coupling between the two hind feet (i.e. homologous coupling) during locomotor cycle. There were no significant differences between the experimental groups at all speeds examined. WT: wild-type, HZ: heterozygotes and Hb9-VG2OFF: Hb9-VGluT2$^{OFF}$. P>0.05.

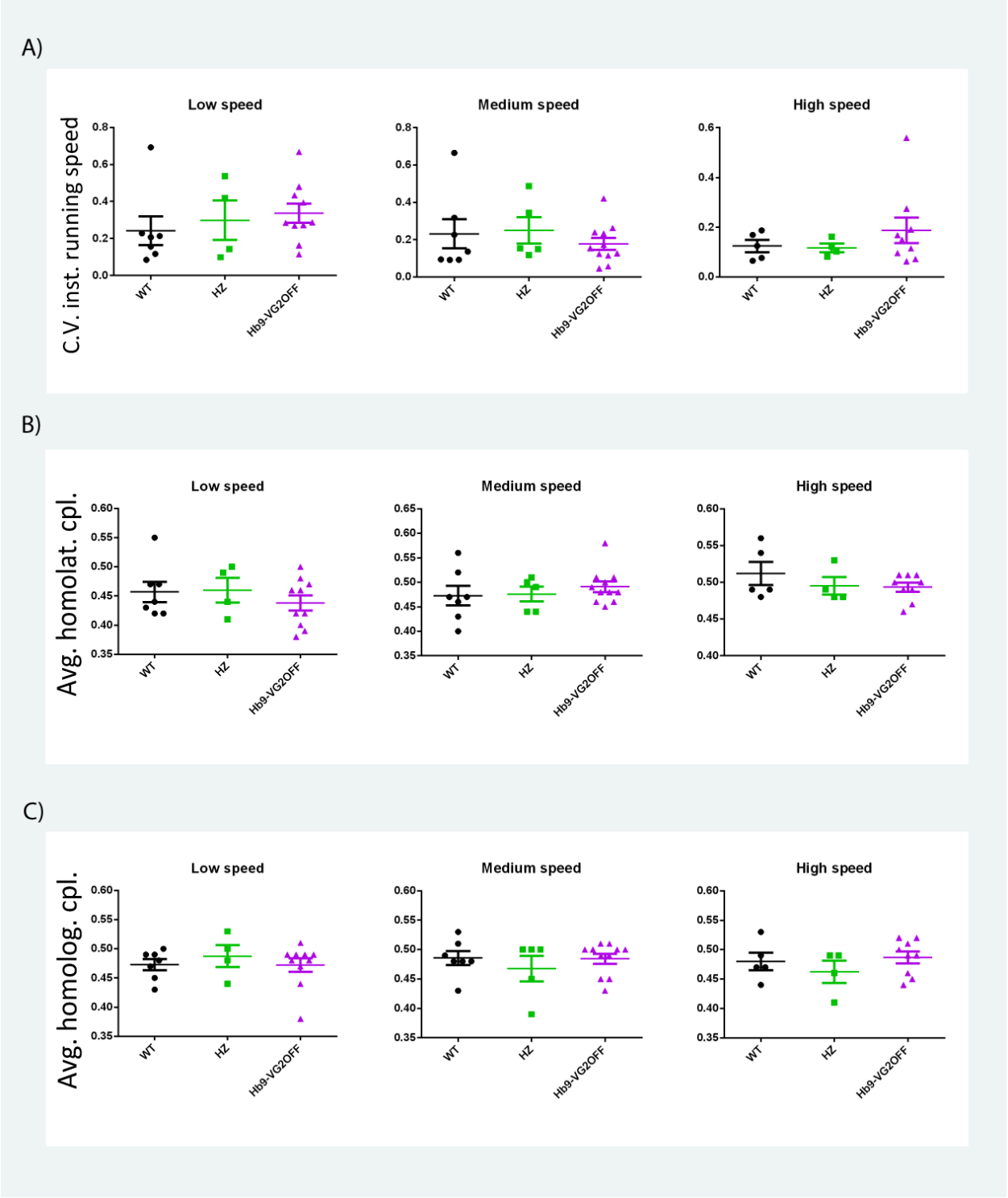


**Figure 3.7. Analysis of locomotor speed and right-left alternation**

**Figure 3.8.** Analysis of gait parameters. No significant difference was observed between the experimental groups for **(A)** total number of step cycles per duration of locomotor activity displayed as stride frequency, **(B)** distance between hind feet during locomotion displayed as C.V. of rear track width or **(C)** variability of stride length at all speeds examined. WT: wild-type, HZ: heterozygotes and Hb9-VG2OFF: Hb9 -VGluT2$^{OFF}$. P>0.05.

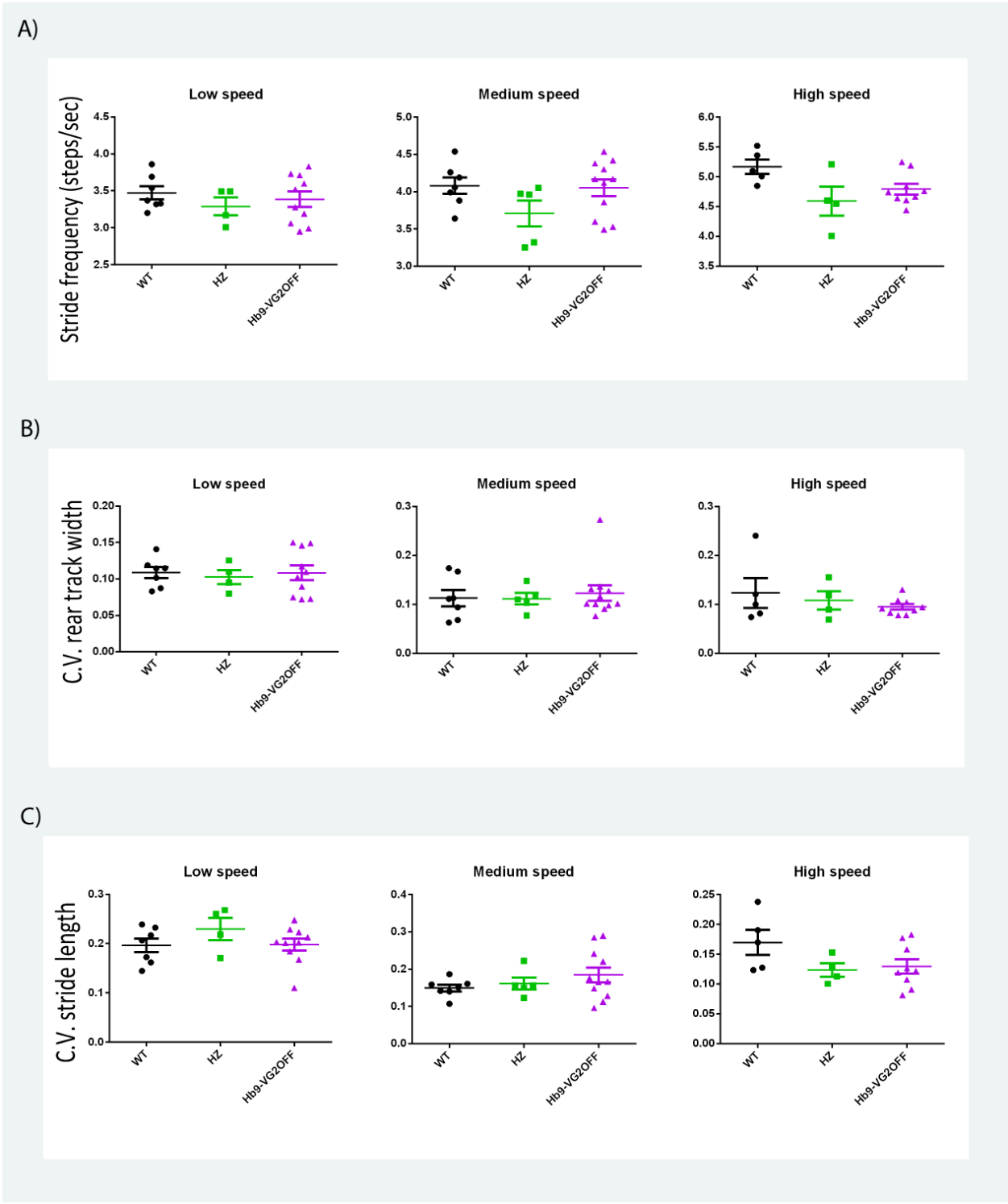


**Figure 3.8. Analysis of gait parameters**

# CHAPTER 4 IDENTIFICATION OF HB9 IN PROJECTIONS IN THE SPINAL CORD

## 4.1 SUMMARY

Motor output is controlled by networks of interconnected cells, many of which are interneurons (INs) that reside within the confines of the spinal cord. Small sized INs that express the homeodomain protein Hb9, termed "Hb9 INs," have pacemaker properties and have been suggested to contribute to locomotor rhythm generation. To get a thorough understanding of what these INs do, it is important to know the cells in the spinal cord with which they communicate. Using a combination of genetic, anatomical and imaging techniques, we identified the regions where Hb9 INs project as well as some of the cells in the spinal network that receive glutamatergic synapses from Hb9 INs. Clusters of Hb9 IN boutons were observed throughout the spinal cord, concentrated in medial lamina VIII, lamina IX, and lamina X. Appositions of boutons with few motoneurons (MNs) as well as Hb9 INs were observed. We also examined appositions with sympathetic preganglionic neurons (SPNs) but found few. These data provide a map to further study the projections of Hb9 INs, and suggest that Hb9 INs may be important in modulating the motor output of specific MN subpopulations.

## 4.2 INTRODUCTION

Behaviour is produced by neural circuits, which in the spinal cord are comprised of numerous populations of INs that can drive diverse functional outputs ranging from

simple reflex actions to more complicated behaviours such as running and swimming. Among the numerous populations of INs in the spinal cord is a group of small INs (8-10 μm somata diameter) that express the homeodomain protein Hb9 (Hb9 INs, Wilson *et al.,* 2005; Hinckley *et al.,* 2005). The role of these neurons in motor behaviour is not known.

The demonstration of pacemaker properties in these neurons led to the suggestion that they are involved in producing the rhythm of locomotor activity. It is now clear that Hb9 INs are not the sole pacemakers of locomotion (Kwan *et al.,* 2009; Chapter 3). But whether they play a role in the timing function of locomotion is not clear (Wilson *et al.,* 2005; Hinckley *et al.,* 2005; Kwan *et al.,* 2009; Masino *et al.,* 2012; Chapter 3).

Key questions remain about the functional anatomy of Hb9 INs. It has been demonstrated that these neurons are glutamatergic, expressing the vesicular glutamate transporter vGluT2, and are located throughout cervical to upper lumbar segments. In 30 μm cross sections, they were found in clusters of two or three INs per cluster in medial lamina VIII and lamina X (Wilson *et al.,* 2005; Hinckley *et al.,* 2005). Evidence from a previous study indicated that in the upper lumbar segments, axons of Hb9 INs project ventrally toward dendrites located between the lateral motor column (LMC) and medial motor column (MMC; Hinckley *et al.,* 2005). The occurrence of Hb9 IN-MN contacts was rare, in addition, other studies failed to demonstrate connections with motoneurons (Wilson *et al.,* 2005). As reviewed by Brownstone and Wilson (2008), the issue of whether they are premotor or not remains unresolved. Terminals of Hb9 INs were also observed on the somata and proximal dendrites of neighbouring Hb9 INs (Wilson *et al.,* 2005; Hinckley *et al.,* 2005), but projections to other spinal neurons have not been studied.

One difficulty in studying the projections of Hb9 INs has been in their identification. In Hb9::eGFP mice, GFP expression is observed in many interneurons that do not express Hb9 (Wilson *et al.,* 2005, Hinckley *et al.,* 2005; Hinckley and Ziskind-Conhaim, 2006; Wilson *et al.,* 2007; Kwan *et al.,* 2009). While they can be identified anatomically in Hb9-lacZ knock-in animals (Wilson *et al.,* 2005; Wilson *et al.,* 2007; Kwan *et al.,* 2009), the ability to definitively trace the axons of Hb9 INs in these animals is limited. In addition, while they can be defined by electrophysiological properties (Wilson *et al.,* 2005; Hinckley *et al.,* 2005; Masino *et al.,* 2012), tracing intracellularly filled axons of neurons in reduced preparations has been difficult and has not led to a definitive answer about their projections. Thus, new models are needed to answer this question.

In this study, we therefore turned to an inducible Cre recombinase mouse model, using Hb9::CreER$^{T2}$ mice. We crossed these with Rosa26$^{fs\text{-}synaptophysin\text{-}Td\ tomato/+}$ mice that express the synaptic vesicle glycoprotein synaptophysin fused with the fluorescent protein Td-tomato after excision of the transcriptional stop sequence flanked by loxP sites in neurons expressing Cre recombinase. Thus, boutons arising from Hb9 INs can be visualised after Tamoxifen administration. The Td-tomato positive boutons could be definitively identified as originating in Hb9 INs because of their co-expression of vGluT2. We demonstrated the spinal cord regions where Hb9 IN axons terminate and examined appositions with other neuronal types. Results showed clusters of Hb9 IN boutons throughout the rostro-caudal extent of the spinal cord, even in the lower lumbar and sacral segments that are devoid of Hb9 INs. In upper lumbar segments, bouton clusters were most abundant in medial lamina VIII, lamina IX, and lamina X. The

projection of Hb9 INs to ventromedial locations of the upper lumbar segments may suggest possible roles of Hb9 INs in the spinal circuits.

## 4.3 METHODS

### 4.3.1 Animals

Hb9::CreER$^{T2}$ mice were crossed with mice possessing the knock-in gene Rosa26$^{fs_synaptophysin_Td\ tomato/+}$ (Ai34D) purchased from Jackson laboratory (Maine). Administration of Tamoxifen to the offspring resulted in CreER activation in cells expressing the homeobox gene HB9 (Chapter 2). Cre recombinase acts to excise the transcriptional stop sequence in the Rosa26 gene leading to the expression of the fusion protein synaptophysin-Td tomato, concentrated in the terminals of Hb9 expressing cells (i.e. conditional expression; reviewed by Sauer, 1998). All mice were of C57BL/6J background and were used in the experiments regardless of sex. Spinal cords were extracted from animals at postnatal days 25-27 to look at the distribution of boutons. Experimental procedures were approved by the University Committee on Laboratory Animals and were in accordance with the Canadian Council on Animal Care guidelines.

### 4.3.2 Preparation and administration of Tamoxifen

To prepare a stock of 20 mg/ml, 100 mg Tamoxifen (T5648-1G) was warmed in 400 µl of 100% ethanol at 37$^{o}$ C for 5 minutes followed by dilution in 5 ml sunflower oil

(w530285). The solution was incubated at 37° C ≥ 1 hour; vigorous shaking was required during incubation to dissolve Tamoxifen. Aliquots of 1-2 ml of Tamoxifen solution were stored at -20° C and warmed up to 37° C prior to injection. Mice were injected between postnatal day 5 and 7 (P5-7) with a dose of 0.1- 0.2 ml of Tamoxifen solution. Injection was performed subcutaneously into the dorsal fat pad on the back of the neck using a 30 G needle. It was notable that the actual absorbed dose of Tamoxifen was variable and less than the dose injected due to post injection leakage at the injection site. Pups were transferred to a clean cage during the injection session (approximately 30 minutes) and were injected by separate needles to avoid inter-individual infection. They were left in the cage for few minutes to allow leakage of excess Tamoxifen through the injection site before returning to their home cage to recover and be nursed.

### 4.3.3 Perfusion and tissue preparation

#### *4.3.3.1 Perfusion*

Before perfusion, mice were injected intraperitoneally (IP) with approximately 0.1 ml of anaesthetic solution (3 ml Ketamine HCl, 1.88 ml Xylocaine, and 5.12 ml saline per 10 ml solution). The effect of anaesthesia was confirmed by the disappearance of hind feet reflexes. The heart was then exposed by cutting along both sides of the ribs to allow insertion of a butterfly needle in the apex of the left ventricle, and a small incision was made in the right atrium to ensure that the administrated solutions would flow through the entire cardiovascular system. First, Ringer's solution (containing 0.5 % Xylocaine) was administrated to clear the blood. Success of this step was determined by

visual cues such as change in the color of the liver from dark red to yellowish brown, and leaking of ringer's solution from the tail vein. This was followed by administration of approximately 200 ml of a 4% paraformaldehyde (PFA) solution in 0.2M PB. Following perfusion, the spinal cords were extracted, cleaned from meninges, and post fixed in PFA at 4$^{o}$C overnight, then transferred to a 30 % sucrose solution for 24-48 hours before sectioning.

#### *4.3.3.2 Sectioning*

Two different methods were used:

1) Spinal cords blocks were frozen in agarose gel and mounted on the vibratome cutting stage using super glue and 4% agar block for support. 50-60 µm floating sections were collected in a rostral to caudal order in 0.1 M PB solution at 2$^{o}$ C and stored in glass vials specified for the position from which the sections were collected. Sections were processed for immunohistochemistry on the same day or stored in glycerol at -20$^{o}$C for later use.

2) Spinal cords were quick frozen in optimal cutting temperature compound (OCT) and stored in -80$^{o}$C before sectioning with cryostat at 50 µm. Sections were collected individually and flattened on microscope slides, then allowed to air dry for 20 minutes. Slides were processed for immunohistochemistry on the same day or kept at -20$^{o}$C for later use.

### 4.3.4 Immunohistochemistry

Two different methods were used:

1) Floating sections were washed in PBS for 10 minutes before incubation in 50% ethanol to enhance antibody (Ab) penetration. After 30 minutes of ethanol incubation, sections were washed with double salt PBS (dsPBS) 3 x 10 minutes and transferred to blocking solution containing 10% donkey serum in 0.3 M Triton X and PBS solution (PBST) for 30 minutes at RT to block any non-specific staining. Tissues were quickly transferred to primary antibody solution and incubated for 48-72 hours at 4$^{o}$ C. The primary antibodies used in this study were diluted in a solution containing 1% donkey serum and PBST (Primary Abs: mouse anti -vGluT2 at 1:1000 and rabbit anti-dsRed at 1:2000 for all experiments except identification of boutons apposing SPNs. Guinea pig anti -vGluT2 at 1:1000, rabbit anti-dsRed at 1:500, goat anti-ChAT at 1:50 and mouse anti nNOS at 1:100 for identification of boutons apposing SPNs). After incubation in primary antibody solution, sections were washed in dsPBS 3 x 10 minutes and transferred to secondary antibody solution to be incubated overnight at 4$^{o}$C. Secondary antibodies were diluted in a solution containing 1% donkey serum and PBST (Secondary Abs: Alexa 488 anti-mouse IgG at 1:400 and Alexa 546 anti-rabbit IgG at 1:400 for all experiments except identification of boutons apposing SPNs. Alexa 488 anti-guinea pig IgG 1:500, Rhodamine red X anti-Rabbit IgG 1:100, DL 405 anti-goat IgG 1:500 and Cy5 anti-mouse IgG 1:500 for identification of boutons apposing SPNs). Finally sections were washed in PBS 1 x 10 minutes and mounted on a microscope slide using a fine tip brush. Sections were mounted using Vectashield mounting medium (Vector laboratories, Burlingame, CA) to enhance fluorescence and minimize fading.

2) Frozen sections were warmed for 5 minutes in RT to remove excess OCT. Sections were segregated using PAP pen and were blocked in immunofluorescence buffer (IF) blocking solution for 1 hour at RT followed by incubation in primary antibody solution diluted in IF blocking solution overnight at 4$^{o}$ C. After incubation, sections were washed in IF blocking solution 3 x 5 minutes at RT before incubation in secondary antibody solution diluted in IF blocking solution for 1 hour at RT. Finally, sections were washed 3 x 5 minutes with PBS and mounted with Vectashield mounting medium (Vector laboratories, Burlingame, CA) to enhance fluorescence and reduce fading.

### 4.3.5 Image acquisition

Confocal images (40x, 63x and 100x) were acquired with a Zeiss LSM 710 - Laser Scanning Confocal Microscope that includes Argon, HeNe and red diode lasers. Images were captured either as 2D snapshots or 3D z-stacks up to approximately 30 µm in thickness. To confirm the validity of the boutons detected in the XY axes, an interval of 0.4-0.6 µm was set between the optical sections in the z stack in order to accurately detect each bouton in more than one optical section in the Z axis (Fogarty *et al.*, 2013). Tiling was used to simultaneously obtain a higher resolution and a larger area of the section of interest. To stitch the tiles together, 5% overlap area was set between neighbouring tiles. The fluorescent intensity of the overlapping area changed from one tile to the next due to photo-bleaching. For this reason, the correlation coefficient of fluorescent intensity was set to 0.7-0.95. Although the tiles were successfully stitched, reduced signal was observable along the overlapping region due to repetitive scanning.

### 4.3.6 Image analysis

#### *4.3.6.1 Detection of Hb9 IN boutons and neuronal surfaces*

To identify the regions where axons terminate, z-stack confocal images were processed in IMARIS 7.6.5 software (Bitplane, Oxford Instruments, CT, USA). Colour parameters (i.e. brightness, contrast, and gamma) were adjusted for each fluorescent channel to facilitate differentiation between fluorescent puncta to be included in the analysis and identification of false positive objects. The spot function was used to convert the fluorescent puncta into artificial spots that could then be processed for further analysis (Fogarty *et al.,* 2013). For both Hb9-Syn-Td tom positive and vGluT2 positive boutons, the diameter of the puncta was 1 μm in the X and Y axes and 2 μm in the Z axis due to point spread function. The fluorescent intensity threshold required to convert a bouton to a spot was set manually. The newly created spots in the two channels were processed for colocalization analysis (threshold for the distance between the spots centers $\leq$ 0.6 μm), and new color channels were created to represent the colocalized boutons. FIJI was then used to create two maximum intensity projection (MIP) images; one from the original confocal image and the other from the colocalized boutons (i.e. spots) of the same image. The original confocal image was used as a guide to manually draw the landmarks of the spinal cord cross section (e.g. laminae, central canal and Clarke's column) using Adobe image illustrator CS5.1. These landmarks were used to identify the regions of the colocalized boutons and were identified using Allen institute spinal cord map (Website: ©2012 Allen Institute for Brain Science. Allen Spinal Cord Atlas [Internet]. Available from: http://mousespinal.brain-map.org/) and Todd *et al.* (2003). To

detect boutons that synapse on the soma and proximal dendrites of specific neurons, an artificial surface based on the fluorescent signal was created in IMARIS to mimic the actual neuronal surface.

#### *4.3.6.2 Bouton density mapping*

All upper lumbar sections examined were from L1 due to the importance of this segment in the initiation of locomotor rhythm (Kiehn and Kjaerulff, 1998; Brownstone and Wilson, 2008). Image J 1.49b was used to align laminae of multiple sections to the corresponding laminae in a template L1 image. The resulting image was adjusted in Adobe Photoshop CS5 to create a 2D image that represented the sum distribution of boutons in multiple L1 cross sections (Figure 4.1). The resulting image was processed in IMARIS to evaluate the positions of the boutons in XY coordinates and to produce a data sheet of the XY values which was used to generate density distribution map of the bouton clusters using the two dimensional kernel density estimation (kde2d) function and RColorBrewer function in R 3.1.1 software (Venables and Ripley, 2002).

#### *4.3.6.3 Quantitative analysis of boutons*

In this study we quantified the number of boutons in lamina IX (MMC versus LMC), and the number of boutons in lamina X (dorsal and ventral to the central canal). To visualize individual Hb9 IN boutons, we chose 100X objective magnification to

capture confocal images in z stacks as described above. Boutons were converted into artificial spots in IMARIS 7.6.5 software (Bitplane, Oxford Instruments, CT, USA), and processed in FIJI to obtain a 2D MIP image of the boutons detected in the 3D z-stack (Figure 4.5.) The region of interest was edited in Adobe Photoshop, and then processed in IMARIS to obtain a numerical value for each bouton (i.e. spots) in the XY axes. By knowing the position of the boutons relative to region of interest, we were able to segregate between the boutons that were detected, for example, dorsal to the central canal and those detected ventral to the central canal. We were able to estimate the number of boutons per 1000 $\mu m^3$ by counting the number of boutons per total volume using the following equation:

Number of boutons per $10^3$ $\mu m^3$= (Total number of boutons/ Total volume in $\mu m^3$) X $10^3$

To quantify the number of boutons in the MMC versus the LMC, we manually created a surface that represented the total area of the MMC and LMC using IMARIS. By counting the number of boutons per total area, we were able to differentiate between the densities of boutons in the MMC versus LMC.

## 4.4 RESULTS

### 4.4.1 Assessment of spinal cord regions where Hb9 IN axons terminate

Knowing where in the spinal cord Hb9 INs axons terminate is necessary to provide a first approximation of which cells Hb9 INs communicate with, which may

suggest what their function might be. The expression of vGluT2 and Td-tomato in Hb9 IN boutons allowed us to visualize the boutons throughout the rostrocaudal axis of the spinal cord in the cervical, thoracic, lower lumbar and sacral segments (Figure 4.2.) suggesting that Hb9 INs project caudally and inter-segmentally. Focusing on upper lumbar segment L1, density distribution maps of bouton clusters are displayed for three animals (Figure 4.3.; n=3 sections/animal). Summation of the bouton clusters distribution in the three animals by lumping the sections from L1 (Figure 4.1.) was then used as a reference to examine the regions of interest in more details (Figure 4.4.). The density distribution map showed clusters of Hb9 IN boutons mainly in the ventral half of the L1 segment. Dense clusters (i.e. hot spots) were observed in lamina X ventral to the central canal, and the medial motoneuron column (MMC) of lamina IX.

### 4.4.2 Assessment of the number of boutons in regions of interest

To confirm the distribution of boutons in hot spots compared to neighbouring regions, we counted the number of Hb9 IN boutons in lamina X of L1 segment, where hot spots were observed in the region ventral to the central canal (Figure 4.5.). Intra-individual variability in three animals showed an average number of 0.290 ± 0.102, 0.317 ± 0.099 and 0.148 ± 0.014 boutons per 1000 $\mu m^3$ in the region dorsal to the central canal compared to 0.533 ± 0.205, 0.459 ± 0.113 and 0.254 ± 0.034 boutons per 1000 $\mu m^3$ in the region ventral to the central canal (Figure 4.6. ; n=3 sections/animal). Despite that animal 3 had lower numbers compared to animal 1 and animal 2 (likely due to variability in sectioning and immunohistochemistry procedures), ratios of dorsal to ventral bouton

counts were similar: 1:1.79, 1:1.42 and 1:1.73 for animal 1, 2 and 3 respectively. In addition, higher counts of boutons were observed in MMC compared to LMC (Table 4.1). Thus, relatively higher count of boutons in hot spots compared to neighbouring regions confirmed the results revealed by density distribution maps.

### 4.4.3 Identification of cells that receive synapses from Hb9 INs

We next focused on whether Hb9 INs send their projections to MNs. The expression of the fusion protein synaptophysin-Td-tomato in Hb9 expressing somata as well as boutons allowed the study of Hb9 IN terminals contacting somata and proximal dendrites of MNs. Appositions were observed in MMC and in LMC (Figure 4.7*A*). Although Hb9 IN-MN appositions were not frequent, their occurrence was relatively higher in MMC compared to LMC (Figure 4.7*B*). In lamina IX, Hb9 IN boutons not apposing the soma or proximal dendrites of MNs were more frequent than boutons apposing the soma and proximal dendrites in both LMC and MMC (Figure 4.7*A*-*B*).

Given the abundance of Hb9 INs boutons in lamina X, we next investigated whether Hb9 INs terminals contacted Hb9 INs and SPNs of the intermediomedial (IMM) column. We found Hb9 IN boutons in apposition to soma and proximal dendrites of Hb9 INs (Figure 4.8.), but observed few contacts on SPNs of the IMM column in upper lumbar (Figure 4.9*A*-*B*), and lower cervical (Figure 4.9*C*) spinal cord segments.

## 4.5 DISCUSSION

The primary goal of this study was to determine the spinal cord regions to which Hb9 INs project. We demonstrated that although Hb9 INs are confined to spinal cord segments above L3 (Wilson *et al.,* 2005; Hinckley *et al.,* 2005), their axons project to all spinal cord segments, including lower lumbar and sacral segments. We also demonstrated clusters of Hb9 IN boutons in the upper lumbar segments specifically in medial lamina VIII, lamina IX and ventral lamina X. Thus, identifying the distribution of Hb9 IN boutons provided us with a first approximation of which neurons in the spinal cord Hb9 INs might be communicating.

Although it has previously been demonstrated that axons of Hb9 INs may project locally (Hinckley *et al.,* 2005), the presence of clusters of Hb9 IN boutons in the lower lumbar and sacral segments demonstrates that these INs extend their axons caudally, and to segments distant to their soma. We focused on the projection of Hb9 INs boutons in the upper lumbar segments (specifically L1 segment) due to the importance of these segments in the initiation, generation, and modulation of hind limb locomotor output (Cowley and Schmidt, 1997; Kiehn and Kjaerulff, 1998; Cazalets *et al.,* 1998 Marcoux and Rossignol, 2000). Axon terminals were detected in various regions of the L1 segment, but preferentially clustered in medial lamina VIII, lamina IX, and ventral lamina X. The abundance of Hb9 IN terminals in the ventral region of L1 segments suggests their involvement in motor circuits such as locomotor CPGs.

In motoneuron pools, our results show that there is greater clustering of Hb9 IN boutons in the MMC compared to the LMC. Moreover, in collaboration with Andrew Todd (Glasgow, Scotland), electron microscopy confirmed that Hb9 IN excitatory synapses were observed on the soma and proximal dendrites of MNs located in the MMC. Nonetheless, these synapses were rare in terms of their quantity per single MN (soma and proximal dendrites) as well as the overall number of MNs that receive them (AJ Todd, personal communication). These findings are consistent with Hinckley *et al.* (2005), who showed apposition of an Hb9 IN terminal on a proximal dendrite of a MN. The effect of Hb9 INs projection to MNs is yet to be known.

Models of mammalian locomotor central pattern generators (CPGs) often consider two "layers": a rhythm generating layer and a pattern forming layer (Rybak *et al.,* 2006). This suggests that rhythm generating INs need not form monosynaptic contacts on MNs but rather on pattern forming cells, which use the original rhythmic discharge to pattern appropriate signals to MNs (Rybak *et al.,* 2006; Brownstone and Wilson, 2008; Griener *et al.,* 2013). Whether the rarity of synapses on the somata and proximal dendrites of MNs indicates that Hb9 INs belong to the rhythm generation layer is not yet clear.

The clusters of boutons in lamina IX that do not appear to form synapses with MN somata and proximal dendrites might be synapsing on the distal dendrites of MNs or other, unidentified premotor INs. Another possibility is that since the dendrites of Hb9 INs extends more than 200 μm in the dorsal as well as the ventral direction (Hinckley *et al.,* 2005), Hb9 INs might be synapsing on their own ventrally projecting dendrites to initiate recurrent excitation. Moreover, Hb9 IN boutons in lamina X were found to form

synapses on somata and proximal dendrites of Hb9 INs, suggesting recurrent synaptic excitation between Hb9 INs. These results agree with previous findings that showed contacts of Hb9 INs on neighbouring Hb9 IN somata using the Hb9::eGFP mouse model (Wilson *et al.,* 2005; Hinckley *et al.,* 2005).

We also investigated Hb9 IN synapses with SPNs in the IMM column. We observed very few clear contacts of Hb9 IN boutons on somata or proximal dendrites of SPNs in lower cervical and upper lumbar segments. The location of Hb9 INs in or near the central autonomic area region (Wilson *et al.,* 2005), not far from pre-sympathetic INs (Deuchars *et al.,* 2005), suggested possible involvement with the autonomic system. But the rarity of direct projections of Hb9 INs to SPNs does not support this hypothesis. Although Hb9 INs are unlikely to provide direct input to SPNs, the abundance of their boutons in the central autonomic area does not exclude that they project to pre-sympathetic INs in this area.

In summary, identifying the regions where Hb9 INs terminate provided a map to examine the specific cell types with which Hb9 INs communicate. Knowing the target neurons of Hb9 INs will provide further insight into their function.

**Table 4.1. Number of Hb9 IN boutons per 500 µm$^2$ in MMC and LMC of L1 segment**

| ID | Section # | MMC | LMC | MMC:LMC Ratio |
|---|---|---|---|---|
| Animal 1 | 1 | 0.041 | 0.038 | 1.08:1 |
| | 2 | 0.06 | 0.063 | 0.95:1 |
| Animal 2 | 1 | 0.039 | 0.011 | 3.55:1 |
| | 2 | 0.043 | 0.051 | 0.84:1 |
| | 3 | 0.059 | 0.015 | 3.93:1 |
| Animal 3 | 1 | 0.011 | 0.008 | 1.38:1 |
| | 2 | 0.023 | 0.018 | 1.28:1 |
| Avg values for animal 1 | | 0.05 | 0.05 | 1:1 |
| Avg values for animal 2 | | 0.047 | 0.026 | 1.81:1 |
| Avg values for animal 3 | | 0.017 | 0.013 | 1.31:1 |

**Figure 4.1** Basic steps for identifying Hb9 IN boutons in spinal cord. **(A)** Converting fluorescent boutons (vGluT2 in green and synaptophysin-Td-tomato in red) to artificial spots in IMARIS (steps 1-2), followed by converting the image from 3D to 2D MIP image in FIJI (step 3) to facilitate drawing the contours of the spinal cord segment using Adobe illustrator (step 4). Step 5 is aligning multiple sections of the same segment from one animal or multiple animals, one lamina at a time, using image J. And finally (step 6) using Adobe Photoshop to combine all the regions together with reference to a template image of the spinal cord segment of interest. **(B)** Topological organization of the laminae in the upper lumbar spinal cord cross section. CC: central canal, IML: intermediolateral cell column, MMC: medial motoneuron column, and LMC: lateral motoneuron column.

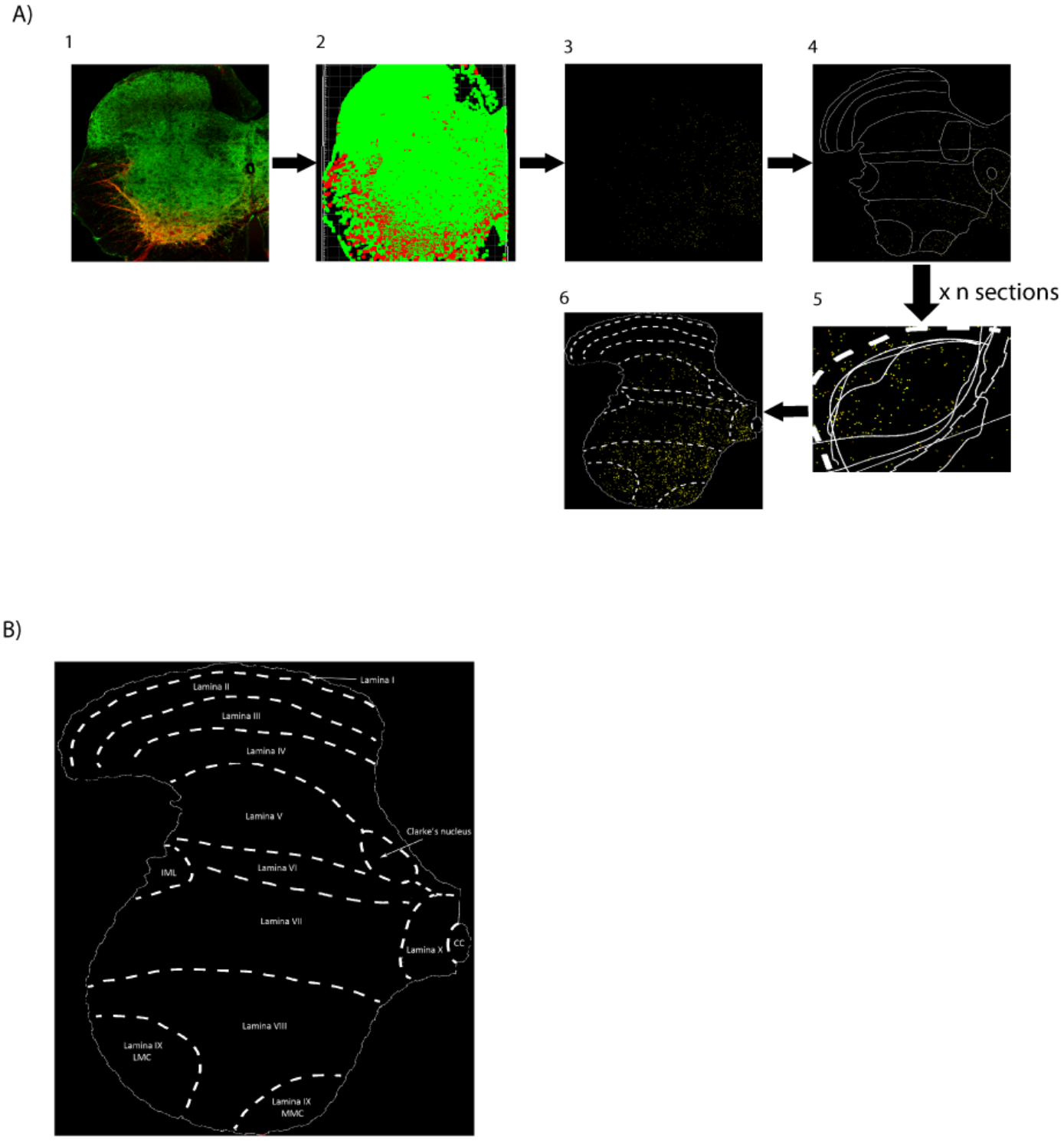


**Figure 4.1. Basic steps for identifying Hb9 INs boutons in the spinal cord**

**Figure 4.2.** Projection of Hb9 INs throughout the rostrocaudal axis of the spinal cord. Hb9 INs projections represented by the colocalization of Td-tomato (red) and vGluT2 (green) are observed in **(A)** cervical, **(B)** thoracic, **(C)** lumbar and **(D)** Sacral segments of the spinal cord and shown as yellow puncta (right). Scale bars: 50 μm

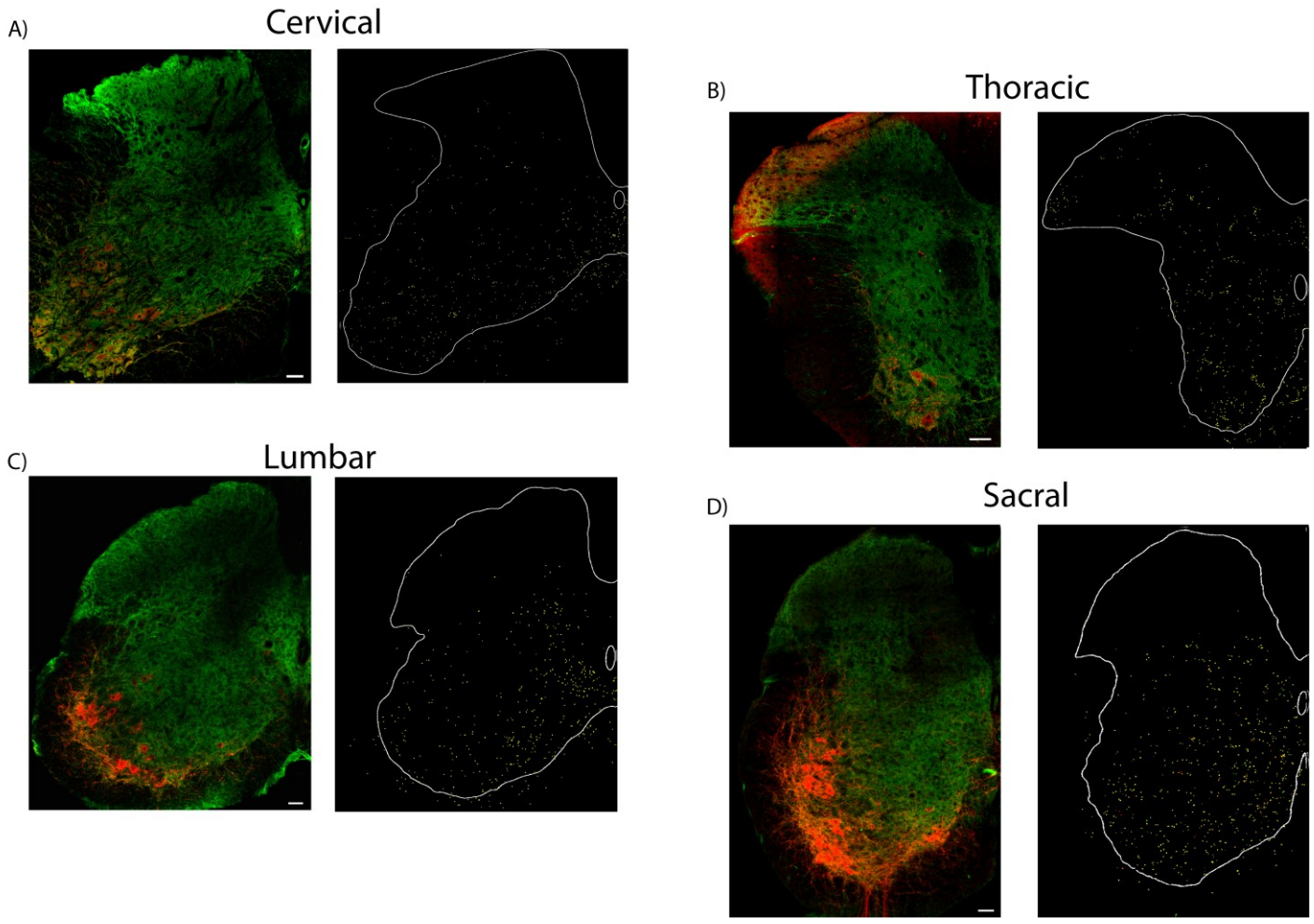


**Figure 4.2. Projection of Hb9 INs throughout the rostrocaudal axis of the spinal cord**

**Figure 4.3** Density distribution maps of bouton clusters in spinal cord segment L1 of three animals. Kde2d performed on Hb9 IN boutons in L1 segment by lumping multiple sections from L1 segment (n=3 sections). Hot spots (high bouton density) are localized in MMC of lamina IX and ventral lamina X in animal 1 **(A)**, medial lamina VII, medial lamina VIII, MMC of lamina IX and ventral lamina X in animal 2 **(B)**, and medial lamina VIII, MMC and LMC of lamina IX in animal 3 **(C)**. Numbers on the color bar represent average bouton density per $\mu m^2$ in an approximately 30μm thick section. Refer to Figure 4.1*B* for the designation of laminae.

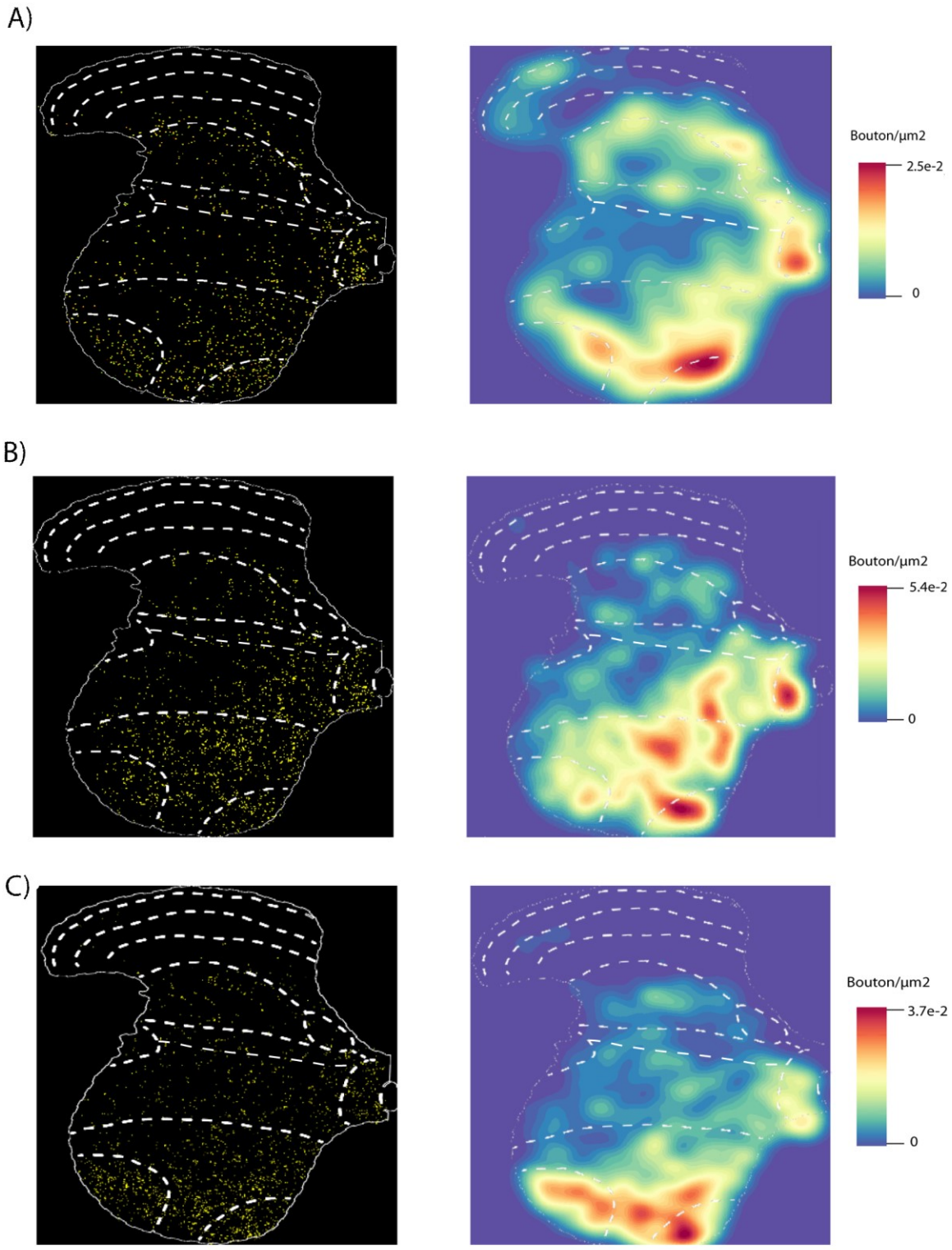


**Figure 4.3. Density distribution maps of bouton clusters in spinal cord segment L1 of three animals**

**Figure 4.4.** Distribution of Hb9 IN bouton clusters in spinal cord segment L1. Lumping density distribution maps of multiple animals resulted in a density distribution map that defines the regions where Hb9 IN boutons are most likely to occur in L1 segment of all animals. The highest chances to find Hb9 IN boutons are in the hot spots. Hot spots are located in MMC and lamina X and with a less density in medial lamina VIII and LMC. Numbers on the color bar represent average bouton density per $\mu m^2$ in an approximately 30μm thick section. Refer to Figure 4.1*B* for the designation of laminae.

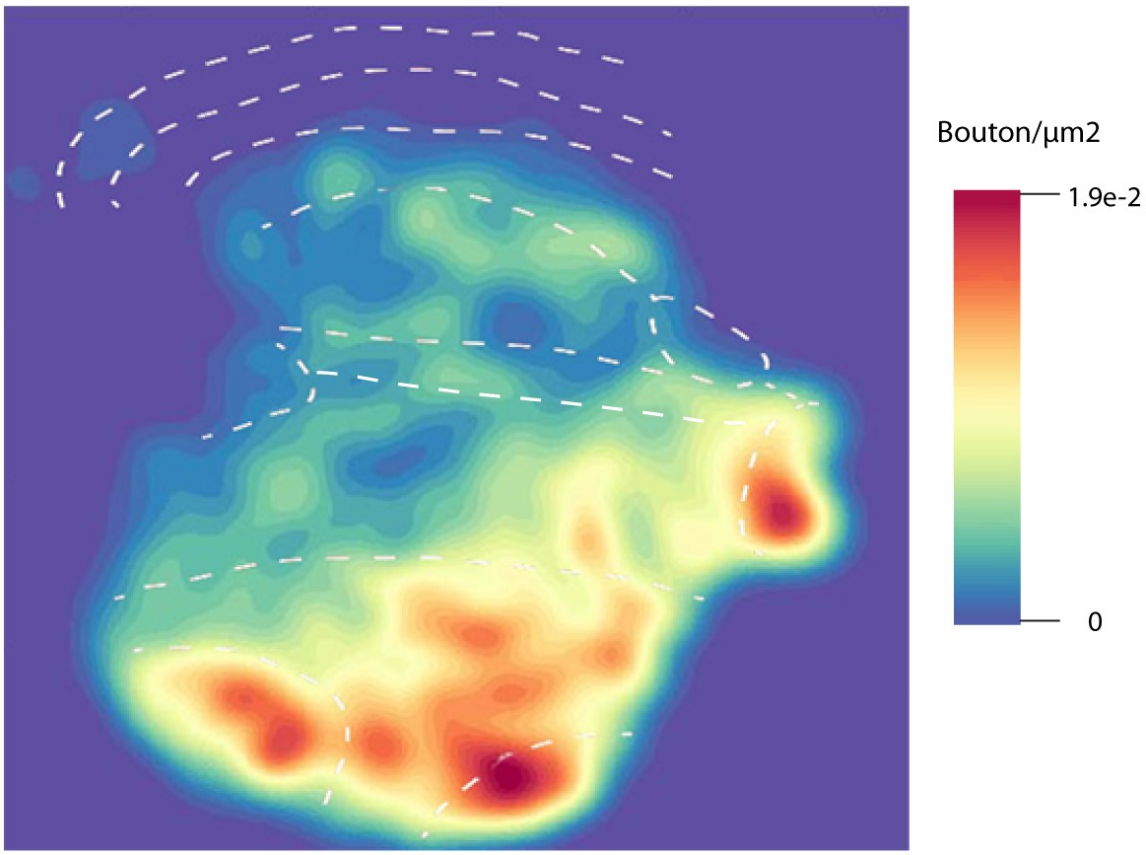


**Figure 4.4. Distribution of Hb9 IN bouton clusters in spinal cord segment L1**

**Figure 4.5.** Basic steps for quantifying Hb9 INs boutons in spinal cord. **(A)** 3D fluorescent boutons (expressing vGluT2 in green and synaptophysin-Td-tomato in red) are converted to artificial spots in IMARIS, followed by conversion to a 2D MIP image in FIJI (step 2). The 2D MIP image was then processed again in IMARIS to obtain a co-ordinate value for each bouton (step 3), by knowing the value in the Y axis that corresponds to the central canal (CC) midline, boutons were readily segregated into those that are dorsal to the CC vs those that are ventral to the CC. By counting the total number of boutons per total volume of the region dorsal to the CC (Step 4), for example, we were able to obtain the number of boutons per 1 $\mu m^3$. Multiplying this value by 1000 allowed us to obtain a normalized value for the number of boutons per 1000 $\mu m^3$. Value of the Z component of the total volume is known from the z stack thickness. Blue oval represents CC.

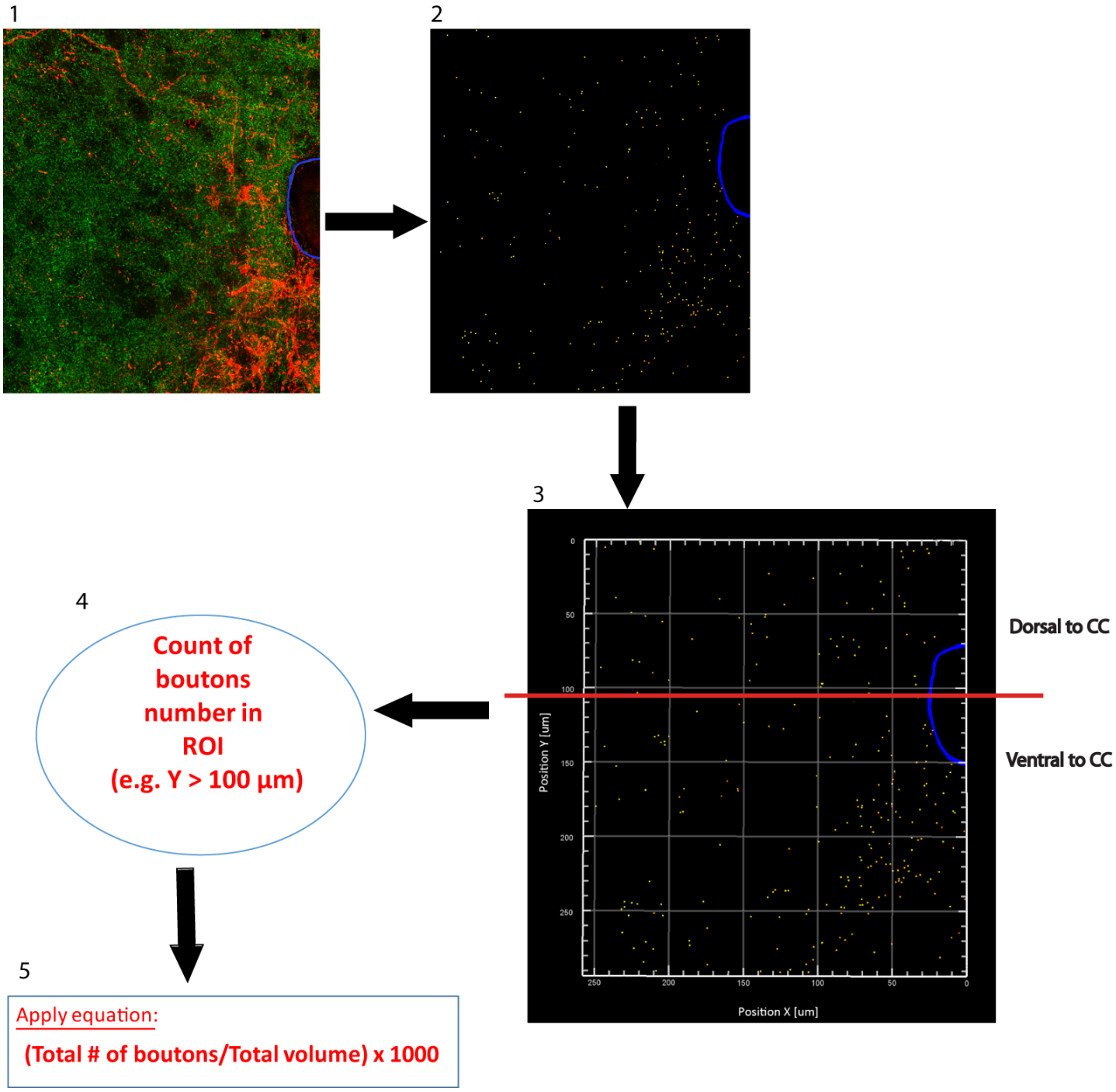


**Figure 4.6. Basic steps for quantifying Hb9 INs boutons in spinal cord.**

**Figure 4.6.** Bouton count in hotspots versus neighbouring regions. Average and SD of the number of Hb9 IN boutons per 1000 $\mu m^3$ in the region dorsal to the central canal (gray) compared to the region ventral to the central canal (blue) of lamina X in 3 different animals. Animal 1 and 2: floating sections, animal 3: cryostat sections. Refer to Figure 4.1*B* for the designation of laminae.

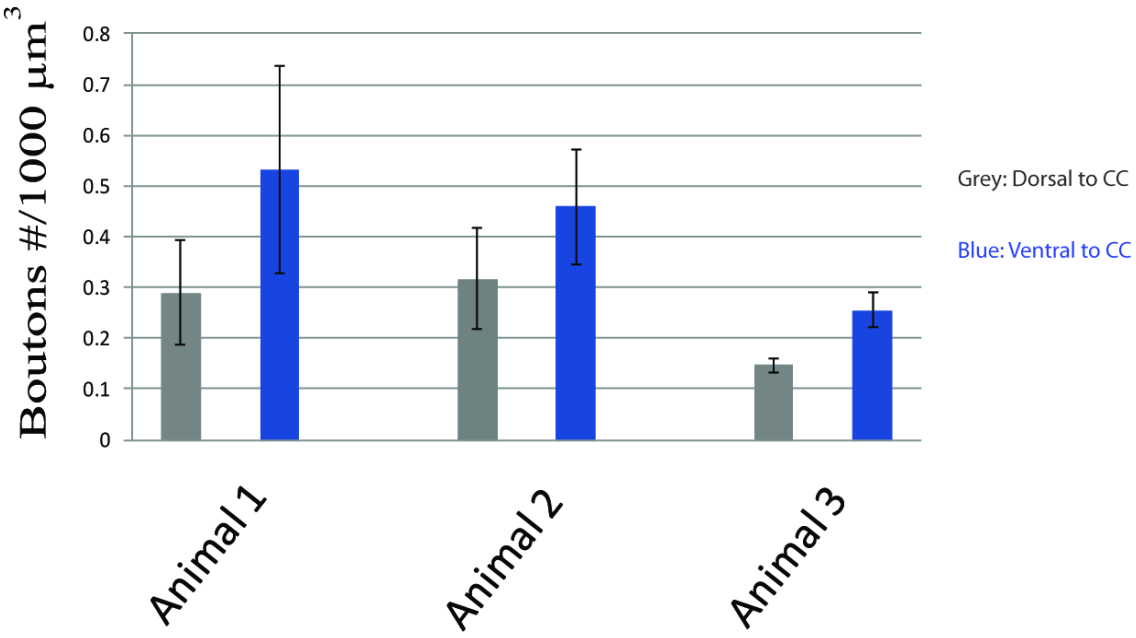


**Figure 4.7. Bouton count in hotspots versus neighbouring regions**

**Figure 4.7.** Projection of Hb9 INs to somata and proximal dendrites of MNs in the upper lumbar segments. **(A)** Maximum intensity projection image of the ventral most region of approximately 10 μm thick upper lumbar segment section showing MNs (expressing synaptophysin-Td-tomato) that received contacts from Hb9 INs projections (expressing synaptophysin-Td-tomato and vGluT2), and a fraction of MNs that did not receive any Hb9 IN contacts. Hb9 IN boutons shown as yellow puncta are distributed in laminae VIII and IX (MMC and LMC). Hb9 INs projections on MNs surfaces are within yellow. One MMC MN receives extensive Hb9 IN contacts (green box) and is magnified in **(B)**. Boutons (arrowheads) contact soma and proximal dendrite of the same neuron at different optical sections in the Z axis **(Bi)** and **(Bii).** Refer to Figure 4.1*B* for the designation of laminae. Scale bar: 10 μm for A and B.

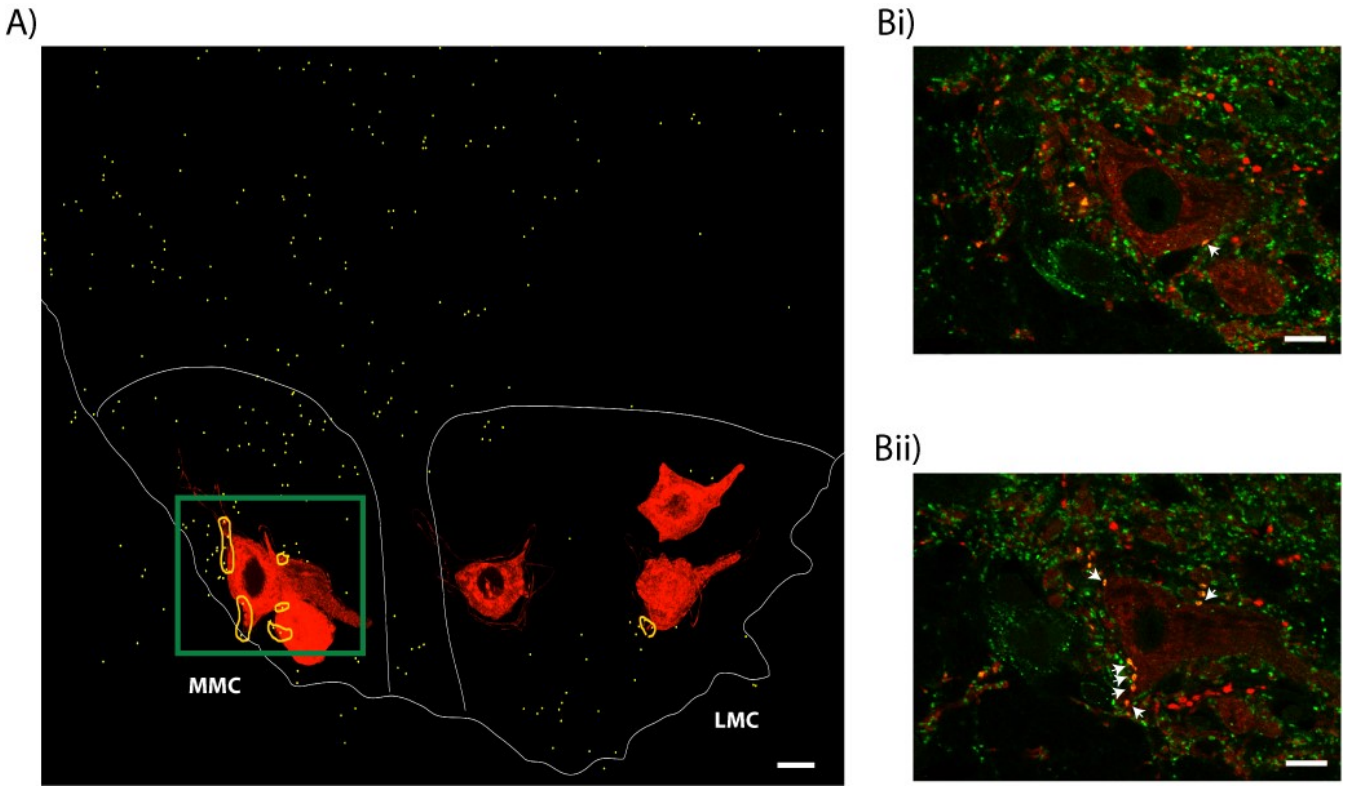


**Figure 4.8. Projection of Hb9 INs to somata and proximal dendrites of MNs in the upper lumbar segments**

**Figure 4.8.** Projection of Hb9 INs to somata and proximal dendrites of Hb9 INs in the upper lumbar segments. **(A)** Maximum intensity projection image of approximately 10 μm thick section of the region near the central canal (lamina X) displays the surfaces of two Hb9 INs (expressing synaptophysin-Td-tomato) and Hb9 IN boutons (expressing synaptophysin-Td-tomato and vGluT2) as yellow puncta. Hb9 IN boutons projecting to Hb9 INs surfaces are within yellow. Hb9 IN boutons (arrowheads) contacting the surface of the Hb9 IN on the left hand side **(Bi)**, and the surface of the Hb9 IN on the right hand side **(Bii)**. Refer to Figure 4.1*B* for the designation of laminae**.** Scale bar: 5 μm for A and B.

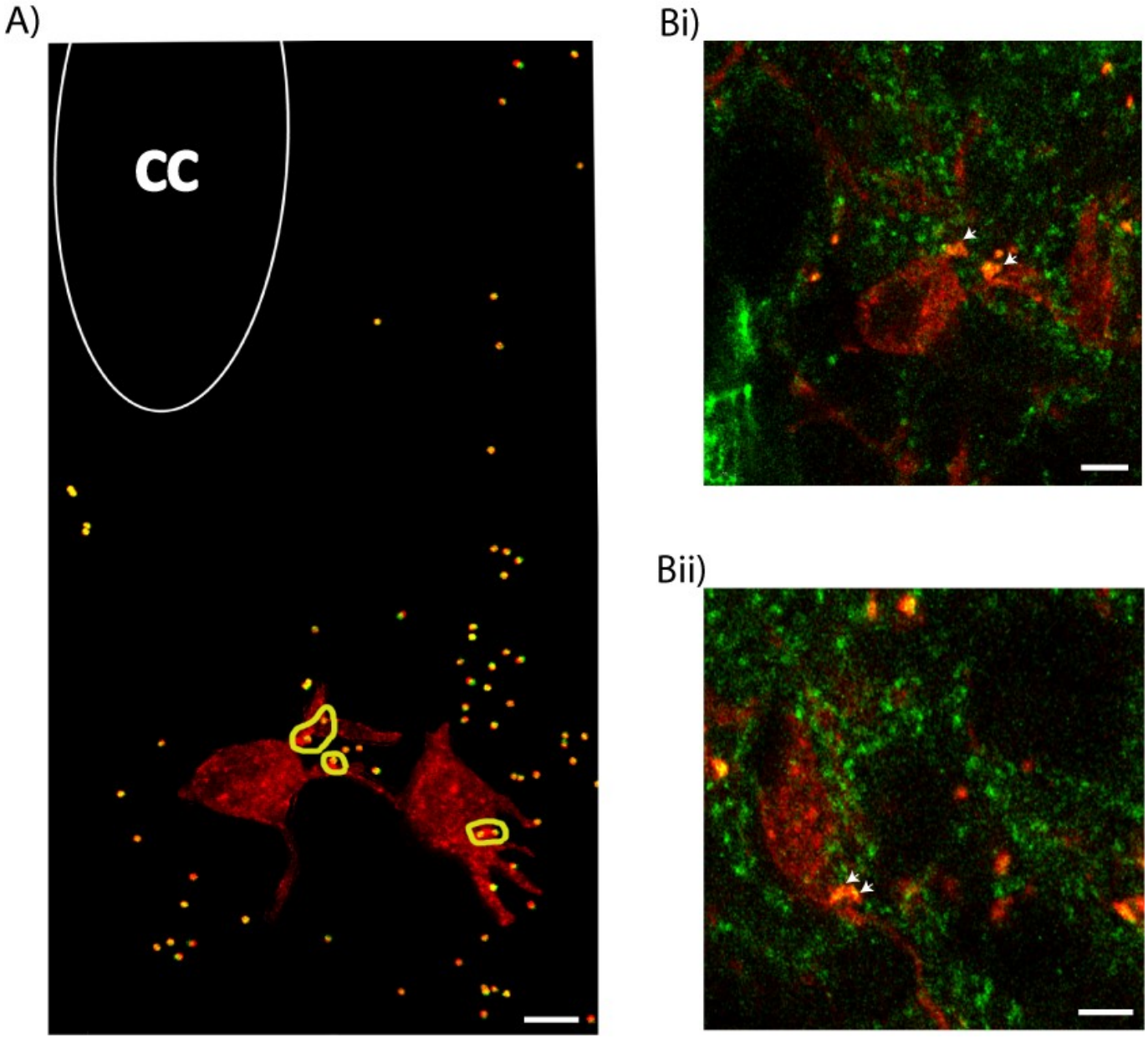


**Figure 4.9. Projection of Hb9 INs to somata and proximal dendrites of Hb9 INs in the upper lumbar segments**

**Figure 4.9.** Appositions of Hb9 INs on somata and proximal dendrites of SPNs in the upper lumbar and lower cervical segments. Artificial surfaces (in Magenta) and spots in (green and red) were created to represent the SPNs and Hb9 INs boutons respectively and facilitate their detection. Appositions of Hb9 INs (expressing synaptophysin-Td-tomato in red and vGluT2 in green) on somata and proximal dendrites of SPNs (expressing nNOS in white and ChAT in blue) were rare. For example, in the upper lumbar segments **(A)** and **(B),** only one apposition of Hb9 INs was observed per SPN soma on few SPNs (arrowheads). No appositions were observed on SPNs of the central autonomic area in the lower cervical segment **(C**). Refer to Figure 4.1*B* for the designation of laminae**.** Dashed oval represent central canal. Scale bars: 10 µm for A, 5 µm for B and 20 µm for C.

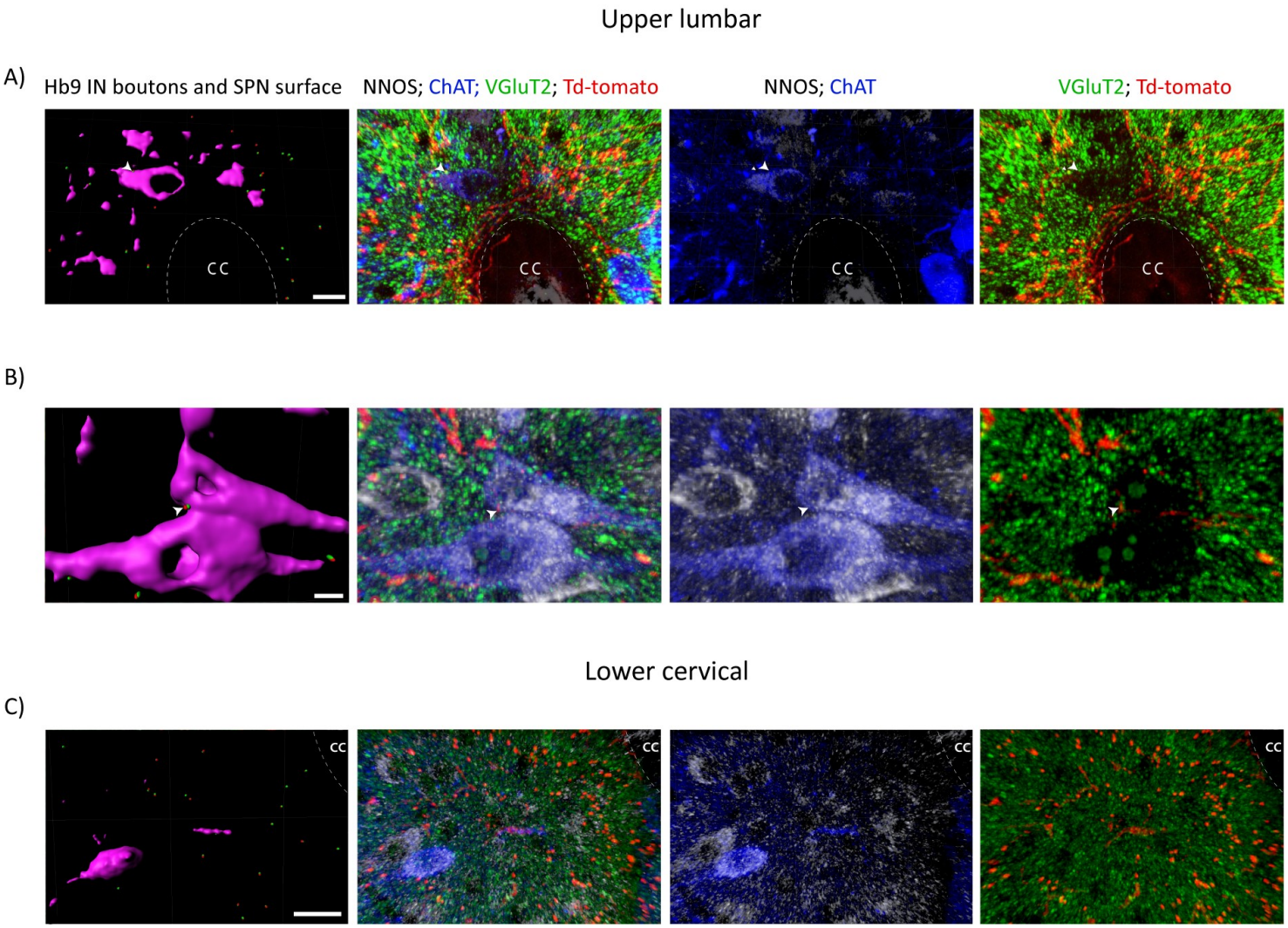


**Figure 4.10. Appositions of Hb9 INs on somata and proximal dendrites of SPNs in the upper lumbar and lower cervical segments**

# CHAPTER 5 DISCUSSION

## 5.1 SUMMARY

The objective of this thesis was to study the effect of glutamatergic transmission by Hb9 INs on locomotor behaviour and to anatomically identify the regions where they project in the spinal cord. In Chapter 2, we introduced a new mouse model in which expression of $CreER^{T2}$ is specific to Hb9 expressing cells, and proved successful recombination upon conditional activation of CreER. In Chapter 3, we tested the effect of conditional silencing of chemical transmission by Hb9 INs on treadmill locomotion. We tested locomotor variability and various gait parameters but did not observe significant differences between Hb9-$VGluT2^{OFF}$, heterozygote, and wild-type littermate mice. Finally, in Chapter 4, we introduced a map of axonal projections of Hb9 INs and found that they terminate throughout the rostrocaudal axis of the spinal cord. We focused on the projections that terminate in the upper lumbar segments due to the importance of these segments in initiating locomotor rhythm and in modulating the locomotor pattern of hind limbs. We observed high density clustering of Hb9 IN boutons in medial lamina VIII, lamina IX and ventral lamina X. Looking at specific populations of neurons located in the regions of clustering, we found appositions on soma and proximal dendrites of Hb9 INs as well as on selective MNs in the MMC. We found rare appositions with SPNs in upper lumbar and lower cervical segments.

Collectively, these results validate the efficacy of the Hb9::$CreER^{T2}$ mouse model in manipulating the expression and excision of target genes specifically in Hb9 INs. Examining locomotor behaviour of Hb9-$VGluT2^{OFF}$ mice suggested that glutamatergic

transmission by Hb9 INs is not critical in generating the rhythm or in modulating the pattern of locomotion at low, moderate or high locomotor speeds. Nonetheless, synaptic contacts formed by Hb9 INs on selective MN pools in the MMC suggests that they might be involved in the motor output to specific axial muscle groups. In addition, our results and others (Wilson *et al.,* 2005; Hinckley *et al.,* 2005) that show appositions with somata and proximal dendrites of Hb9 INs suggest the occurrence of recurrent excitation in Hb9 INs. We will discuss the relevance of this thesis work to the field of motor control and explore future directions towards understanding the spinal control of locomotor behaviour.

## 5.2 GENERAL DISCUSSION

The use of the newly introduced Hb9::CreER$^{T2}$ mouse model in this study allowed expression/excision of selective genes in Hb9 INs (Chapter 2). We were able to specifically target Hb9 expressing cells, which has proven difficult in the Hb9::eGFP mice used in previous studies due to ectopic expression of GFP in Hb9 negative cells (Wilson *et al.,* 2005; Hinckley *et al.,* 2005; Kwan *et al.,* 2009). Furthermore, we demonstrated that the use of Hb9$^{Cre/+}$mice did not restrict expression of reporter proteins to Hb9 expressing neurons (Chapter 2). Thus, identification of Hb9 INs in those mouse models required additional steps, such as confirmation of morphology and electrophysiological properties (Wilson *et al.,* 2005; Hinckley *et al.,* 2005; Kwan *et al.,* 2009).

By crossing Hb9::CreER$^{T2}$ with vGluT2$^{flox/flox}$ mice, we generated an inducible mouse model that lacks vGluT2 in Hb9 INs (Hb9-VGluT2$^{OFF}$). This allowed us to study the effects of silencing glutamatergic transmission by Hb9 INs on locomotor behaviour (Chapter 3). No significant difference was observed in treadmill locomotor variability or in locomotor pattern when compared to heterozygotes and wild-type littermates at low, moderate and high speeds, suggesting that the absence of glutamatergic transmission by Hb9 INs did not affect the rhythmic nature of treadmill locomotor pattern at any of the speeds examined. Previous studies have shown that Hb9 INs fulfill many anatomical and electrophysiological characteristics required for rhythm generators (Wilson *et al.,* 2005; Hinckley *et al.,* 2005; Brownstone and Wilson, 2008; Kwan *et al.,* 2009; Masino *et al.,* 2012). But Kwan *et al.* (2009), showed that the onset of firing in ventral roots preceded that of the Hb9 INs, suggesting they are not the sole pacemakers of locomotion. We sought to determine whether they play any role in locomotor rhythmogenesis, and thus first sought to eliminate their chemical transmission. As this had no discernible effect on locomotion, we suggest that they do not play a significant role. However, it is possible that they play a role through non-glutamatergic transmission, such as through electrical synapses (Hinckley and Ziskind-Conhaim *et al.,* 2006; Wilson *et al.,* 2007). It is also possible that there was compensation between the times of activating CreER at postnatal days 5-7, and the time during which locomotor experiments took place at postnatal days 23-37, although no obvious effect was noted during this interval on their behaviour in cages. Another possibility is that glutamatergic transmission by Hb9 INs control the locomotor output of types of locomotion different from those tested, such as those that require the activation of different muscle groups, such as axial muscles (Schilling, 2011;

Horner and Jayne, 2014; Bagnall *et al.,* 2014). To get a further understanding of possible roles of Hb9 INs, we sought to study their projections throughout the spinal cord and to identify neuronal subpopulations that are postsynaptic to Hb9 INs (Chapter 4).

By crossing of Hb9::CreER$^{T2}$ mice with Rosa26$^{fs\text{-}synaptophysin\text{-}Td\ tomato/+}$, we generated mice that express Td-tomato specifically in the boutons of Hb9 expressing cells. We then studied the projections of Hb9 INs by looking at Td-tomato positive/vGluT2 positive terminals to create a map by which we can gain insight into the role of glutamatergic transmission by Hb9 INs (Chapter 4). Observing high density clusters in ventral lamina X, medial lamina VIII and medial lamina IX of upper lumbar segments indicated that Hb9 INs synapse on neuronal subpopulations located in these regions. We studied appositions on MNs, Hb9 INs and SPNs of the IMM column. Interestingly, preliminary data indicate that only some MNs in the MMC were postsynaptic to Hb9 INs as confirmed using electron microscopy in collaboration with the Todd lab (Glasgow, Scotland). The fact that these synapses are few and selective to specific MN subpopulations, questions the significance of these synapses on overall locomotor behaviour.

We also found appositions with the soma and proximal dendrites of Hb9 INs which extends previous findings that investigated GFP/vGluT2 colocalization using the Hb9::eGFP mouse model (Wilson *et al.,* 2005; Hinckley *et al.,* 2005). This result suggests that Hb9 INs form recurrent synapses to initiate mutual or self-excitation.

Lastly, we examined appositions with SPNs in the IMM of upper lumbar as well as lower cervical segments, but found few. The projection of Hb9 INs to the central

autonomic area as well as their presence in this area (Wilson *et al.,* 2005; Deuchars, 2007), suggested that Hb9 INs could be pre-sympathetic INs. However, we found that there were rare appositions with SPNs, indicating that Hb9 INs do not provide significant direct sympathetic input. Another possibility is that they may be modulating sympathetic outflow via a disynaptic pathway by forming synaptic contacts on pre-sympathetic INs (Deuchars *et al.,* 2005). Thus, the role of Hb9 INs on the sympathetic outflow requires investigation.

In this thesis, we showed that glutamatergic transmission by Hb9 INs is not critical for treadmill locomotion. We also provided an axon terminal map and identified some neuronal subpopulations post-synaptic to Hb9 INs. Future research in identifying neuronal subpopulations located in the hot spots of these maps could provide more insight to the function of chemical transmission by Hb9 INs.

## 5.3 COMMENTS ON FUTURE RESEARCH OF HB9 INS

We have answered an outstanding question regarding locomotor rhythmogenesis by demonstrating that glutamatergic transmission by Hb9 INs had no discernible effect on locomotor behaviour. Furthermore, we provided a density distribution map of axonal terminals of Hb9 INs. Nevertheless, the role of Hb9 INs in spinal cord function remains to be determined.

Studying the locomotor output in an isolated spinal cord preparation after silencing glutamatergic transmission by Hb9 INs may provide answers to the effect of

these INs on core spinal networks. *In vitro* spinal cord preparations provide a way to study spinal networks in isolation of descending and sensory inputs (Chizh *et al.,* 1998; Jiang *et al.,* 1999; Whelan *et al.,* 2000; Hinckley *et al.,* 2005; Kwan *et al.,* 2009; Brownstone *et al.,* 2011)

One possibility to be explored is that Hb9 INs may be contributing to rhythm generation through electrical synapses (Wilson *et al.,* 2007; Hinckley and Ziskind-Conhaim, 2006; Sieling *et al.,* 2014). Studying the effect of silencing electrical coupling involving Hb9 INs on locomotor behaviour will provide an answer to whether these INs contribute to locomotor rhythmogenesis via other means of synapses. This could be done using a similar strategy as in this thesis, by crossing Hb9::CreER$^{T2}$ with Cx36$^{flox/flox}$ mice to silence the electrical transmission by Hb9 INs (Wellershaus *et al.,* 2008; Campbell *et al.,* 2011).

Studying axonal projections of Hb9 INs revealed synaptic contacts on specific MN subpopulations in the MMC. The rarity of synapses on the soma and proximal dendrites of MNs raises two questions: 1) Are synapses between Hb9 INs and MNs significant? And 2) why Hb9 INs/MNs synapses seem to preferentially target specific MNs in the MMC? Stimulating Hb9 INs and recording from postsynaptic MNs using electrophysiological techniques and $Ca^{2+}$ imaging may provide an answer as to whether the effects of these synapses are significant. On the other hand, injecting retrograde rabies virus in various muscles to identify the specific MNs post synaptic to Hb9 INs, and knowing the role of these muscles in locomotion, may add specificity to the identity of the MNs targeted (Stepien *et al.,* 2010). The presence of synapses on specific MMC MN pools suggests that Hb9 INs manipulate specific axial muscles. Behavioural tests on

forms of locomotion that involve the axial muscles, such as swimming, by observing the overall behaviour and/or recording the activity from axial muscles after silencing glutamatergic transmission by Hb9 INs using EMG, may reveal whether Hb9 INs are indeed involved in different forms of locomotion. Thus, the effect of projections of Hb9 INs to MNs is yet to be demonstrated.

This work provides a basis for future studies aimed to identify the roles of Hb9 INs, as well as an approach towards the study of spinal INs that may be involved in locomotion. In addition, we have provided a method to facilitate the identification of the post-synaptic targets of genetically definable spinal neurons.

# BIBLIOGRAPHY


Alaynick WA, Jessell TM, Pfaff SL (2011) SnapShot: spinal cord development. Cell 146:178-178 e171.

Anderson TM, Abbinanti MD, Peck JH, Gilmour M, Brownstone RM, Masino MA (2012) Low-threshold calcium currents contribute to locomotor-like activity in neonatal mice. Journal of neurophysiology 107:103-113.

Arber S (2012) Motor circuits in action: specification, connectivity, and function. Neuron 74: 975-989.

Arber S, Han B, Mendelsohn M, Smith M, Jessell TM, Sockanathan S (1999) Requirement for the homeobox gene Hb9 in the consolidation of motor neuron identity. Neuron 23: 659-674.

Ausborn J, Mahmood R, El Manira A (2012) Decoding the rules of recruitment of excitatory interneurons in the adult zebrafish locomotor network. Proc Natl Acad Sci U S A 109: E3631-3639.

Austin S, Ziese M, Sternberg N (1981) A novel role for site-specific recombination in maintenance of bacterial replicons. Cell 25:729-736.

Bagnall MW, McLean DL (2014) Modular organization of axial microcircuits in zebrafish. Science 343:197-200.

Beare JE, Morehouse JR, DeVries WH, Enzmann GU, Burke DA, Magnuson DS, Whittemore SR (2009) Gait analysis in normal and spinal contused mice using the TreadScan system. Journal of neurotrauma 26: 2045-2056.

Betz UA, Voßhenrich CA, Rajewsky K, Müller W (1996) Bypass of lethality with mosaic mice generated by Cre-loxP-mediated recombination. Curr Biol 6: 1307-1316.

Briscoe J, Pierani A, Jessell TM, Ericson J (2000) A homeodomain protein code specifies progenitor cell identity and neuronal fate in the ventral neural tube. Cell 101:435-445.

Brown, TG. (1911) The intrinsic factors in the act of progression in the mammal. Proc. R. Soc. Lond., B 84: 308–319.

Brown TG. (1912) The factors in rhythmic activity of the nervous system. Proc R Soc Lond., B 85: 278–89.

Brownstone RM, Bui TV (2010) Spinal interneurons providing input to the final common path during locomotion. Progress in brain research 187:81-95.

Brownstone RM, Krawitz S, Jordan LM (2011) Reversal of the late phase of spike frequency adaptation in cat spinal motoneurons during fictive locomotion. Journal of neurophysiology 105:1045-1050.

Brownstone RM, Wilson JM (2008) Strategies for delineating spinal locomotor rhythm-generating networks and the possible role of Hb9 interneurones in rhythmogenesis. Brain research reviews 57:64-76.

Buchanan JT, Cohen AH (1982) Activities of identified interneurons, motoneurons, and muscle fibers during fictive swimming in the lamprey and effects of reticulospinal and dorsal cell stimulation. Journal of neurophysiology 47: 948-960.

Bui TV, Akay T, Loubani O, Hnasko TS, Jessell TM, Brownstone RM (2013) Circuits for grasping: spinal dI3 interneurons mediate cutaneous control of motor behavior. Neuron 78: 191-204.

Burke RE, Degtyarenko AM, Simon ES (2001) Patterns of locomotor drive to motoneurons and last-order interneurons: clues to the structure of the CPG. Journal of neurophysiology 86: 447-462.

Campbell RE, Ducret E, Porteous R, Liu X, Herde MK, Wellerhaus K, Sonntag S, Willecke K, Herbison AE (2011) Gap junctions between neuronal inputs but not gonadotropin-releasing hormone neurons control estrous cycles in the mouse. Endocrinology 152: 2290-2301.

Carr PA, Huang A, Noga BR, Jordan LM (1995) Cytochemical characteristics of cat spinal neurons activated during fictive locomotion. Brain research bulletin 37: 213-218.

Chau D, Johns DG, Schramm LP (2000) Ongoing and stimulus-evoked activity of sympathetically correlated neurons in the intermediate zone and dorsal horn of acutely spinalized rats. Journal of neurophysiology 83: 2699-2707.

Cazalets JR, Bertrand S, Sqalli-Houssaini Y, Clarac F (1998) GABAergic control of spinal locomotor networks in the neonatal rat. Annals of the New York Academy of Sciences 860: 168-180.

Chizh BA, Headley PM, Paton JF (1998) Coupling of sympathetic and somatic motor outflows from the spinal cord in a perfused preparation of adult mouse *in vitro*. The Journal of physiology 508 ( Pt 3): 907-918.

Cohen AH, Ermentrout GB, Kiemel T, Kopell N, Sigvardt KA, Williams TL (1992) Modelling of intersegmental coordination in the lamprey central pattern generator for locomotion. Trends in neurosciences 15: 434-438.

Conway BA, Hultborn H, Kiehn O (1987) Proprioceptive input resets central locomotor rhythm in the spinal cat. Exp Brain Res 68:643-656.

Cowley KC, Schmidt B (1997) Regional distribution of the locomotor pattern-generating network in the neonatal rat spinal cord. J Neurophysiol 77: 247-259.

Crone SA, Zhong G, Harris-Warrick R, Sharma K (2009) In mice lacking V2a interneurons, gait depends on speed of locomotion. The Journal of neuroscience : the official journal of the Society for Neuroscience 29: 7098-7109.

Dai X, Noga BR, Douglas JR, Jordan LM (2005) Localization of spinal neurons activated during locomotion using the c-fos immunohistochemical method. Journal of neurophysiology 93: 3442-3452.

Deuchars SA (2007) Multi-tasking in the spinal cord--do 'sympathetic' interneurones work harder than we give them credit for? The Journal of physiology 580:723-729.

Deuchars SA, Milligan CJ, Stornetta RL, Deuchars J (2005) GABAergic neurons in the central region of the spinal cord: a novel substrate for sympathetic inhibition. The Journal of neuroscience : the official journal of the Society for Neuroscience 25:1063-1070.

Edgerton, V.R., Grillner, S., Sjostrom, A., Zangger, P., 1976. Central generation of locomotion in vertebrates. In: Herman, R.M., Grillner, S., Stein, P.S.G., Stuart, D.G. (Eds.), Neural Control of Locomotion, vol. 18. Plenum Press, New York, pp. 439–464.

El Manira A, Tegner J, Grillner S (1994) Calcium-dependent potassium channels play a critical role for burst termination in the locomotor network in lamprey. Journal of neurophysiology 72:1852-1861.

Feil R, Brocard J, Mascrez B, LeMeur M, Metzger D, Chambon P (1996) Ligand-activated site-specific recombination in mice. Proc Natl Acad Sci U S A 93:10887-10890.

Feil S, Valtcheva N, Feil R (2009) Inducible Cre mice. Methods in molecular biology 530:343-363.

Feldman JL, Del Negro C (2006 ) Looking for inspiration: new perspectives on respiratory rhythm. Nat Rev Neurosci 7:232-242.

Fogarty MJ, Hammond LA, Kanjhan R, Bellingham MC, Noakes PG (2013) A method for the three-dimensional reconstruction of Neurobiotin-filled neurons and the location of their synaptic inputs. Frontiers in neural circuits 7:153.

Gosgnach S, Lanuza GM, Butt SJ, Saueressig H, Zhang Y, Velasquez T, Riethmacher D, Callaway EM, Kiehn O, Goulding M (2006) V1 spinal neurons regulate the speed of vertebrate locomotor outputs. Nature 440:215-219.

Griener A, Dyck J, Gosgnach S (2013) Regional distribution of putative rhythm-generating and pattern-forming components of the mammalian locomotor CPG. Neuroscience 250:644-650.

Grillner S (1991) Recombination of motor pattern generators. Curr Biol 1:231-233.

Grillner S, McClellan A, Perret C (1981) Entrainment of the spinal pattern generators for swimming by mechano-sensitive elements in the lamprey spinal cord *in vitro*. Brain Res 217:380-386.

Grillner S, Zangger P (1975) How detailed is the central pattern generation for locomotion? Brain Res 88:367-371.

Grillner S, Deliagina T, Ekeberg O, el Manira A, Hill RH, Lansner A, Orlovsky GN, Wallen P (1995) Neural networks that co-ordinate locomotion and body orientation in lamprey. Trends in neurosciences 18:270-279.

Grillner S, Jessell TM (2009) Measured motion: searching for simplicity in spinal locomotor networks. Current opinion in neurobiology 19:572-586.

Grillner S, Matsushima T (1991) The neural network underlying locomotion in lamprey--synaptic and cellular mechanisms. Neuron 7:1-15.

Gu H, Marth JD, Orban PC, Mossmann H, Rajewsky K (1994) Deletion of a DNA polymerase beta gene segment in T cells using cell type-specific gene targeting. Science 265:103-106.

Hagglund M, Borgius L, Dougherty KJ, Kiehn O (2010) Activation of groups of excitatory neurons in the mammalian spinal cord or hindbrain evokes locomotion. Nature neuroscience 13:246-252.

Hagglund M, Dougherty KJ, Borgius L, Itohara S, Iwasato T, Kiehn O (2013) Optogenetic dissection reveals multiple rhythmogenic modules underlying locomotion. Proc Natl Acad Sci U S A 110:11589-11594.

Han P, Nakanishi ST, Tran MA, Whelan PJ (2007) Dopaminergic modulation of spinal neuronal excitability. The Journal of neuroscience : the official journal of the Society for Neuroscience 27:13192-13204.

Harrison KA, Druey KM, Deguchi Y, Tuscano JM, Kehrl JH (1994) A novel human homeobox gene distantly related to proboscipedia is expressed in lymphoid and pancreatic tissues. The Journal of biological chemistry 269:19968-19975.

Hinckley CA, Hartley R, Wu L, Todd A, Ziskind-Conhaim L (2005) Locomotor-like rhythms in a genetically distinct cluster of interneurons in the mammalian spinal cord. Journal of neurophysiology 93:1439-1449.

Hinckley CA, Ziskind-Conhaim L (2006) Electrical coupling between locomotor-related excitatory interneurons in the mammalian spinal cord. The Journal of neuroscience : the official journal of the Society for Neuroscience 26:8477-8483.

Hnasko TS, Chuhma N, Zhang H, Goh GY, Sulzer D, Palmiter RD, Rayport S, Edwards RH (2010) Vesicular glutamate transport promotes dopamine storage and glutamate corelease *in vivo*. Neuron 65:643-656.

Hoess R, Abremski K, Sternberg N (1984) The nature of the interaction of the P1 recombinase Cre with the recombining site loxP. Cold Spring Harbor symposia on quantitative biology 49:761-768.

Hoess RH, Ziese M, Sternberg N (1982) P1 site-specific recombination: nucleotide sequence of the recombining sites. Proc Natl Acad Sci U S A 79:3398-3402.

Horner AM, Jayne BC (2014) Lungfish axial muscle function and the vertebrate water to land transition. PloS one 9:e96516.

Hughes GM, Wiersma AG (1960) The co-ordination of swimmeret movements in the crayfish, Procambarus clarkii. . J Exp Biol 37:657–670.

Iizuka M, Kiehn O, Kudo N (1997 ) Development in neonatal rats of the sensory resetting of the locomotor rhythm induced by NMDA and 5-HT. Exp Brain Res 114:193-204.

Indra AK, Warot X, Brocard J, Bornert JM, Xiao J, Chambon P, Metzger D (1999) Temporally-controlled site-specific mutagenesis in the basal layer of the epidermis: comparison of the recombinase activity of the tamoxifen-inducible Cre-ERT and Cre-ERT2 recombinases Nucleic Acids Research 27:4324–4327.

Jessell TM (2000) Neuronal specification in the spinal cord: inductive signals and transcriptional codes. Nature reviews Genetics 1:20-29.

Jiang Z, Carlin KP, Brownstone RM (1999) An *in vitro* functionally mature mouse spinal cord preparation for the study of spinal motor networks. Brain research 816:493-499.

Johnson RL, Tabin C (1995) The long and short of hedgehog signaling. Cell 81:313-316.

Kerman IA, Enquist LW, Watson SJ, Yates BJ (2003) Brainstem substrates of sympatho-motor circuitry identified using trans-synaptic tracing with pseudorabies virus recombinants. The Journal of neuroscience : the official journal of the Society for Neuroscience 23:4657-4666.

Kiehn O (2006) Locomotor circuits in the mammalian spinal cord. Annu Rev Neurosci 29:279-306.

Kiehn O, Kjaerulff O ( 1998) Distribution of central pattern generators for rhythmic motor outputs in the spinal cord of limbed vertebrates. Ann N Y Acad Sci 860:110-129.

Kiehn O, Butt SJB (2003) Physiological, anatomical and genetic identification of CPG neurons in the developing mammalian spinal cord. Progress in Neurobiology 70:347-361.

Kwan AC, Dietz SB, Webb WW, Harris-Warrick RM (2009) Activity of Hb9 interneurons during fictive locomotion in mouse spinal cord. The Journal of neuroscience : the official journal of the Society for Neuroscience 29:11601-11613.

Lakso M, Sauer B, Mosinger B Jr, Lee EJ, Manning RW, Yu SH, Mulder KL, Westphal H (1992) Targeted oncogene activation by site-specific recombination in transgenic mice. Proc Natl Acad Sci U S A 89:6232-6236.

Lansner A, Kotaleski JH, Grillner S (1998) Modeling of the spinal neuronal circuitry underlying locomotion in a lower vertebrate. Annals of the New York Academy of Sciences 860:239-249.

Lanuza GM, Gosgnach S, Pierani A, Jessell TM, Goulding M (2004) Genetic identification of spinal interneurons that coordinate left-right locomotor activity necessary for walking movements. Neuron 42:375-386.

Li WC, Roberts A, Soffe SR (2009) Locomotor rhythm maintenance: electrical coupling among premotor excitatory interneurons in the brainstem and spinal cord of young Xenopus tadpoles. The Journal of physiology 587:1677-1693.

Lundberg, A., 1981. Half-centres revisited. In: Szentagothai, P.M., Hamori, J. (Eds.), Motion and Organization Principles: 28th International Congress of Physiological Sciences. Pergamon Press, Budapest.

MacLean JN, Cowley KC, Schmidt BJ (1998) NMDA receptor-mediated oscillatory activity in the neonatal rat spinal cord is serotonin dependent. Journal of neurophysiology 79:2804-2808.

Madden CJ, Morrison SF (2006) Serotonin potentiates sympathetic responses evoked by spinal NMDA. The Journal of physiology 577:525-537.

Marcoux J, Rossignol S (2000) Initiating or blocking locomotion in spinal cats by applying noradrenergic drugs to restricted lumbar spinal segments. The Journal of neuroscience : the official journal of the Society for Neuroscience 20:8577-8585.

Marigo V, Tabin CJ (1996) Regulation of patched by sonic hedgehog in the developing neural tube. Proc Natl Acad Sci U S A 93:9346-9351.

Marina N, Taheri M, Gilbey MP (2006) Generation of a physiological sympathetic motor rhythm in the rat following spinal application of 5-HT. The Journal of physiology 571:441-450.

Masino MA, Abbinanti MD, Eian J, Harris-Warrick RM (2012) TTX-resistant NMDA receptor-mediated membrane potential oscillations in neonatal mouse Hb9 interneurons. PloS one 7:e47940.

McCall RB, Gebber GL, Barman SM (1977) Spinal interneurons in the baroreceptor reflex arc. The American journal of physiology 232:H657-665.

McCrea DA, Rybak IA (2008) Organization of mammalian locomotor rhythm and pattern generation. Brain research reviews 57:134-146.

Metzger D, Clifford J, Chiba H, Chambon P (1995) Conditional site-specific recombination in mammalian cells using a ligand-dependent chimeric Cre recombinase. Proc Natl Acad Sci U S A 92:6991-6995.

Miller CO, Johns DG, Schramm LP (2001) Spinal interneurons play a minor role in generating ongoing renal sympathetic nerve activity in spinally intact rats. Brain research 918:101-106.

Mulloney B, Smarandache C (2010) Fifty Years of CPGs: Two Neuroethological Papers that Shaped the Course of Neuroscience. Frontiers in behavioral neuroscience 4.

Nishimaru H, Kakizaki M (2009) The role of inhibitory neurotransmission in locomotor circuits of the developing mammalian spinal cord. Acta physiologica 197:83-97.

Ohta Y, Grillner S (1989) Monosynaptic excitatory amino acid transmission from the posterior rhombencephalic reticular nucleus to spinal neurons involved in the control of locomotion in lamprey. Journal of neurophysiology 62:1079-1089.

Panayi H, Panayiotou E, Orford M, Genethliou N, Mean R, Lapathitis G, Li S, Xiang M, Kessaris N, Richardson WD, Malas S (2010) Sox1 is required for the specification of a novel p2-derived interneuron subtype in the mouse ventral spinal cord. The Journal of neuroscience : the official journal of the Society for Neuroscience 30:12274-12280.

Perkel DH, Mulloney B (1974) Motor pattern production in reciprocally inhibitory neurons exhibiting postinhibitory rebound. Science 185:181-183.

Pierani A, Moran-Rivard L, Sunshine MJ, Littman DR, Goulding M, Jessell TM (2001) Control of interneuron fate in the developing spinal cord by the progenitor homeodomain protein Dbx1. Neuron 29:367-384.

Rekling JC, Shao XM, Feldman JL (2000) Electrical coupling and excitatory synaptic transmission between rhythmogenic respiratory neurons in the preBotzinger complex. The Journal of neuroscience : the official journal of the Society for Neuroscience 20:RC113.

Roberts A, Soffe SR, Wolf ES, Yoshida M, Zhao FY (1998) Central circuits controlling locomotion in young frog tadpoles. Annals of the New York Academy of Sciences 860:19-34.

Russell DF, Hartline DK (1978) Bursting neural networks: a reexamination. Science 200:453-456.

Rybak IA, Shevtsova NA, Lafreniere-Roula M, McCrea DA (2006) Modelling spinal circuitry involved in locomotor pattern generation: insights from deletions during fictive locomotion. The Journal of physiology 577:617-639.

Saha MS, Miles RR, Grainger RM (1997) Dorsal-ventral patterning during neural induction in Xenopus: assessment of spinal cord regionalization with xHB9, a marker for the motor neuron region. Developmental biology 187:209-223.

Saint-Amant L, Drapeau P (2001) Synchronization of an embryonic network of identified spinal interneurons solely by electrical coupling. Neuron 31:1035-1046.

Sasaki K, Cropper EC, Weiss KR, Jing J (2013) Functional differentiation of a population of electrically coupled heterogeneous elements in a microcircuit. The Journal of neuroscience : the official journal of the Society for Neuroscience 33:93-105.

Sauer B (1998 ) Inducible Gene Targeting in Mice Using the Cre/lox System. Methods 14:381-392.

Sauer B, Henderson N (1989 ) Cre-stimulated recombination at loxP-containing DNA sequences placed into the mammalian genome. Nucleic Acids Res 17:147-161.

Scherrer G, Low SA, Wang X, Zhang J, Yamanaka H, Urban R, Solorzano C, Harper B, Hnasko TS, Edwards RH, Basbaum A (2010) VGLUT2 expression in primary afferent neurons is essential for normal acute pain and injury-induced heat hypersensitivity. Proc Natl Acad Sci U S A 107:22296-22301.

Schilling N (2011) Evolution of the axial system in craniates: morphology and function of the perivertebral musculature. Frontiers in zoology 8:4.

Sieling F, Bedecarrats A, Simmers J, Prinz AA, Nargeot R (2014) Differential roles of nonsynaptic and synaptic plasticity in operant reward learning-induced compulsive behavior. Curr Biol 24:941-950.

Stepien AE, Tripodi M, Arber S (2010) Monosynaptic rabies virus reveals premotor network organization and synaptic specificity of cholinergic partition cells. Neuron 68:456-472.

Stuart DG, Hultborn H (2008) Thomas Graham Brown (1882--1965), Anders Lundberg (1920-), and the neural control of stepping. Brain research reviews 59:74-95.

Su CY, Menuz K, Reisert J, Carlson JR (2012) Non-synaptic inhibition between grouped neurons in an olfactory circuit. Nature 492:66-71.

Taccola G, Nistri A (2004) Low micromolar concentrations of 4-aminopyridine facilitate fictive locomotion expressed by the rat spinal cord *in vitro*. Neuroscience 126:511-520.

Talpalar AE, Bouvier J, Borgius L, Fortin G, Pierani A, Kiehn O (2013) Dual-mode operation of neuronal networks involved in left-right alternation. Nature 500:85-88.

Tanabe Y, Jessell TM (1996) Diversity and pattern in the developing spinal cord. Science 274:1115-1123.

Tang X, Chander AR, Schramm LP (2003) Sympathetic activity and the underlying action potentials in sympathetic nerves: a simulation. American journal of physiology Regulatory, integrative and comparative physiology 285:R1504-1513.

Tazerart S, Vinay L, Brocard F (2008) The persistent sodium current generates pacemaker activities in the central pattern generator for locomotion and regulates the locomotor rhythm. The Journal of neuroscience : the official journal of the Society for Neuroscience 28:8577-8589.

Thaler J, Harrison K, Sharma K, Lettieri K, Kehrl J, Pfaff SL (1999) Active suppression of interneuron programs within developing motor neurons revealed by analysis of homeodomain factor HB9. Neuron 23:675-687.

Todd AJ, Hughes DI, Polgar E, Nagy GG, Mackie M, Ottersen OP, Maxwell DJ (2003) The expression of vesicular glutamate transporters VGLUT1 and VGLUT2 in neurochemically defined axonal populations in the rat spinal cord with emphasis on the dorsal horn. The European journal of neuroscience 17:13-27.

Traub RD (1995) Model of synchronized population bursts in electrically coupled interneurons containing active dendritic conductances. Journal of computational neuroscience 2:283-289.

Venables, W. N. and Ripley, B. D. (2002) Modern Applied Statistics with S. Fourth edition. Springer

Wellershaus K, Degen J, Deuchars J, Theis M, Charollais A, Caille D, Gauthier B, Janssen-Bienhold U, Sonntag S, Herrera P, Meda P, Willecke K (2008) A new conditional mouse mutant reveals specific expression and functions of connexin36 in neurons and pancreatic beta-cells. Experimental cell research 314:997-1012.

Whelan P, Bonnot A, O'Donovan MJ (2000) Properties of rhythmic activity generated by the isolated spinal cord of the neonatal mouse. Journal of neurophysiology 84:2821-2833.

Wilson, D.M., 1961. The central control of flight in the locust. J. Exp.Biol. 38, 471–490.

Wilson D (1966) Central nervous mechanisms for the generation of rhythmic behaviour in arthropods. Symp Soc Exp Biol 20:199-228.

Wilson DM, Wyman RJ (1965) Motor output patterns during random and rhythmic stimulation of locust thoracic ganglia J Biophys 5:121-143.

Wilson JM, Cowan AI, Brownstone RM (2007) Heterogeneous electrotonic coupling and synchronization of rhythmic bursting activity in mouse Hb9 interneurons. Journal of neurophysiology 98:2370-2381.

Wilson JM, Hartley R, Maxwell DJ, Todd AJ, Lieberam I, Kaltschmidt JA, Yoshida Y, Jessell TM, Brownstone RM (2005) Conditional rhythmicity of ventral spinal interneurons defined by expression of the Hb9 homeodomain protein. The Journal of neuroscience : the official journal of the Society for Neuroscience 25:5710-5719.

Zagoraiou L, Akay T, Martin JF, Brownstone RM, Jessell TM, Miles GB (2009) A cluster of cholinergic premotor interneurons modulates mouse locomotor activity. Neuron 64:645-662.

Zhang Y, Narayan S, Geiman E, Lanuza GM, Velasquez T, Shanks B, Akay T, Dyck J, Pearson K, Gosgnach S, Fan CM, Goulding M (2008) V3 spinal neurons establish a robust and balanced locomotor rhythm during walking. Neuron 60:84-96.

Ziskind-Conhaim L, Mentis GZ, Wiesner EP, Titus DJ (2010) Synaptic integration of rhythmogenic neurons in the locomotor circuitry: the case of Hb9 interneurons. Annals of the New York Academy of Sciences 1198:72-84

Ziskind-Conhaim L, Wu L, Wiesner EP (2008) Persistent sodium current contributes to induced voltage oscillations in locomotor-related hb9 interneurons in the mouse spinal cord. Journal of neurophysiology 100:2254-2264.